UNIVERSITY OF CALIFORNIA SAN DIEGO

The Temporal, Histological, and Transcriptional Behavior of Biological Programs in Skeletal Muscle After Rotator Cuff Tear and Repair

A Dissertation submitted in partial satisfaction of the requirements
for the degree Doctor of Philosophy

in

Bioengineering

by

Laura S. Vasquez-Bolanos

Committee in Charge:

Professor Samuel R. Ward, Chair
Professor Adam J. Engler, Co-Chair
Professor Kim Cooper
Professor Andrew McCulloch
Professor Elsa Sanchez-Lopez
Professor Anshuman Singh

2023

The Dissertation of Laura S. Vasquez-Bolanos is approved, and it is acceptable in quality and form for publication on microfilm and electronically.

University of California San Diego

2023

DEDICATION

I would like to thank Sam for taking me under his wing in 2019 when I decided to join his lab. Sam was an amazing mentor who knew how to comfort me during difficult times yet motivate and push me forward during other moments. I am very grateful for his mentorship and support throughout especially when I asked for a break from the PhD to explore an internship, both when I left and when I came back to wrap up my dissertation. I am also thankful for Severin, Mary, Shannon, Mac, Sydnee, and Isabella, all members at one point of the Ward lab that helped me with not only presentations, papers, and experiments, but also the joys of talking science, orthopedics, or dog mom things. I am grateful for the friendships I made during an unprecedented time (aka the pandemic), and for the advice that got me through the last bit of my PhD once everyone else had finished.

A lot of my dissertation was done unfortunately in my bedroom so shoutout to my roommates during the bulk of my PhD, Austin and Josh, for being amazing friends to talk science with and for supporting me through Quals and my first paper submission. I would also like to thank my partner, Greg, who defend their PhD a few years before me, and helped me tremendously during the challenging slumps, by helping me see the bigger picture. Likewise, at the end of the PhD during the most stressful time, he helped care for me, making sure I had the fuel to keep going and an audience to practice my defense with. I really could not have done it without you by my side Greg. Although my dog Wilbur cannot read, I would like to emphasize the instrumental role he played, as I got him 6 months into my PhD, right before the pandemic, he was a huge emotional support throughout the whole process and very much enjoyed the work from home part. In conclusion, I am so appreciative to my family, friends and many programs such as McNair, Cornell Diversity Programs in Engineering, NSF GRFP, Sloan scholar, for supporting me along the way

in many ways, but especially reminding me that even as a first-generation, under-represented minority, to dream big and that I too, deserved to be there.

TABLE OF CONTENTS

LIST OF FIGURES

LIST OF SUPPLEMENTAL DATA

1. Chapter 2 published at: https://www.frontiersin.org/articles/10.3389/fphys.2021.707116/full#supplementary-material
2. Chapter 3 published at: https://www.frontiersin.org/articles/10.3389/fphys.2023.1164055/full#supplementary-material
3. Chapter 4 file: Vasquez-Bolanos_WGCNA-GOEnrichmentTable.xlsx

ACKNOWLEDGEMENTS

Chapter 2, in full, is a reprint of the material as it appears in the Journal of Physiology 2021. Laura S Vasquez-Bolanos, Michael C Gibbons, Severin Ruoss, Isabella T Wu, Mario Vargas-Vila, Sydnee A Hyman, Mary C Esparza, Donald C Fithian, John G Lane, Anshuman Singh A, Chanond A Nasamran CA, Kathleen M Fisch, and Samuel R Ward. The dissertation author was the primary investigator of this material.

Chapter 3, in full, is a reprint of the material as it appears in the Journal of Physiology, 2023. Laura S Vasquez-Bolanos, Michael C Gibbons, Severin Ruoss, Isabella T Wu, Mary C Esparza, Donald C Fithian, John G Lane, Anshuman Singh, Chanond A Nasamran, Kathleen M Fisch, Samuel R Ward. The dissertation author was the primary investigator of this material.

Chapter 4, in full, is currently being prepared for submission for publication of this material. Laura S Vasquez-Bolanos, Shannon N Bremner, Mary C Esparza, Donald C. Fithian, John G. Lane, Anshuman Singh, Elsa Sanchez-Lopez, Samuel R Ward. The dissertation author was the primary investigator of this material.

VITA

2019 Bachelor of Science, Mechanical Engineering, Cornell University

2023 Doctor of Philosophy, Bioengineering, University of California San Diego

ABSTRACT OF THE DISSERTATION

The Temporal, Histological, and Transcriptional Behavior of Biological Programs in Skeletal Muscle After Rotator Cuff Tear and Repair

by

Laura S. Vasquez-Bolanos

Doctor of Philosophy in Bioengineering

University of California San Diego, 2023

Professor Samuel Ward, Chair
Professor Adam Engler, Co-Chair

Rotator cuff tears affect 1 in 5 individuals over the age of 60, leading to muscle atrophy, degeneration, fibrosis, and fatty infiltration. These changes observed in muscle are persistent regardless of treatment or surgical repair, and the progression to this irreversible degenerative muscle state is poorly understood. The purpose of this work was to investigate the temporal histological and transcriptomic behavior of biological programs after rotator cuff tear and repair in a rabbit model. We performed RNAseq at 1, 2, 4, 8, and 16 weeks after tear and 1, 2, 4, and 8

weeks after repair to identify the transcriptional profile of biological programs (*i.e.* inflammation, adipogenesis, apoptosis). After detecting a strong immune system signature, we evaluated the number of immune cells and markers of proliferation/cell cycle histologically. Post-tenotomy there was a clear orchestration of biological programs largely related to inflammation and energetics at early timepoints, a progression towards adipogenesis and apoptosis that subsided by 8 weeks, and a resurgence of various programs including inflammation, fibrosis, and apoptosis at 16 weeks. Post-repair there was a lack of a regenerative response to mechanical re-loading, but instead, a strong resurgence of inflammation, adipogenesis, fibrosis and apoptosis at 2 weeks that subsided by 8 weeks. Relative to the immune system, there was a significant increase in neutrophil numbers at 1 and 4 weeks post-tenotomy, but few to none post-repair. There was a significant increase in CD163+ macrophages at 2 week post-tenotomy and 1 and 2 weeks post-repair. This increase was also seen regionally post-repair, with more CD163+ (M2c) macrophages found in regions of muscle degeneration compared to regions of non-degenerated muscle at almost all timepoints (1, 2, 4 weeks). In conclusion, we identified a temporal transcriptional profile of biological programs such as inflammation, adipogenesis and fibrosis and highlighted contrasting immune system behaviors of neutrophils and CD163+ macrophages in muscle after rotator cuff tear and repair. These data provide a time-resolved framework for understanding myocyte-inflammatory cell-progenitor cell interactions that are poorly understood in muscle. Translationally, these data provide context for transcriptional and cell-based assays of human tissue that can only be procured cross-sectionally in time, and they shed light onto potential therapeutic targets that may augment muscle recovery after tendon repair in patients with rotator cuff injuries.

Chapter 1 INTRODUCTION

Rotator cuff (RC) tears affect 1 in 5 individuals over the age of 60, and these tears lead to significant disability (Lehman et al., 1995; Colvin et al., 2012; Sayampanathan et al., 2017; Collin et al., 2019; Yamamoto et al., 2010). As a result, there is a significant healthcare expense incurred by this population of individuals who typically undergo a range of treatment options such as physical therapy, injectables, and surgical intervention (Gerber et al., 2007; Gladstone et al., 2007; Collin et al., 2018 & 2019. The initial process in rotator cuff disease often manifests as a tear in the tendon, which can occur due to a variety of factors including age, overuse, or trauma (Bartolozzi et al., 1994; Yamamoto et al., 2010; Saccomanno et al., 2016). This tear disrupts the normal biomechanics of the shoulder, ultimately leading to muscle unloading and retraction which leads to structural changes in the musculature.

These changes include atrophy, characterized by increased contractile protein turnover and diminished protein synthesis (Bialek et al., 2011; Bonaldo et al., 2013). However, as RC disease progresses, atrophied muscle can evolve into muscle fibers accumulating structural damage, resulting in altered sarcomere structure, degeneration, leading to muscle fiber death (Gibbons et al. 2017). This process is more complex than the unloading-induced muscle atrophy seen in other disuse models (Clark et al., 2009; Bialek et al, 2011), because RC disease has been theorized to include not only unloading, but also overloading of regions of muscle, which can lead to abnormal shear stress (as seen in eccentric contraction; Darr et al., 1987; Schoenfeld, 2012). Ultimately this contributes to changes in muscle architecture, such as muscle fiber reorientation, increases in the pennation angle (Lieber et al., 2000; Meyer et al., 2004) and decreases in sarcomere length (Gibbons et al., 2016; Tomioka et al., 2009), due to altered biomechanics and prolonged changes in loading patterns. Over time, the atrophied muscle may also undergo fatty infiltration, where fat

cells replace muscle fibers, leading to a decrease in muscle quality and function (Gibbons et al., 2017). Torn human RC muscle has been characterized to lose up to 40-60% of muscle volume and contain 10-40% of fat content (Matsumura et al., 2017; Gibbons et al., 2018). Additionally, at chronic stages of RC disease fibrosis is thought to accumulate with excessive deposit of extracellular matrix in the muscle, and sheep and canine animal models have suggested a possible correlation with increased muscle stiffness (Gerber et al., 2004; Safran et al., 2005; Silldorff et al., 2014; Sato et al., 2015). Some of these changes are secondary consequences of the tendon tear, but some may be primary, and in either case they contribute to the progression of the disease and exacerbate functional impairment and disability (Shen et al., 2008; Kim et al., 2010; Goutallier et al., 2003; Gladstone et al., 2007).

Surgical intervention, specifically tendon repair, is a common treatment strategy aimed at restoring the normal anatomy and biomechanics of the rotator cuff (Cofield et al., 2001). Theoretically, by reattaching the torn tendon to its original insertion site on the humerus, the mechanical environment of the shoulder is restored, which should promote muscle recovery (Davidson et al., 2000). For example, in a mouse animal model, restoration of tendon to bone connectivity, restored muscle atrophy (Thomopoulos et al., 2015). However, after surgical repair of the rotator cuff, the muscle structural changes such as muscle atrophy and fatty infiltration observed after tear have been proven to be irreversible in humans and pathphysiologically relevant pre-clinical animal models such as sheep and rabbi (Gerber et al., 2000; Gerber et al., 2004; Gerber et al., 2007; Gladstone et al., 2007). In fact, the degree of muscle atrophy and fatty infiltration at the time of surgery can highly influence the outcome of the repair, with more severe changes associated with a higher risk of repair failure (Harryman et al., 1991; Goutallier et al., 2003; Gladstone et al., 2007). The state of the muscle can actually continue degrading after repair with

an increase in fibrosis, degeneration and fat (Davis et al., 2015; Gibbons et al., 2017). This lack of muscle recovery following tendon repair underscores the complexity of rotator cuff disease and highlights the need for a deeper understanding of the underlying biological mechanisms contributing to.

The mechanisms behind the persistent muscle changes following tendon repair are not understood. The persistence of muscle atrophy and fatty infiltration following tendon repair suggests that these changes may be driven by intrinsic muscle pathology, independent of the tendon tear and subsequent repair. This has led to a growing interest in exploring the molecular and cellular mechanisms underlying these muscle changes, with a particular focus on the role of various biological programs: inflammation, fibrosis, adipogenesis and more. Various theories involving the activation and silencing of muscle fibro-adipogenic progenitors and muscle satellite cells have been considered (Lee et al., 2019; Lee et al., 2020), but on their own, does not explain the irreversible state of muscle after rotator cuff tear and repair. There is likely a multifactorial orchestration of events taking place, involving a complex interplay of biological and mechanical factors. This may explain why the current approach of studying specific cells and components in muscle has not resulted in clear answer on the cause or targets for improvement after surgical repair (Bianco et al., 2019; Chung et al., 2013; Shah et al., 2017).

In order to understand the abnormal interplay among cells and molecular programs, a template acute muscle injury/regeneration model that is well studied must be used as a comparison. Cardiotoxin-induced muscle injury in mice has been extensively studied along multiple biological axes, including transcriptomics, as a model for muscle regeneration due to its reproducibility and the robustness of the regenerative response (Hirata et al., 2003; Garry et al., 2016). Following cardiotoxin injection, there is an initial phase of necrosis where muscle fibers are damaged, leading

to an inflammatory response characterized by the infiltration of neutrophils (within hours to first few days) and macrophages (within hours to the first few days) (Heredia et al., 2013). The literature indicates that these immune cells play a crucial role in clearing necrotic debris and orchestrating the subsequent regenerative response (Howard et al., 2020). Particularly, macrophages undergo a phenotypic transition from a pro-inflammatory to an anti-inflammatory state, which is essential for the progression of muscle regeneration (Wang et al., 2014; Howard et al., 2020). Concurrently, satellite cells, the resident stem cells in muscle, are activated (0-2 days), begin to proliferate (1-7 days), differentiate (3.5 days – 1 month), and mature (7 days to 1 month+) to replace the damaged muscle fibers (Hawke et al., 2003; Garry et al., 2016). These processes are regulated by a complex network of molecular signals, including growth factors, cytokines, and extracellular matrix components (Yan et al., 2003; Wang et al., 2022). The muscle then undergoes a remodeling phase to restore its structure and function (Dumont et al., 2015). Despite the robust regenerative response, it is important to note that repeated or severe cardiotoxin-induced injuries can impair muscle similarly to chronic RC disease, lead to fibrosis and impaired muscle function (Suetta et al., 2013; Wang et al., 2022).

Understanding a well-studied muscle injury/regeneration system and its cell and transcriptional behavior, prompts a similar desired approach to investigate muscle after rotator cuff tear and repair. Specifically, transcriptomics can be used to elucidate the up and down regulation of specific biological programs, and therefore, the mechanisms contributing to the muscle dysfunction. However, to date, the majority of human transcriptomics research has specifically focused on top differentially regulated genes in programs such as myogenesis, inflammation, adipogenesis, and fibrosis in a valid, yet biased manner (Reardon et al., 2001, Shah et al. 2017, Steinbacher et al., 2010, Choo et al., 2014, Gibbons et al., 2018, Ren et al., 2018). For instance,

Gibbons et al. (2018) explored gene expression in a range of biological programs (5-10 genes in each program) involved in rotator cuff disease and correlated these results to the heterogenous tissue composition of degenerated muscle often found in human, identifying distinct transcriptional behaviors. Given the complexity of the biological programs, a single timepoint of gene expression data often from a limited number of transcripts only gives us a small window into what could be happening in the muscle more globally.

There are even fewer studies that have used more unbiased transcriptional sequencing approaches at multiple time points, but studies have identified shared pathways between human and animal models, such as inflammation, extracellular matrix remodeling, and apoptosis, which are significantly influenced during the progression of rotator cuff tears. For instance, Gumucio et al. (2018) conducted a comprehensive analysis using RNAseq, which unbiasedly sequences all transcripts available in the sampled tissue, in a rat rotator cuff tenotomy and neurotomy model, at 10, 30, and 60 days and identified that mitochondrial function was impaired after tear injury possibly contributing to lipid accumulation. Similarly, Lee et al. (2018) used RNA microarray to assess biological programs transcriptionally in a mouse rotator cuff tenotomy at 1 and 4 weeks post-tenotomy and identified relevant significant genes involved in aging, apoptosis, atrophy, and fatty acid transport. However, there are problems associated with these data sets. For example, the interpretation of biological activity in small animal models that do not recapitulate the level of fat, degeneration, and fibrosis found in human muscles or requires a non-physiologic neurotomy in addition to a tenotomy to induce any meaningful muscle atrophy and degeneration (Rowshan et al., 2010) has questionable translational relevance.

Conversely, sheep are the gold standard for studying rotator cuff changes (Gerber et al., 2004) because they recapitulate the muscle morphology changes observed in humans, but are

costly in terms of resources and time, which limits their use as a high throughput model. Currently, there are limited transcriptomic studies in sheep, and they focus on mitochondrial dysfunction, and are limited to two different time points post-tenotomy: 2 and 16 weeks post-tenotomy (Fluck et al., 2017 & 2020). Given the broad lack of understanding related to the cause of muscle atrophy, fatty infiltration, and fibrosis in progressive RC disease, there is an unmet need to establish the time-dependent transcriptional activity after these injuries.

Similarly, understanding muscle recovery (or lack of recovery) after surgical tendon repair is pivotal to our understanding of the mechanisms contributing to the persistent state of the muscle atrophy and fibrosis. There is translational value in identifying possible changes within the acute to chronic window of injury and the implicated biological mechanisms induced after surgical repair. Most of the research to date focuses on acute repair, where a tenotomy and repair are performed simultaneously, so surgical techniques/biologic augmentation may be explored in parallel to acute tendon healing (Sun et al., 2020; Li et al., 2018; Ozbaydar et al., 2008; Su et al., 2018; Chung et al., 2013; Honda et al., 2017; Kwon et al., 2018; Yoon et al., 2018; Ruoss et al., 2018a). However, this does not represent the complex human scenario of delayed repair. For example, in older patients, symptomatic tears develop over years and do not undergo surgical repair for months or years after diagnosis. As a result, there is less literature exploring the more human, and pathophysiologically relevant, approach of performing a delayed repair. When delayed repair is implemented, the model systems are typically sheep and rabbit (Gerber et al., 1999, Gerber et al., 2000, Davidson et al., 2000; Matsumoto et al., 2002; Gerber et al., 2004; Gerber et al., 2009; Rubino et al., 2008; Steinbacher et al., 2010; Coleman et al, 2003, Farshad et al., 2011, Uhthoff et al., 2014; Ren et al., 2018; Ruoss et al., 2018b, & Wu et al., 2022). However, even in

these systems, there is very little to no transcriptional data available, let alone time-dependent transcriptional data.

This dissertation aims to meet the unmet need of understanding the biological activity associated with rotator cuff tear and repair. Understanding the time-dependent transcriptional changes in injured and repaired rotator cuff muscles would provide insight into the mechanisms of muscle maladaptation and the opportunity for future studies to target specific pathways in an attempt to mitigate disease progression and accelerate recovery.

Chapter 2 TRANSCRIPTIONAL TIME COURSE AFTER ROTATOR CUFF TEAR

Abstract

Rotator cuff (RC) tears are prevalent in the population above the age of 60. The disease progression leads to muscle atrophy, fibrosis, and fatty infiltration in the chronic state, which is not improved with intervention or surgical repair. This highlights the need to better understand the underlying dysfunction in muscle after RC tendon tear. Contemporary studies aimed at understanding muscle pathobiology after RC tear have considered transcriptional data in mice, rats and sheep models at 2-3 time points (1 to 16 weeks post injury). However, none of these studies observed a transition or resurgence of gene expression after the initial acute time points. In this study, we collected rabbit supraspinatus muscle tissue with high temporal resolution (1, 2, 4, 8, 16 weeks) post-tenotomy (n=6/group), to determine if unique, time-dependent transcriptional changes occur. RNA sequencing and analyses were performed to identify a transcriptional timeline of RC muscle changes and related morphological sequelae. At 1-week post-tenotomy, the greatest number of differentially expressed genes was observed (1069 up/873 down) which decreases through 2 (170/133), 4 (86/41), and 8 weeks (16/18), followed by a resurgence and transition of expression at 16 weeks (1421/293), a behavior which previously has not been captured or reported. Broadly, 1-week post-tenotomy is an acute time point with expected immune system responses, catabolism, and changes in energy metabolism, which continues into 2 weeks with less intensity and greater contribution from mitochondrial effects. Expression shifts at 4 weeks post-tenotomy to fatty acid oxidation, lipolysis, and general up-regulation of adipogenesis genes. The effects of previous weeks' transcriptional dysfunction present themselves at 8 weeks post-tenotomy with enriched DNA damage binding, aggresome activity, ECM-receptor changes and significant expression of genes known to induce apoptosis. At 16 weeks post-tenotomy, there is a range of

enriched pathways including ECM constituent binding, mitophagy, neuronal activity, immune response, and more, highlighting the chaotic nature of this time point and possibility of a chronic classification. Transcriptional activity correlated significantly with histological changes and were enriched for biologically relevant pathways such as lipid metabolism. These data provide platform for understanding the biological mechanisms of chronic muscle degeneration after RC tears.

Key Words: Rotator cuff, Transcriptome analysis, Time series data, Rotator cuff muscle dysfunction, Muscle biology, Tenotomy, Muscle unloading, Muscle atrophy

Introduction

Rotator cuff (RC) tears are prevalent in the general population with an incident rate of 20% after the age of 60 (Collin et al. 2019). Although rotator cuff repairs are used to treat this condition, time between tear and repair can influence the success of surgery (Gladstone et al. 2018). However, clinical studies have proven that repair does not improve or reverse the muscle atrophy and fatty infiltration observed at chronic states of disease (Gerber et al. 2000, Gladstone et al. 2018). This highlights the need to better understand what dysfunction in RC tears is leading to persistent muscle atrophy and fatty infiltration to determine potential targets for reversibility.

The rabbit model is an advantageous system to use to study this question due to similar morphological changes such as increased fat, fibrosis and degeneration (Rubino et al., 2007, Farshad et al., 2012, Valencia et al., 2018, Hyman et al., 2020, Hyman et al., 2021, Vargas-Vila et al., 2021) to what is observed in the supraspinatus (SSP) in humans (Gibbons et al., 2017) without the need of a neurectomy as in smaller animal models (Rowshan et al., 2010). The major physiological changes noted in this model include significant decrease in muscle fiber cross-

sectional area (CSA) at 4 and 16 weeks, degeneration of muscle fibers with a ~25% muscle mass reduction after 16 weeks, and an increase in collagen and fat between 4 to 16 weeks (Rubino et al., 2007, Farshad et al., 2012, Valencia et al., 2018, Hyman et al., 2020, Hyman et al., 2021, Vargas-Vila et al., 2021). Understanding the progression of rotator cuff disease before repair may help determine the potential effectiveness of a surgical intervention with or without adjuvant therapeutics.

Currently, few human studies have characterized gene expression in RC muscle after tendon tear and how it relates to the severity of muscle changes (Reardon et al., 2001, Shah et al. 2017, Steinbacher et al., 2010, Choo et al., 2014, Gibbons et al., 2018, Ren et al., 2018), but these data could not be related to a time course neither compared to a healthy control. Gene expression data with two or more time points have been collected in a mouse RC tear model and a rat tenotomy and neurectomy model (Lee et al., 2018, Gumicio et al., 2018, Hu et al., 2019), typically focusing on specific programs and gene overlap over the time series. However, even fewer studies have considered the mechanistic effects of muscle unloading in an animal RC tear model which properly recapitulates the human pathophysiology of fatty infiltration. One example includes the sheep RC tear model, which recapitulates human pathophysiology (Gerber et al., 2004) and has been used to consider the role of mitochondrial dysfunction with transcriptomics at two different time points (2 & 16 weeks post-tenotomy) (Fluck et al., 2017 & 2020). Given the lack of a broad understanding of the progression of RC disease there is an unmet need to investigate the development in a time dependent manner with greater time and transcriptional resolution.

This study aims to establish transcriptional responses to RC tendon tear as a function of time in the rabbit tenotomy injury model. Sequencing for all genes, rather than select ones, allows for an unbiased analysis of transcriptional changes over time. These data may provide a greater

understanding of how RC tears progress to a chronic state of decreased muscle quality and function. We hypothesize, based on morphological changes previously observed in this model, that transcription of certain genes is time dependent, where early changes would favor atrophy and inflammation and late changes would favor fatty infiltration, degeneration, and fibrosis.

Materials & Methods

Animals

In this study 30 female New Zealand White rabbits (~6 months, Western Oregon Rabbit Company, Philomath, OR) were used to evaluate post-tenotomy transcriptional changes over time (Vargas-Vila et al., 2021). Females were used due to housing safety concerns regarding mixing gender and the ease of sourcing older female animals. All protocols were approved by the University of California, San Diego Institutional Animal Care and Use Committee (protocol #S11246). All animals were assigned a number ID and cage location upon arrival and then at time of harvest were randomized to one of the study groups. Animals were single housed with food and water ad lib, environmental and food enrichment, and visual access to other animals. There were no adverse events in this study and no animals met the criteria for humane early endpoints.

Surgical Procedures

Rabbits were anesthetized with a subcutaneous injection of ketamine and xylazine (35 mg/kg ketamine/5 mg/kg xylazine, MWI Veterinary Supply, Boise, ID). Following intubation, 2-4% isoflurane (VetOne, Boise, ID) was utilized to keep the animals under anesthesia for the duration of the surgery. The surgical site was disinfected, and an incision was made through the skin and deltoid muscle overlying the rotator cuff. After exposing the supraspinatus tendon, a unilateral tenotomy was performed by transecting the tendon at its footprint on the greater tubercle of the humerus. Surrounding soft tissues were bluntly dissected to permit unobstructed retraction of the tendon. To avoid the formation of tissue adhesions, a Penrose drain (Medline, Northfield,

IL) was sutured to the tendon stump. The muscle and skin layers were subsequently sutured and stapled closed, and the animals were allowed to recover. A sham surgery was performed on the contralateral limb of the tenotomy to serve as a control for the procedure where only the skin was cut, tendon isolated, and then stitched up as normal. An E-collar was placed on the animals to prevent suture ripping, and after 10 days, the collar and any remaining staples were removed (Vargas-Vila et al., 2021).

Muscle Harvesting

After the study, animals were euthanized at 5 time points; 1 week, 2 weeks, 4 weeks, 8 weeks and 16 weeks post-tenotomy. At the specified time points, animals were euthanized with an intravenous overdose of pentobarbital (Beuthanasia, 120 mg/kg, MWI Veterinary Supply, Boise, ID). The supraspinatus muscles from both shoulders were harvested and divided into four regions with the central tendon serving as the muscle midline between the anterior and posterior sides of the muscle. These four regions included anterior lateral (A1), posterior lateral (P1), anterior medial (A2), and posterior medial (P2), and one full-muscle thickness fragment was harvested from each location. The harvested muscle regions were pinned to in vivo length and flash frozen in liquid nitrogen-chilled isopentane for storage at -80 C (Vargas-Vila et al., 2021).

RNA Extraction

The muscle samples from the P1 region were removed from -80 degrees C and brought to a cryostat where they were allowed to come up to -20 degrees C. The P1 region was chosen due to consistently presenting the most affected region of muscle in this rotator cuff injury model compared to the anterior and medial regions (Vargas-Vila et al., 2021). One notable difference is his region experiences the greatest fiber type changes with increased type II and decreased type I influencing the metabolic activity (Vargas-Vila et al., 2021). A 50-75mg piece was removed from

the center of each pinned region and placed in a pyrogen-free tube. RNA extraction was performed using the QIAGEN Fibrous Tissue mini kit on a QIAGEN Qiacube robot (QIAGEN, Germantown, MD). In brief, the tissue was immersed in buffer RLT and disrupted by bead in the QIAGEN TissueLyser II, (QIAGEN, Germantown, MD) before being transferred to the Qiacube for RNA extraction. Samples were digested with Proteinase K, (QIAGEN, Germantown, MD) prior to extraction. A DNase digestion step was included in the protocol. RNA was stored at -80 degrees C.

RNA Sequencing

Total RNA was assessed for quality using an Agilent Tapestation 4200, and samples with an RNA Integrity Number (RIN) greater than 8.0 were used to generate RNA sequencing libraries using the TruSeq Stranded mRNA Sample Prep Kit (Illumina, San Diego, CA). Samples were processed following manufacturer's instructions, modifying RNA shear time to five minutes. Resulting libraries were multiplexed and sequenced with 75 basepair (bp) single reads (SR75) to a depth of approximately 25 million reads per sample on an Illumina HiSeq400. Samples were demultiplexed using bcl2fastq Conversion Software (Illumina, San Diego, CA).

RNAseq Analysis

Quality control of the raw fastq files was performed using the software tool FastQC (Andrews et al., 2010). Sequencing reads were aligned to the rabbit genome (Ensembl OryCun2.0) using the STAR v2.5.1a aligner (Dobin et al., 2013). Read quantification was performed with RSEM (Li et al., 2011) (v1.3.0) and Ensembl annotation (Oryctolagus_cuniculus.OryCun2.0.91.gtf). The R BioConductor packages edgeR (Robinson et al., 2010) and limma (Richie et al., 2015) were used to implement limma-voom (Law et al., 2014) followed by empirical Bayes technique for differential expression analysis. Lowly expressed

genes were filtered out (cpm > 1 in at least one sample). Trimmed mean of M-values (TMM) normalization was applied (Robinson et al., 2010). The experimental design was modeled upon time point and treatment (~0 +time_treatment) with contrasts (Tenotomy – Sham) for each time point and all samples. All results will be presented as the tenotomy time point compared to sham unless specified otherwise. From the empirical Bayes result, differentially expressed (DE) genes were defined by an adjusted P-value < 0.05 (based on the moderated t-statistic using the Benjamini-Hochberg (BH) method to control the false discovery rate (Benjamini et al., 2001)) and a |log2FC| >1. G:Profiler was used to map rabbit Ensemble IDs to human Ensemble IDs, Entrez IDs and symbols (Raudvere et al., 2019). Of the 11,535 total genes, 1210 were not mapped to human and 296 were duplicates and were removed for the analysis. The resulting genes with Entrez IDs correspond to the set of 'background or detected genes' consisting of 10,029 genes. We removed one 8 week sample that we identified as an outlier using PCA plots and unsupervised hierarchical clustering. With n=6 animals per group, we were sufficiently powered to identify significantly differentially expressed genes with a power of 72%. Volcano plots were created using Enhanced Volcano package (v.1.60). Heatmaps were created using clustermap in the seasborn package (Waskom, 2021). The Venn Diagram was produced using Van de Peer lab tools. RT-qPCR validation was not used in this study due to the robust nature of RNAseq methods and data analysis and supporting literature (Coenye, 2021, Feng, 2010).

Enrichment Analysis

Assignment of functional categories was based on the Gene Ontology (GO) categories 'Biological process', 'Molecular function' and 'Cellular component'. Enrichment analysis of GO categories was performed in R (version 4.0.2; http://www.r-project.org) using the 'weight01' method from the Bioconductor topGO (v. 2.40.0) package with the org.Hs.eg.db_3.11.4 human

database (Alexa & Rahnenfuhrer, 2020 & Carlson, 2019). Node size was set to 10, and Fisher's exact test was used for assessing GO term significance. Overrepresentation of functional categories was calculated for DE genes as compared with the 10,030 'background' genes, and significant GO terms were identified as those having P-value <0.05. KEGG analysis was also done in R using KEGGREST package (v. 1.28.0) with list of pathways and genes. A Wilcox rank-sum test was performed for each pathway, the Entrez ID along with the adjusted p-values of the gene expression as input. Testing whether p-values of genes included in that pathway are smaller than outside p-values. Overrepresentation of KEGG pathways was calculated for DE genes as compared with the 10,030 'background' genes, and significant KEGG pathways were identified as those having a p-value <0.05.

Gene Pathways of Interest

To highlight the changes in common genetic programs of interest, the rotator cuff muscle literature was searched to build a list of essential genes found in programs such as myogenesis, inflammation, adipogenesis, and fibrosis (Gibbons, 2018). Additional genes relating to adipogenesis identified as correlated with rotator cuff radiographic assessments (Shah et al., 2017) were also included. The final lists were compared to other RC transcriptome analyses in other animal models (Gumucio et al., 2019, Lee et al., 2018, Fluck et al., 2020) for confirmation of overlap although in more broadly described categories.

Correlation Analysis

Weighted correlation network analysis (WGCNA) was performed using WGCNA R package (v. 1.70-3) (Langdelder & Horvath, 2008) with transcriptional and phenotypic data (Supp. Data 2.6) with the tenotomy only samples as there was no significance found in the combined analysis. This analysis works by building an unbiased network of modules which represents a

cluster of genes, and then correlations can be investigated with phenotype traits through gene membership. The phenotypic data included in this study is fiber area, central nucleation, fat quantification, collagen content, and degeneration, all of which are reported in detail elsewhere (Vargas-Vila et al., 2021) but are from the same animals used in this study. However, Hematoxylin and Eosin-stained (H & E) stained sections of representative muscles in each group, at each time point, can be seen in Fig. 2.1.

Results

Transcriptome profiles changed from acute to chronic state

Visually there were obvious structural muscle changes over time between post-tenotomy and sham samples (Fig. 2.1). Changes included decreased muscle cross-sectional area, increased muscle degeneration, and increased fat and collagen deposition (Vargas-Vila et al., 2021).

At 1 week post-tenotomy, the initial acute time point, there was substantial number of significantly up- and down-regulated DE genes (Fig. 2.2A), followed by a sharp decrease in differentially regulated transcripts at 2 (Fig. 2.2B), 4 (Fig. 2.2C), and 8 weeks post-tenotomy (Fig. 2D). However, at 16 weeks post-tenotomy (Fig. 2.2E) there was a resurgence in the number of DE genes, which considers this time point at a chronic state because although the expression is similar in intensity to 1 week post-tenotomy (Fig. 2.2A), it had more up-regulated genes than down-regulated genes. The difference between the labeled genes in Fig. 2.2A-E include that the genes at 1 week post-tenotomy do not appear in the described top 10 genes at any other time point, meanwhile there was overlap with the other time points, although with no clear commonality. Each time point's corresponding principal component analysis (Fig. 2.2F-J) illustrated that standard analytical methods easily separate tenotomy from sham.

The Venn diagram (Fig. 2.3A) shows the distribution of DE genes between each time point post-tenotomy, where 1 week had 1111 unique genes, 2 weeks with 27, 4 weeks with 9, 8 weeks

with 2 and 16 weeks post-tenotomy with 876. There are 6 DE genes (KLHL34, LSMEM2 (Leucine Rich Single-Pass Membrane Protein 2), UCP2 (Uncoupling Protein 2), TP63 (Tumor Protein P63), MYT1L (Myelin Transcription Factor 1 Like), ADPRHL1 (ADP-Ribosylhydrolase Like 1)) in common at all the time points which generally have to do with energy or transcription factors. The 1 week and 16 weeks post-tenotomy time points uniquely shared 581 DE genes (only 25% of their respective total DE genes). The total amount of DE genes by week was 1942 with 1069 up and 873 down for 1 week, 303 with 170 up and 133 down for 2 weeks, 127 with 86 up and 41 down for 4 weeks, 34 with 16 up and 18 down for 8 weeks and 1714 with 1421 up and 293 down for 16 weeks post-tenotomy (Fig. 2.3B). Despite 1 and 16 weeks post-tenotomy shared an approximately equivalent number of DE genes, instead of the DE genes being split by up- and down-regulated as seen at the 1 week post-tenotomy, the 16 weeks post-tenotomy demonstrated 83% of up-regulated DE genes (Fig. 2.3B). This contrast between 1 and 16 weeks post-tenotomy can also be demonstrated by the clustering in the heatmap. The clustering grouped 5 out of 6 of 1 week post-tenotomy samples separately from 16 weeks post-tenotomy (Fig. 2.3C). The sham samples generally clustered together with some tenotomy sample exceptions (Fig. 2.3C).

Enrichment analysis

To determine the larger scale function the DE genes, overrepresentation analyses were performed using GO and KEGG at each time point (Fig. 2.4). For 1 week post-tenotomy, the GO cellular component (yellow bars –Fig. 2.4A) was enriched for transcripts relating to mitochondria. The molecular function (green bars –Fig. 2.4A) was enriched for transcripts related to energy, and transporter and transferase activity. Biological processes (blue bars –Fig. 2.4A) were enriched regarding catabolic, metabolic and signaling specific pathways.

GO analysis at 2 weeks post-tenotomy continued to be enriched for components relating to mitochondria, molecular function relating to enzymes of the electron transport chain for ATP, NADH, cytochrome-c and iron-sulfur binding (Fig. 2.4B). The electron transport chain activity continued to be in enriched in the biological process along with positive regulation of the calcineurin-NFAT signaling cascade (Fig. 2.4B).

At 4 weeks post-tenotomy, the cellular components were enriched for complexes related to signaling and neurotransmission (Fig. 2.4C). Molecular function at 4 weeks was enriched for binding (activin, IGF1, I-SMAD), catalytic activity on DNA, and proton transport (Fig. 2.4C). There was continued enrichment of positive regulation of the calcineurin-NFAT signaling cascade at 4 weeks in biological process along with response of vitamin A and leucine (Fig. 2.4C). This was the first time point where positive regulation of fatty acid oxidation appeared along with negative regulation of protein import into the nucleus.

The percent of genes in a given GO term decreases over time and was at its lowest at 8 weeks post-tenotomy, with most having 25% or less genes in the term (Fig. 2.4D). The cellular components had broad enrichment at 8 weeks, ranging from aggresome, Z-disc, synapse, mitochondrial envelope to nucleus (Fig. 2.4D). Interestingly, damaged DNA binding and transcription repressor activity appeared enriched in molecular function at 8 weeks, along with ubiquitin protease activity, virus receptor activity, and antioxidant activity (Fig. 2.4D). Positive regulation of calcineurin-related signaling again was enriched in biological process at 8 weeks with more regulation related to IL-8, translation in response to stress, and skeletal muscle cell differentiation.

An increase of ~50% in significant genes within a GO term from 8 weeks post-tenotomy to 16 weeks post-tenotomy was seen with a range of cellular components enriched for the synapse,

collagen trimer, mitochondrial respiratory chain complex I, and pseudopodium (Fig. 2.4E). Molecular function at 16 weeks was enriched for binding (PDGF, collagen, proteoglycan, phosphatidylinositol-4-phosphate) and extracellular matrix constituents (Fig. 2.4E). Positive regulation of reactive oxygen species (ROS) generation was enriched in biological process at 16 weeks, along with synapse maturation, axonal transport of mitochondrion, leukocytes rolling, and membrane fission (Fig. 2.4E).

KEGG analyses highlighted changes of broader pathways over time (Fig. 2.5). At 1 week post-tenotomy, all metabolism terms were significantly enriched and generally continued into 2 weeks post-tenotomy (Fig. 2.5 – metabolism). Metabolism at 4 weeks post-tenotomy identified new enriched metabolism terms such as tryptophan metabolism (Fig. 2.5 – amino acid metabolism), retinol metabolism (Fig. 2.5 – vitamins and cofactors metabolism), sugar metabolism (Fig. 2.5 – carbohydrate metabolism), cholesterol metabolism, and steroid biosynthesis (Fig. 2.5 – lipid metabolism). Only glycine, serine, threonine metabolism (Fig. 2.5 – amino acid metabolism) and biosynthesis of unsaturated fatty acid (Fig. 2.5 – lipid metabolism) were enriched at 8 weeks post-tenotomy. By 16 weeks post-tenotomy there were only a few pathways in each metabolism category that were enriched significantly. In the signaling transduction cluster, MAPK, FoxO, Rap1 signaling pathways were the only terms enriched at all time points. Most terms in this cluster were enriched at 16 weeks post-tenotomy with 5 pathways (cGMP-PKG, Apelin, Wnt, Hedgehog, Sphingolipid signaling pathway) that became enriched only at this time point. Focusing on the immune system cluster, there was a clear activation of all terms at 1 week which decreased slightly by 2 weeks, was not present at 4 weeks and only antigen processing and presentation was enriched at 8 weeks, but by 16 weeks post-tenotomy there was a reactivation of many of the 1 week terms in addition to B and T cell receptor signaling pathway (Fig. 2.5 – immune system). There were a

few enriched terms in the endocrine system cluster at 1, 2 and 4 weeks with double the number at 8 weeks and over 9 at 16 weeks post-tenotomy (Fig. 2.5 – endocrine system). At 4 weeks post-tenotomy, regulation of lipolysis in adipocytes, insulin resistance and signaling pathway were enriched and continued to be at 16 weeks post-tenotomy along with many more endocrine system terms. 16 weeks post-tenotomy also had many significantly enriched terms in the nervous system cluster which contrasted with the behavior at 1 week post-tenotomy. The cell processes cluster highlighted terms with the cell environment where 1 week post-tenotomy was enriched for apoptosis, ABC transporters, cytokine-cytokine receptor interaction, 2 weeks with ribosome, 4 weeks with p53 signaling pathway, 8 weeks with neuroactive ligand-receptor interaction, adherens junction, and 16 weeks with mitophagy and ubiquitin mediated proteolysis.

Gene programs of interest changed over time after tear

Using a literature-driven approach, specific genes from the literature relating to myogenic, anti-myogenic (suppressing muscle formation, cell death, degradation), adipogenic, inflammation, and fibrotic programs were highlighted across the five time points (Fig. 2.6). The myogenic program (Fig. 2.6 – green bars) was activated the strongest after 1 week post-tenotomy (Fig. 2.6A) and was faint or not significant at all other time points (Fig. 2.6B-E). The anti-myogenic program (Fig. 2.6 – red bars) was also expressed strongly at 1 week post-tenotomy with continued expression at all the time points, although with fewer genes at the 2-8 week time points, and then presented a second robust response at 16 weeks. Although some genes within the adipogenic program (Fig. 2.6 – yellow bars) were significantly expressed in 1 and 2 weeks, the entire program was fully expressed initially at 4 weeks and again at 16 weeks post-tenotomy. Inflammation (Fig. 2.6 – orange bars) was observed with a large expression at 1 week post-tenotomy and decreasing through 8 weeks, with a resurgence at 16 weeks. The fibrotic program (Fig. 2.6 – pink bars) was

also initially expressed at 1 week with fewer expressed genes at 2 weeks followed by no significant genes at 4 and 8 weeks (Fig. 2.6 C,D – dashed bars) and another robust response at 16 weeks post-tenotomy (Fig. 2.6E).

Transcriptional data correlations with phenotypic traits

WGCNA revealed gene modules significantly related to phenotype characteristics quantified by histology (Fig. 2.7). Modules 10 and 4 encompass the greatest number of significant correlations with phenotype traits, and genes in these modules were significantly enriched for interesting pathways related to lipid metabolism, and general RNA activity (Supp. Data 2.8). The phenotype traits degeneration ($p=0.07$) and collagen content ($p=0.03$) were only correlated with module 10, which is enriched for lipid metabolism. The strongest correlation coefficient (-0.71, $p=2e-05$) is associated with the centralized nuclei trait (a marker of muscle degeneration-regeneration) and module 13 which is enriched for pathways related to DNA binding and regulation. Centralized nuclei trait is also correlated significantly to modules 9, 11, and 14 and these genes are enriched for skeletal muscle adaptation/fast-slow fiber transition, endoplasmic reticulum related protein binding, and ubiquitin-like protease activity respectively (Fig. 2.7 & Supp. Data 2.8). Module 7 is significantly associated with interfascicular fat and fat & degeneration phenotype traits whose genes are enriched for interesting pathways as Ragulator complex which is anchored to lipid rafts in late endosomes and protein import related to peroxisomes membrane (Fig. 2.7 & Supp. Data 2.8).

Discussion

The purpose of this study was to establish transcriptional changes as a function of time in a rabbit RC tear model. We hypothesize, based on morphological changes previously observed in this model, that transcription of certain genes is time dependent, where early changes would favor atrophy and inflammation and late changes would favor fatty infiltration, degeneration, and

fibrosis. There were clear transcriptional differences between each time point, which support the concept of differential timing of inflammation, adipogenesis, fibrosis, and cell death programs that lead to muscle atrophy, degeneration, and fatty infiltration. Likewise, phenotypic traits correlated significantly with gene groupings in unbiasedly defined modules which were enriched for biological relevant pathways such as lipid metabolism.

At 1 week post-tenotomy, as expected, there was a large transcriptional response in both up- and down regulation (Fig. 2A, Fig. 2.3B). Functional enrichment elucidates that these genes are related to the immune system, energy metabolism, catabolism and a wide range of signaling pathways we would expect to see at an acute response to injury (Fig. 2.4A, 2.5A). 2 weeks post-tenotomy the response trends in areas of metabolism, particularly with the mitochondria (Fig. 2.4B), signaling pathways, and immune system with fewer enriched terms (Fig. 2.5). Overall, 2 weeks post-tenotomy had a more muted response than the previous week with greater emphasis on ubiquinone, a metabolite involved in the electron transport chain in the mitochondria and free-radical scavenger antioxidant, related build up (Fig. 2.4B).

A turning point appeared to occur at 4 weeks post-tenotomy where the expression, despite decreasing from 2 weeks (Fig. 2.2C), shares a greater overlap of DE genes with the 16 weeks time point as opposed to 1 and 2 weeks (Fig. 2.3A). The enrichment analyses supported the gene shift towards lipids and adipogenesis, with enriched pathways of positive regulation of fatty acid oxidation (Fig. 2.4C) and regulation of lipolysis in adipocytes (Fig. 2.6). Likewise, when literature-specific adipogenesis genes were considered, this time point demonstrated significant upregulation of these genes (Fig. 2.6C).

The 8 weeks post-tenotomy time point, with only 34 DE genes, was the time point with the lowest levels of DE expression demonstrating a possible trend towards steady state of transcription

expression (Fig. 2.2D, 2.3). These genes are related to GO terms associated with DNA damage binding, transcription repression, regulation of translation in response to stress, and interestingly aggresome, which serves as a location for misfolded proteins and is used when there is too much protein degradation for the cell to handle (Fig. 2.4D). These changes are all associated with low transcriptional activity and degradation. ECM-receptor interaction, including neuroactive ligand-receptor interaction, GAP junctions first appeared enriched at this time point highlighting a change in the cell environment (Fig. 2.6). Given how few significant genes there were at 8 weeks post-tenotomy, only CIDEA, TP63, TEAD4 from the literature specific genes (Fig. 2.6D) were significantly expressed in the anti-myogenic category, which interestingly, are related to apoptosis.

At 16 weeks post-tenotomy, a resurgence in expression, well after the acute stage response, suggests the possibility of a unique, chronic transcriptional signature. Based on morphology from previous studies (Vargas-Vila et al., 2021), this was when fatty infiltration was most present. Transcriptionally, there are 876 unique DE genes at 16 weeks post-tenotomy not present at any other time point highlighting the difference in response from 1 week post-tenotomy (Fig 2.2A). Positive regulation of superoxide (a type of ROS) anion generation, ubiquitin mediated proteolysis, general immune system response was enriched at this time point (Fig. 2.4E, 2.4). Similarly, extracellular matrix (ECM) binding such as collagen, proteoglycans, neuronal activity relating to synapse components, maturation and axonal transport of mitochondrion are enriched (Fig. 2.4E, 2.4). Mitophagy, in particular, was enriched at this time point suggesting there was sufficient mitochondrial damage/stress that needed to be degraded by autophagy. Not including the myogenic specific genes, all literature-based programs are significantly expressed and more so than at any other time point (Fig. 2.6E).

The distribution of DE genes with the first acute time point having the most and the decrease of expression (Fig. 2.2) was similar to other transcriptional time-series studies (Lee et al., 2020, Gumucio et al., 2019) in a mouse RC tear model (1 and 4 weeks) and a rat (10, 30, 60 days) RC tear and denervation model. However, neither of these studies captured what was observed at the 16 weeks post-tenotomy time point (Fig. 2.2E), which was a resurgence of expression to a similar level of the most acute time point at 1 week post-tenotomy, but with 876 new genes (Fig. 2.3A) and a greater ratio of up-regulated genes instead of down-regulated (Fig. 2.3B) where autophagy and ECM binding dominate. These studies also demonstrated a large overlap of DE genes at all recorded time points (Gumucio et al., 2019, Hu et al. 2019, Lee et al. 2020), which does not encompass the RC tear progression over time since this study only recorded 6 genes in common at all time points (Fig. 2.3). This is an advantage of this study due to the time and sequence resolution used in order to capture unique time points during RC tear progression. In regard to enrichment there were similar trends in expression of ECM related genes increasing over-time in a rat tenotomy and neurectomy model (Gumucio et al., 2019) which was similar to the genes in the literature-defined fibrotic program that increased at 16 weeks post-tenotomy in this study (Fig. 2.6).

In a more clinically relevant sheep RC tear model (Fluck et al., 2017 & 2020), with two time points (2 & 16 weeks) highlighted that there were 350 transcripts reported different at either time point. Enrichment analyses highlighted similarities with pathways related to focal adhesions, calcium binding, and extracellular space, which were also enriched at 16 weeks post-tenotomy in our study (Fig. 2.5). Comparing to a human qPCR study of torn RC muscle (Gibbons et al., 2018), the gene expression across the cell programs in our study at 16 weeks post-tenotomy (Fig. 2.6E) closely resembled biopsies taken from high-fat characterized muscle compared to no-muscle or

intact biopsies (Gibbons et al., 2018). Highlighting essential genes from the literature, we observed the adipogenic pathway expressed starting at 4 and 16 weeks post-tenotomy (Fig. 2.6). Likewise, the difference between 1- and 16 weeks post-tenotomy emphasizes how expression shifts towards more adipogenic and fibrotic genes.

Given a unique, chronic transcriptional profile which emphasized ROS build up, protein degradation, change in ECM/cell environment, the cause(s) leading to these changes merit further investigation to better understand the mechanisms of chronic fatty, fibrotic muscle atrophy observed in RC disease. Some intriguing possibilities based on these data are; changes in metabolism with the mitochondria and oxidative stress, late stage dysregulation of the inflammatory system, or a combination of metabolic and inflammatory dysregulation encouraging autophagy. These potential hypotheses, and other based on these unique data, should be tested mechanistically by deliberately manipulating this now better-defined system.

We are unaware of any other correlation between RNAseq data and muscle structural changes over time in RC muscle. Specifically, unbiased gene sets were correlated with histological measurements in our tenotomy samples, where certain gene sets correlated positively with most histological measurements (Fig. 2.7). The fact that there was an obvious statistical correlation between transcriptional activity and structure reinforces our confidence in the physiological significance of the RNAseq data presented in this study. Importantly, although sets of genes, as opposed to individual genes or even pathways, are likely most relevant to the broad degenerative changes seen in tenotomized muscle, we are not implying that direct cause-effect relationships between specific gene set dysregulation and structural changes as observed in this analysis. That being said, the connection between altered lipid metabolism, DNA regulation, and ubiquitination are all logically appealing pathways to probe contributing to future studies in the muscle

physiology field along with better understanding RC tear injury dysfunction. Future studies will need to manipulate gene sets, or pathways, positively and negatively to determine if they are mechanistically related to degeneration. Additionally, given the heterogeneity of muscle degeneration across individual muscles, relating transcriptional activity to specific regions of muscle will be a valuable technological advance.

Conclusion

Defining transcriptional changes in a RC tear model such as rabbit, which is more similar to human RC disease progression, allows for the possibility of further mechanistic studies to understand the muscle dysfunction leading to muscle atrophy and fatty infiltration observed. The field needs to better understand the progression of tear in order to make more informed decisions regarding RC repair and therapeutics. This study outlines the timeline of transcriptional changes in muscle after RC tear such as the immune response at 1 week post-tenotomy, mitochondrial activity at 2 weeks post tenotomy, adipogenesis active at 4 weeks post-tenotomy, transcriptional steady state at 8 weeks post-tenotomy, and not previously reported resurgence of transcription at 16 weeks post-tenotomy, which may represent a chronic transcriptional signature, and correlates gene sets to structural muscle changes over time.

Acknowledgements

This chapter, in full, is a reprint of the material as it appears in the Journal of Frontiers in Physiology, 2021. Laura S Vasquez-Bolanos, Michael C Gibbons, Severin Ruoss, Isabella T Wu, Mario Vargas-Vila, Sydnee A Hyman, Mary C Esparza, Donald C Fithian, John G Lane, Anshuman Singh A, Chanond A Nasamran CA, Kathleen M Fisch, and Samuel R Ward. The dissertation author was the primary investigator of this material.

Figures

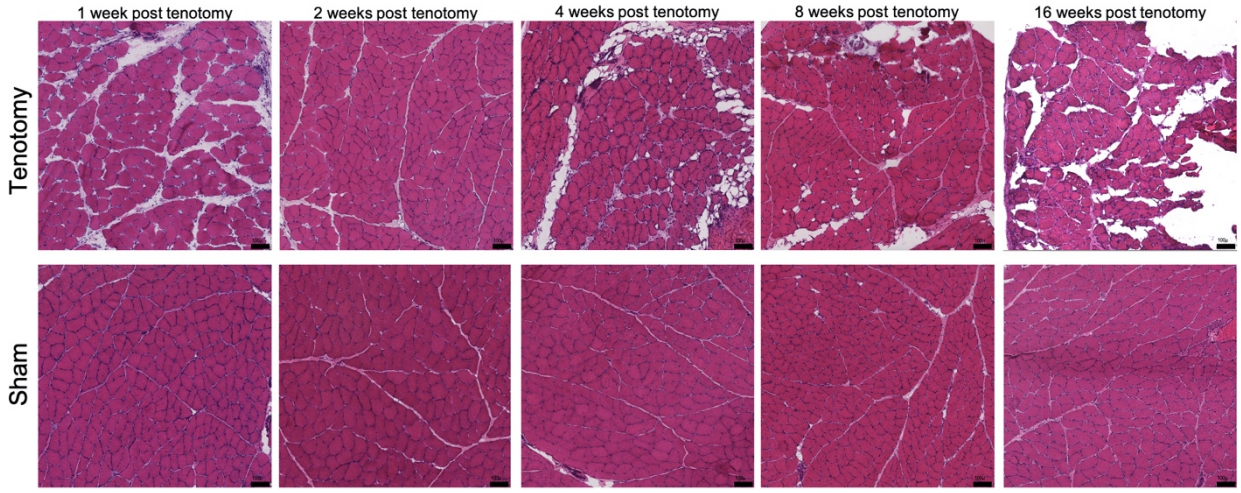

Figure 2.1: Post-Tenotomy Representative histological H & E sections of muscle.

Representative histological H & E sections of muscle at each time point for post-tenotomy and sham. Demonstrating over time a decrease in muscle CSA, muscle mass, increase in collagen content and fat reported in Vargas-Vila et al., 2021. Scale bar 100 um.

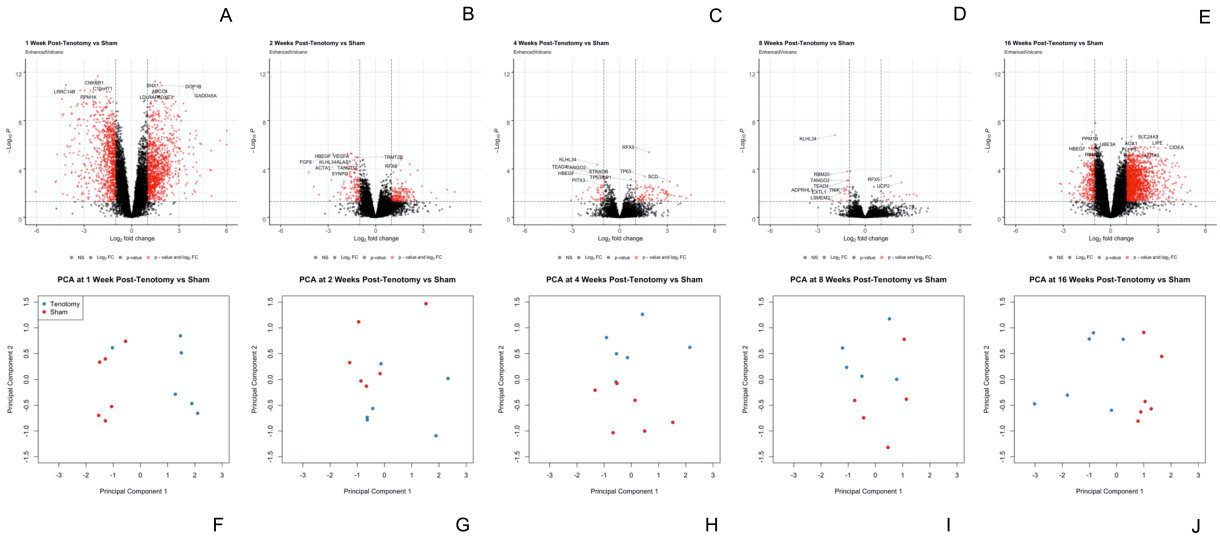

Figure 2.2: Post-Tenotomy Volcano & PCA plots.

Volcano plots highlight differentially expressed (DE) genes (red dots) at each time point post-tenotomy defined as a logFC >1 and an adjusted p-value <0.05 (A-E). The genes labeled in each volcano plot (Fig. 2A-E) consist of the top 10 genes with the smallest p-value. Corresponding PCA plots (F-J) at each time point demonstrate that the analytical methods separate tenotomy and sham.

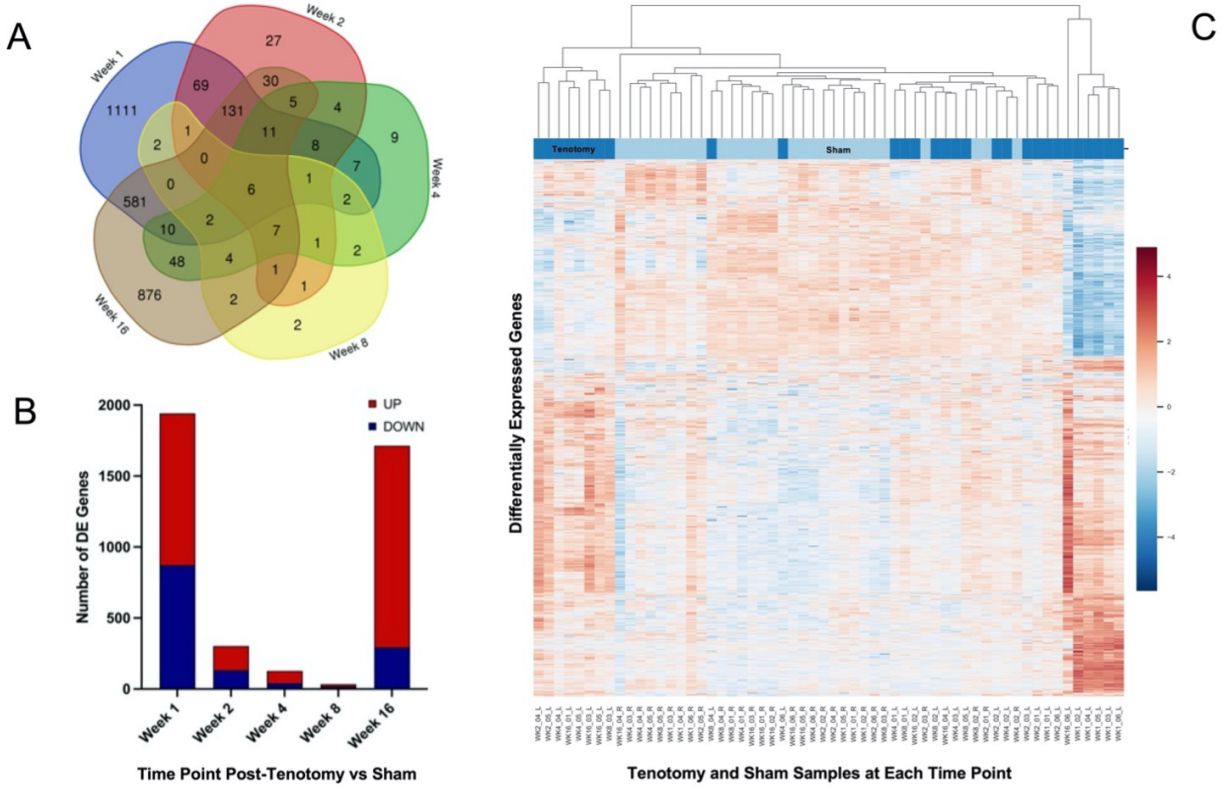

Figure 2.3: Post-Tenotomy DE genes distribution across time.

Distribution of samples by tenotomy vs sham and DE genes over each time point post-tenotomy. Venn diagram (A) highlights the DE genes at each time point and the overlap with other time points. The bar chart displays the number of DE genes which are up or down regulated at each timepoint (C). Data in the heatmap is presented as normalized expression for each tenotomy and sham sample at each time point post-tenotomy with a z-score scale by rows and an average hierarchical clustering by columns.

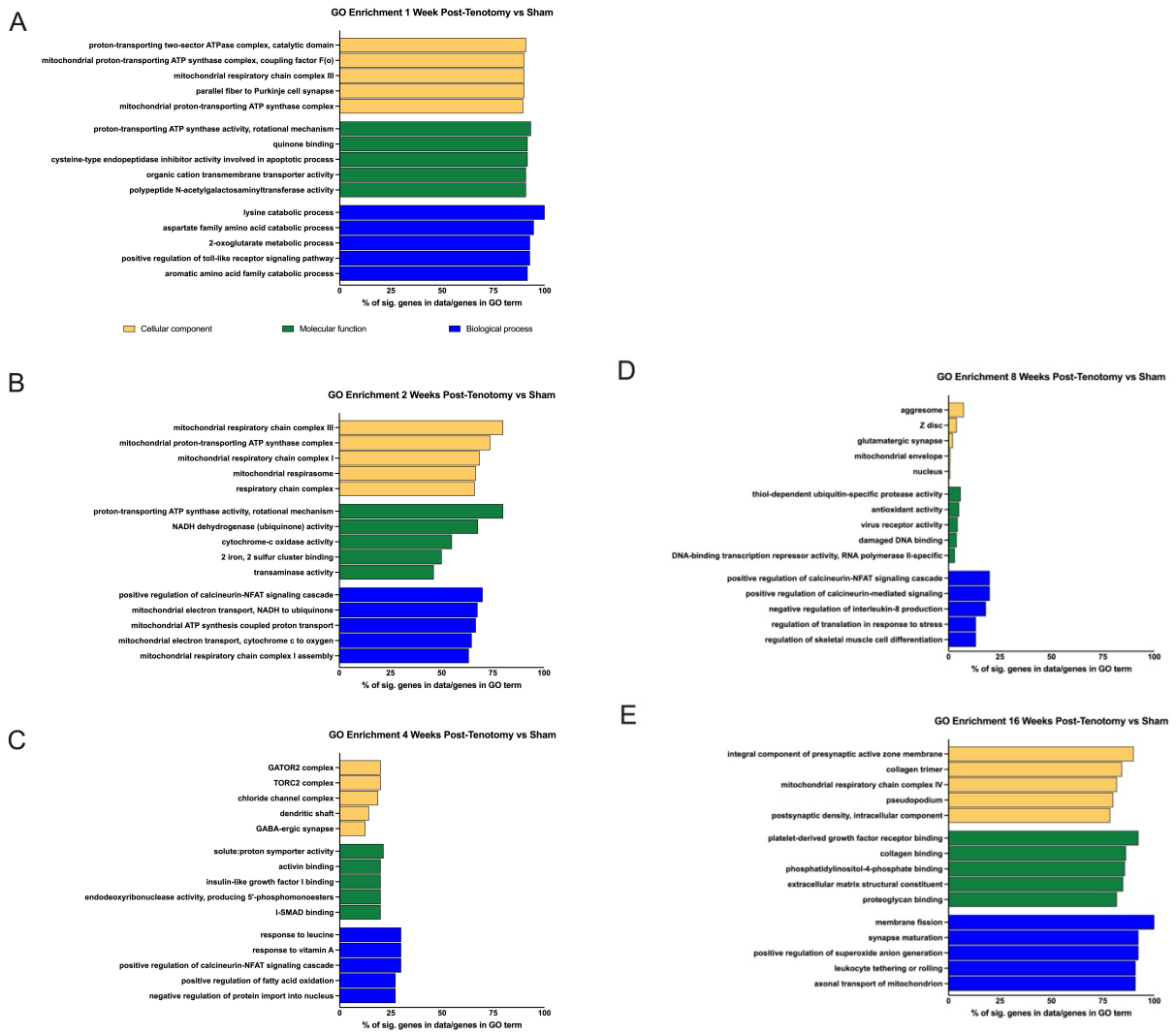

Figure 2.4: Post-Tenotomy GO Enrichment analysis by timepoint.

GO enrichment analysis for (A) 1 week post-tenotomy, (B) 2 weeks post-tenotomy, (C) 4 weeks post-tenotomy, (D) 8 weeks post-tenotomy, and (E) 16 weeks post-tenotomy. Data presented as top 5 greatest gene coverage (# of significant genes/total genes in GO term) in each category: cellular component (yellow), molecular function (green), biological process (blue).

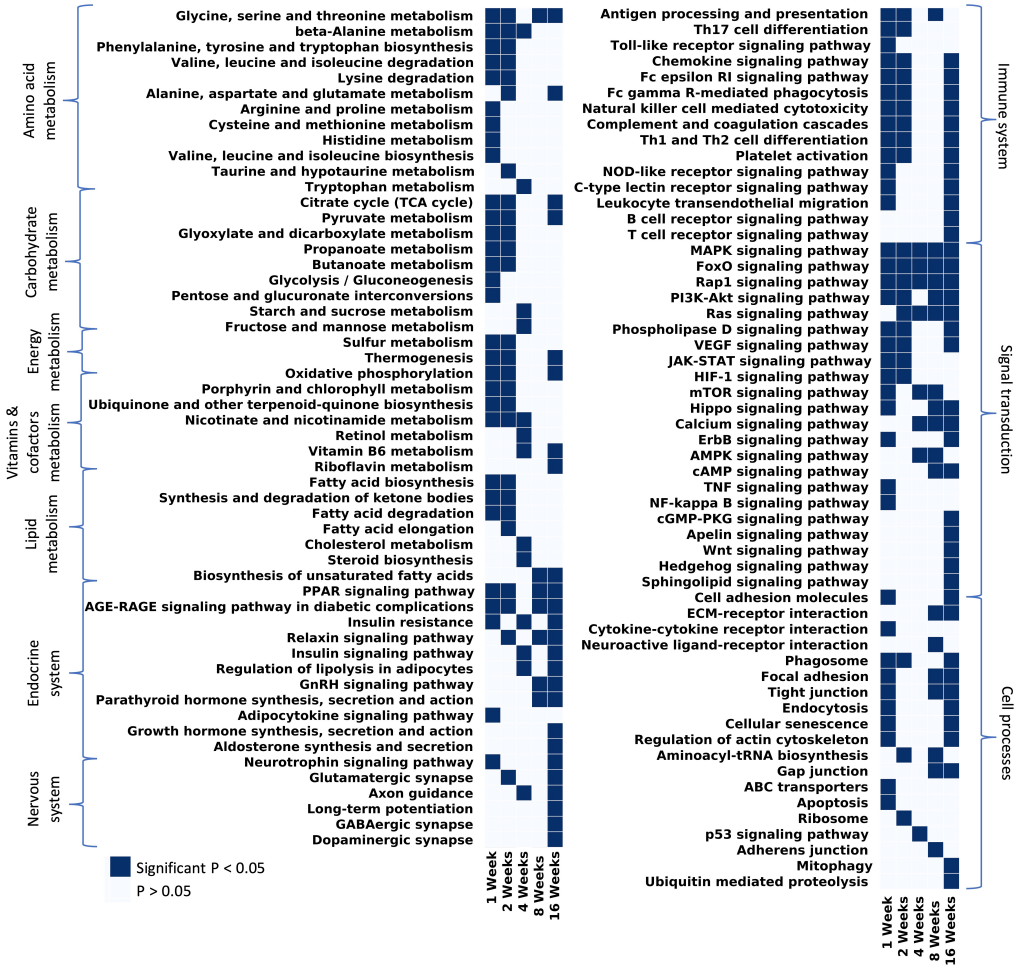

Figure 2.5: Post-Tenotomy KEGG Enrichment analysis by timepoint.

Considering all pathways that have at least 1 significant p-value and filtering out disease/tissue specific pathways, the remaining pathways were grouped by KEGG hierarchy into amino acid metabolism, carbohydrate metabolism, vitamins and cofactors metabolism, energy metabolism, lipid metabolism, endocrine system, nervous system, immune system, signal transduction, cell processes.

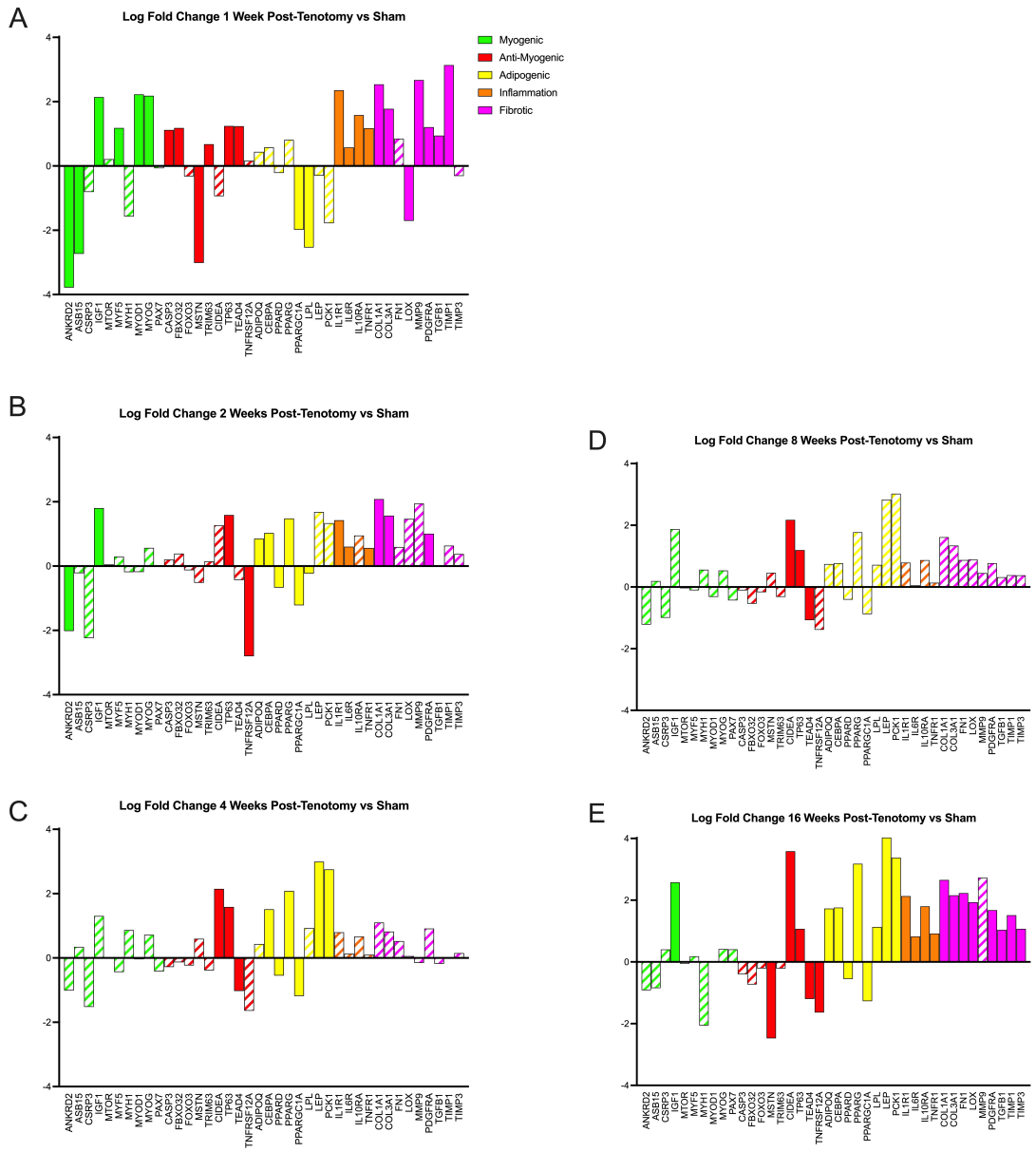

Figure 2.6: Post-Tenotomy Literature based gene expression.

Changes in transcriptome of genetic programs of interest at (A) 1 week post-tenotomy, (B) 2 weeks post-tenotomy, (C) 4 weeks post-tenotomy, (D) 8 weeks post-tenotomy, and (E) 16 weeks post-tenotomy. Log fold change (logFC) is the difference of Tenotomy and Sham. Solid bars represent a significant adjusted p-value ($p<0.05$) and partially filled in bars are not significant. Green bars represent myogenic related genes, red represents anti-myogenic, yellow represents adiopogenic, orange represents inflammation and pink represents fibrotic genes. Data are presented as average logFC.

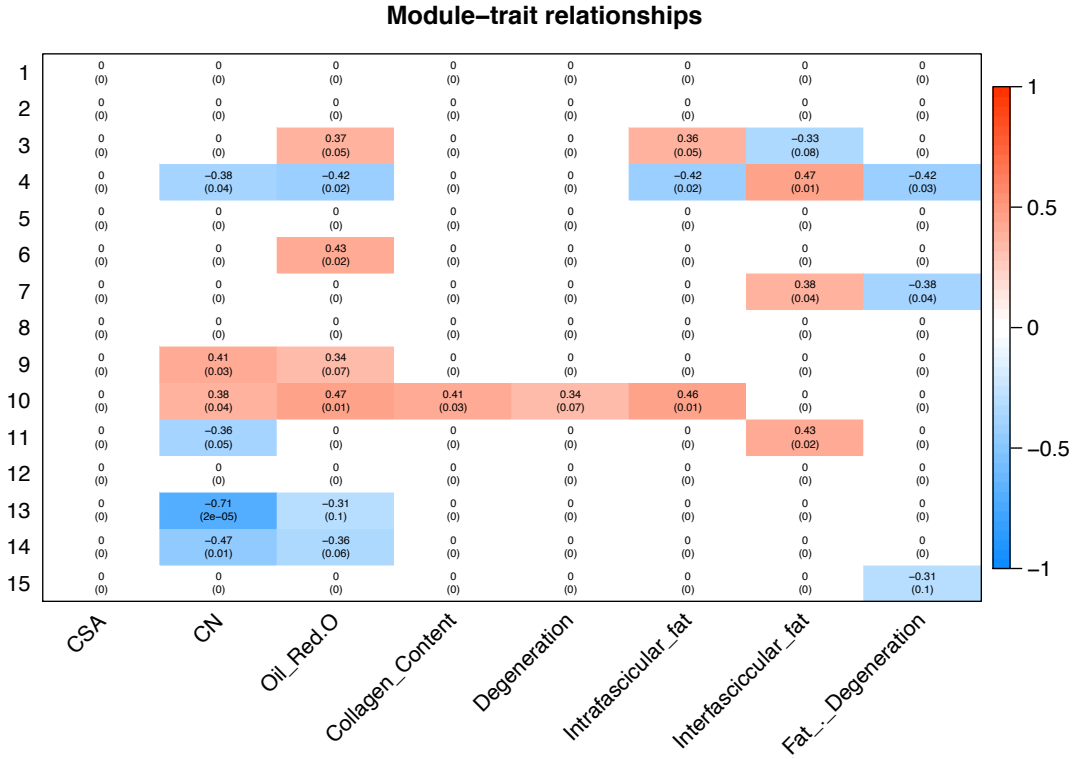

Figure 2.7: Post-Tenotomy Module-trait relationship plot.

The modules are listed 1-15 on the left and the phenotypic traits are on the bottom. The scale bar represents the correlation coefficient and is the first number listed in each cell, and the number in parentheses is the p-value. Only cells with a p-value equal or less than 0.1 were selected to be displayed and the white cells with zeros represent cells with a p-value > 0.1 for clarity of which modules correlate with which phenotypic traits.

Chapter 3 TRANSCRIPTIONAL TIME COURSE AFTER ROTATOR CUFF REPAIR IN 6 MONTH OLD FEMALE RABBITS

Abstract

Introduction: Rotator cuff tears are prevalent in the population above the age of 60. The disease progression leads to muscle atrophy, fibrosis, and fatty infiltration, which is not improved upon with surgical repair, highlighting the need to better understand the underlying biology impairing more favorable outcomes.

Methods: In this study, we collected supraspinatus muscle tissue from 6 month old female rabbits who had undergone unilateral tenotomy for 8 weeks at 1, 2, 4, or 8 weeks post-repair (n=4/group). RNA sequencing and enrichment analyses were performed to identify a transcriptional timeline of rotator cuff muscle adaptations and related morphological sequelae.

Results: There were differentially expressed (DE) genes at 1 (819 up/210 down), 2 (776/120), and 4 (63/27) weeks post-repair, with none at 8 week post-repair. Of the time points with DE genes, there were 1092 unique DE genes and 442 shared genes, highlighting that there are changing processes in the muscle at each time point. Broadly, 1-week post-repair differentially expressed genes were significantly enriched in pathways of metabolism and energetic activity, binding, and regulation. Many were also significantly enriched at 2 weeks, with the addition of NIF/NF-kappaB signaling, transcription in response to hypoxia, and mRNA stability alongside many additional pathways. There was also a shift in transcriptional activity at 4 weeks post-repair with significantly enriched pathways for lipids, hormones, apoptosis, and cytokine activity, despite an overall decrease in the number of differentially expressed genes. At 8 weeks post-repair there were no DE genes when compared to control. These transcriptional profiles were correlated with the histological findings of increased fat, degeneration, and fibrosis. Specifically, correlated gene sets were enriched for fatty acid metabolism, TGF-B-related, and other pathways.

Discussion: This study identifies the timeline of transcriptional changes in muscle after RC repair, which by itself, does not induce a growth/regenerative response as desired. Instead, it is predominately related to metabolism/energetics changes at 1 week post-repair, unclear or asynchronous transcriptional diversity at 2 weeks post-repair, increased adipogenesis at 4 weeks post-repair, and a low transcriptional steady state or a dysregulated stress response at 8 weeks post-repair.

Keywords: Rotator cuff repair, Transcriptome analysis, Time series data, Rotator cuff muscle dysfunction, Muscle biology, Muscle atrophy.

Introduction

Rotator cuff (RC) tears are prevalent in the general population over the age of 60 (MacDermid et al., 2004; Yamamoto et al., 2010d; Sayampanathan et al., 2017; Collin et al. 2019) with over 400,000 surgical repairs performed in the U.S. yearly (McElvany et al., 2015). Clinical studies demonstrate that surgical repair does not improve or reverse the muscle atrophy and fatty infiltration developed at chronic states of disease (Gerber et al. 2000; Gladstone et al. 2007; Galatz et al., 2004; Cho et al., 2009; Park et al., 2015). This is counter to what is expected because with muscle loading, as it is well documented that hypertrophy and growth/regeneration transcriptional programs are active (Perry & Rudnick, 2000; Bodine et al., 2001; Flück et al., 2005; Glass, 2005; Dalbo et al., 2011; Egerman & Glass, 2014;). This disconnect between reloading and a positive anabolic response could be related to altered mechanotransduction, signaling, transcriptional activity, protein synthesis, or myofibrillar assembly.

The biological activity (specifically transcriptional activity and histology) of muscle after RC tear has been more aggressively investigated than after surgical RC repair in a range of animal

models from mice, rats, rabbits, and sheep (Gibbons et al., 2017; Hu et al., 2019; Chaudhury et al., 2016; Choo et al., 2014, Flück et al., 2017 & 2020; Tashjian et al., 2020; Lee et al., 2018; Derwin et al., 2010; Rowshan et al., 2010; Vasquez-Bolanos et al., 2021). All models have advantages and disadvantages. For example, mice and rats require a tenotomy and neurotomy to reproduce the muscle structural phenotypes observed in humans, thereby negating the possibility of a functional repair. Rabbit and sheep appear to undergo fatty infiltration and atrophy changes without the associated nerve injury required in small animals, but sheep are generally more expensive and time intensive, making rabbits an appealing model choice for RC injury and repair.

In the RC surgical repair literature, there is a larger focus on acute repair, where a tenotomy and repair are performed simultaneously, and surgical techniques/biologic augmentation are explored in parallel to acute tendon healing (Sun et al., 2020; Li et al., 2018; Ozbaydar et al., 2008; Su et al., 2018; Chung et al., 2013; Honda et al., 2017; Kwon et al., 2018; Yoon et al., 2018; Ruoss et al., 2018a). However, this does not represent the complex human scenario of delayed repair. For example, in older patients, symptomatic tears develop over years and do not undergo surgical repair for months or years after diagnosis. As a result, there is less literature exploring the more human, and pathophysiologically relevant, approach of performing a delayed repair. When delayed repair is implemented, the model systems are typically sheep and rabbit (Gerber et al., 1999, Gerber et al., 2000, Davidson et al., 2000; Matsumoto et al., 2002; Gerber et al., 2004; Gerber et al., 2009; Rubino et al., 2008; Steinbacher et al., 2010; Coleman et al, 2003, Farshad et al., 2011, Uhthoff et al., 2014; Ren et al., 2018; Ruoss et al., 2018b, & Wu et al., 2022). The rabbit delayed RC repair exhibits an advantage over the sheep model in terms of decreased cost and time.

Similar models, such as disuse followed by resistance exercise, have demonstrated a hypertrophy biological activity response with the reloading of an atrophied muscle (Fluck et al.,

2005; Dalbo et al., 2011). A delayed repair, likewise, should induce an anabolic response in the muscle, due to reloading of the muscle mechanically. However, to date, there are no time series, transcriptional analyses in muscle after repair in either a sheep or rabbit model system. As a result, it is unclear whether a delayed RC surgical repair promotes growth or regeneration of an atrophied muscle after tear as expected from the loading or reloading of muscle in other model systems. Given the lack of knowledge related to the influence of delayed surgical tendon repair on muscle recovery, there is a need for a pre-clinical model to explore the biological state of the muscle after a tear injury and surgical repair of the tendon. This study aims to fill that gap by elucidating the time-dependent transcriptional changes in muscle after tendon repair using a well-established, chronic rabbit RC tear and repair model. Thus, the primary contribution of this manuscript is a first transcriptome-wide, and time resolved, data set of biological activity after chronic tear and repair. Given the typical anabolic response observed in muscle (re)loading, we hypothesize that a hypertrophy growth and regenerative muscle response will be present at the transcriptional level after reloading of the muscle via surgical repair of the tendon

Materials & Methods

Animals

In this study 21 skeletally mature female New Zealand White rabbits (~6 months, Western Oregon Rabbit Company, Philomath, OR) were used to evaluate post-repair transcriptional changes over time. Females were used due to housing safety concerns regarding mixing gender and the ease of sourcing older female animals. All protocols were approved by the University of California, San Diego Institutional Animal Care and Use Committee (protocol #S11246). All animals were assigned a number ID and individual cage location upon arrival and then at time of harvest were randomized to one of the study groups. Animals were single housed with food and water ad lib, environmental and food enrichment, and visual access to other animals. There were

initially 4 rabbits in the 1 and 8 week post-repair groups, and 5 rabbits in the 2 and 4 weeks post-repair groups. One rabbit in the 4 weeks post-repair group was sacrificed before repair due to lack of appetite and weight loss, leaving n=4 at every timepoint except 2 weeks post-repair (n=5). These tissues were also used in a prior study of histology (Wu et al., 2022).

Surgical Procedures

Rabbits were anesthetized with a subcutaneous injection of ketamine and xylazine (35 mg/kg ketamine/5 mg/kg xylazine, MWI Veterinary Supply, Boise, ID). Following intubation, 2-4% isoflurane (VetOne, Boise, ID) was utilized to keep the animals under anesthesia for the duration of the surgery. The left supraspinatus muscle served as the experimental side in all animals, with the right shoulder as an unoperated control, as described previously (Vargas-Vila et al., 2021). In brief, an open anterior approach was performed on the left shoulder, followed by sharp transection of the left supraspinatus tendon from its footprint on the greater tuberosity of the humerus. The surrounding soft tissues were bluntly dissected to allow unhindered retraction of the tendon stump and distal muscle. After securing a Penrose drain to the tendon stump to prevent scar formation between the tendon and surrounding soft tissue, the incision was closed in layers. Rabbits were then allowed individual cage activity with routine post-operative care. A fentanyl patch was placed on the back for pain control for 3 days, and the animals were monitored daily for 2 weeks post-operatively. At 8 weeks post-tenotomy, all animals underwent an open repair of the torn tendon. The repair was performed using a modified locking suture with anterior and posterior bone tunnels to restore the tendon footprint to the humeral head. The same anesthesia (subcutaneous injection of ketamine and xylazine), surgical approach and closure, and post-operative protocols (fentanyl patch and daily monitoring) were used for the surgical repair operations (Wu et al., 2022).

Rabbits were monitored two times/day for the duration of the study, once by animal care staff and once by lab staff. In addition to having a fentanyl patch provided at the time of the procedure, animals were monitored for breakthrough pain and distress by looking for signs of chewing or excessive attention to surgical site, reduced food and water consumption, poor self-manicure (lack of grooming or rough coat), abnormal gait, reduced activity or inactivity, teeth grinding, weight loss, vocalizations, and redness and swelling around the eyes. When signs of pain were present, buprenorphine was administered, and a veterinary consult was requested. Of the 16 rabbits, only two rabbits exhibited some swelling, and no additional medication was needed. Quality of the repair was assessed by visual inspection (suture knots are confirmed to be intact and the distal tendon remains approximated to the humerus), and any re-tears or unusual findings were recorded and reported. Only one rabbit had an unusual small region of scar tissue in the muscle.

Muscle Harvesting

After the study, animals were euthanized at 4 time points; 1 week, 2 weeks, 4 weeks, and 8 weeks post-repair. At the specified time points, animals were euthanized with an intravenous overdose of pentobarbital (Beuthanasia, 120 mg/kg, MWI Veterinary Supply, Boise, ID). The supraspinatus muscles from both shoulders were harvested and divided into four regions with the central tendon serving as the muscle midline between the anterior and posterior sides of the muscle. These four regions included anterior lateral (A1), posterior lateral (P1), anterior medial (A2), and posterior medial (P2), and one full-muscle thickness fragment was harvested from each location. The harvested muscle regions were pinned to in vivo length and flash frozen in liquid nitrogen-chilled isopentane for storage at -80 C degrees (Wu et al., 2022).

RNA Extraction

As previously described (Vasquez-Bolanos et al., 2021) the muscle samples from the P1 region were removed from -80 degrees C and brought to a cryostat where they were allowed to come up to -20 degrees C. The P1 region was chosen due to consistently presenting the most affected region of muscle in this rotator cuff injury model compared to the anterior and medial regions (Vargas-Vila et al., 2021). A 50-75mg piece was removed from the center of each pinned region and placed in a pyrogen-free tube. RNA extraction was performed using the QIAGEN Fibrous Tissue mini kit on a QIAGEN Qiacube robot (QIAGEN, Germantown, MD). In brief, the tissue was immersed in buffer RLT and disrupted by bead in the QIAGEN TissueLyser II, (QIAGEN, Germantown, MD) before being transferred to the Qiacube for RNA extraction. Samples were digested with Proteinase K, (QIAGEN, Germantown, MD) prior to extraction. A DNase digestion step was included in the protocol. RNA was stored at -80 degrees C.

RNA Sequencing

Total RNA was assessed for quality using an Agilent Tapestation 4200, and samples with an RNA Integrity Number (RIN) greater than 8.0 were used to generate RNA sequencing libraries using the TruSeq Stranded mRNA Sample Prep Kit (Illumina, San Diego, CA). Samples were processed following manufacturer's instructions, modifying RNA shear time to five minutes. Resulting libraries were multiplexed and sequenced with 75 basepair (bp) single reads (SR75) to a depth of approximately 25 million reads per sample on an Illumina HiSeq400. Samples were demultiplexed using bcl2fastq Conversion Software (Illumina, San Diego, CA).

RNAseq Analysis

Quality control of the raw fastq files was performed using the software tool FastQC (Andrews et al., 2010). There was one animal that was partially filtered out at this step, the experimental sample at the 8 week time point. Sequencing reads were aligned to the rabbit genome

(Ensembl OryCun2.0) using the STAR v2.5.1a aligner (Dobin et al., 2013). Read quantification was performed with RSEM (Li et al., 2011) (v1.3.0) and Ensembl annotation (Oryctolagus_cuniculus.OryCun2.0.91.gtf). The R BioConductor packages edgeR (Robinson et al., 2010a) and limma (Ritchie et al., 2015) were used to implement limma-voom (Law et al., 2014) followed by empirical Bayes technique for differential expression analysis. Lowly expressed genes were filtered out (cpm > 1 in at least one sample). Trimmed mean of M-values (TMM) normalization was applied (Robinson et al., 2010b). The experimental design was modeled upon time point and treatment (~0 +time_treatment) with contrasts (Repair – Control) for each time point and all samples. All results will be presented as the tenotomy time point compared to sham unless specified otherwise. From the empirical Bayes result, differentially expressed (DE) genes were defined by an adjusted P-value < 0.05 (based on the moderated t-statistic using the Benjamini-Hochberg (BH) method to control the false discovery rate (Benjamini et al., 2001) and a |log2FC| >1 (Supplementary Data 3.1).

To identify human orthologs of rabbit genes, G:Profiler was used to map rabbit Ensemble IDs to human Ensemble IDs, Entrez IDs and symbols (Raudvere et al., 2019) (Supplementary Data 3.2). Of the 11,604 total genes, 1237 were not mapped to human and 255 were duplicates and were removed for the analysis. The resulting genes with Entrez IDs correspond to the set of 'background or detected genes' consisting of 10,112 genes.

Based on the biological coefficient of variation of 0.419 observed in our data, with a sequencing depth of 20 million reads/sample, we are powered to detect a 2-fold change with 64% power with n = 4 per group. Volcano plots were created using Enhanced Volcano package (v.1.60). Heatmaps were created using clustermap in the seasborn package (Waskom, 2021). The Venn Diagram was produced using Van de Peer lab tools. RT-qPCR validation was not used in this study

due to the robust nature of RNAseq methods and data analysis and supporting literature (Coenye, 2021 & Feng, 2010).

Enrichment Analysis

Assignment of functional categories was based on the Gene Ontology (GO) categories 'Biological process', 'Molecular function' and 'Cellular component'. Enrichment analysis of GO categories was performed in R (version 4.0.2; http://www.r-project.org) using the 'weight01' method from the Bioconductor topGO (v. 2.40.0) package with the org.Hs.eg.db_3.11.4 human database (Alexa & Rahnenfuhrer, 2020 & Carlson, 2019). Node size was set to 10, and Fisher's exact test was used for assessing GO term significance. Overrepresentation of functional categories was calculated for DE genes as compared with the 10,112 'background' genes, and significant GO terms were identified as those having p-value <0.05 (Supplementary Data 3.3). KEGG pathway analysis was also done in R using KEGGREST package (v. 1.28.0) with list of pathways and genes. A Wilcox rank-sum test was performed for each pathway, where Entrez ID along with the adjusted p-values results were used as inputs. Overrepresentation of KEGG pathways was calculated for DE genes as compared with the 10,112 'background' genes, and significant KEGG pathways were identified as those having a p-value <0.05 (Supplementary Data 3.4). All pathways with at least one time point with a significant p-value and filtering out disease/tissue specific pathways, the remaining pathways were grouped by KEGG hierarchy into amino acid metabolism, carbohydrate metabolism, vitamins and cofactors metabolism, energy metabolism, lipid metabolism, endocrine system, nervous system, immune system, signal transduction, cell processes.

Biased Gene Pathways Analysis

To explore well known genes involved in muscle homeostasis and pathology, we specifically probed myogenesis, anti-myogenesis, inflammation, adipogenesis, and fibrosis

programs with genes defined by the literature (Shahidi et al., 2020; Gibbons et al., 2018; Vasquez-Bolanos et al., 2021).

Correlation Analysis

Weighted correlation network analysis (WGCNA) was performed using WGCNA R package (v. 1.70-3) (Langdelder & Horvath, 2008) with transcriptional and phenotypic data (Supplementary Data 3.5) with the repair only samples in order to correlate histological traits with changes due to repair. This analysis identified unbiased modules or sets of genes that are clusters of highly correlated genes (Supplementary Data 3.8). In the combined analysis (both repair and control groups) only two modules correlated significantly with fat. This analysis works by building an unbiased network of modules which represents a cluster of genes, and then correlations (Supplementary Data 3.6) can be investigated with phenotype traits through gene membership. GO enrichment analysis was then performed by GoEnrichmentAnalysis function within the WGCNA R package, and returns the top 10 GO terms of each module (Supplementary Data 3.7). The phenotypic data included in this study is fiber area, central nucleation, fat quantification, collagen content, and degeneration, all of which are reported in detail elsewhere (Wu et al., 2022) but are from the same animals used in this study.

Results

Transcriptome profile changes

At 1 week post-repair compared to control, about 80% of the DE genes were up-regulated (Fig. 3.1A, 3.2A) with a similar trend at 2 weeks (Fig. 3.1B, 3.2A), and 10% of the total number of DE genes at 4 weeks post-repair (Fig. 3.1C, 3.2A). Meanwhile, at 8 weeks post-repair compared to controls, there were no DE genes (Fig. 3.1D, 3.2A). The total amount of significant DE genes by week was 1029 (819 up and 210 down) at 1 week, 896 (776 up and 120 down) at 2 weeks, 90 (63 up and 27 down) at 4 weeks, and 0 at 8 weeks post-repair (Supplementary Data 3.1).

Comparing DE genes between time points, there are 595 unique DE genes at 1 week post-repair, 472 at 2 weeks, 25 at 4 weeks, and none at 8 weeks post-repair. There are 39 genes in common at all the time points that have DE genes (Fig. 3.2B). Week 1 and week 2 uniquely share 377 genes, week 1 and 4 share 18 genes, and week 2 and 4 share 8 genes (Fig. 3.2B). Post-repair gene expression was associated with more up-regulation compared to control (Fig. 3.2C). Specifically, post-repair times points 2 and 4 weeks cluster strongly together and weeks 1 and 8 also cluster together, while the control weeks 1, 2, and 4 cluster strongly with 8 weeks (Fig. 3.2C).

Enrichment analysis

To determine the biological relevance of the DE genes, overrepresentation analyses were performed using GO and KEGG at each time point (Fig 3.3 & 3.4, Supplementary Data 3.3 & 3.4). For 1 week post-repair, GO cellular component terms (Fig. 3.3A) were enriched for parts relating to the mitochondria and collagen ECM (p-value 0.00046). GO molecular function terms (Fig. 3.3A) were enriched for ubiquinone (p-value 0.000000085) and cytochrome c activity (p-value 0.00013) along with translation repressor activity and cofactor and hormone binding (p-value 0.000082; 0.000084, 0.00015). GO Biological process terms (Fig. 3.3A) were enriched for the citric acid (TCA) cycle, mitochondrial electron transport chain components, and mitochondrial translational elongation and termination (p-value 0.0000000031; 0.000000047; 0.00000076; 0.00000036).

GO analysis at 2 weeks post-repair terms were enriched for components of the mitochondria and ECM, in addition to extracellular exosome (p-value 0.000000000000036; 0.000027; 0.000000015). For molecular function, DE genes were enriched for pathways of ubiquinone and cytochrome-c activity (p-value 0.00000000000079; 0.00021) along with polysaccharide and collagen binding (p-value 0.00027; 0.00054). The electron transport chain

activity continues in the biological process terms along with regulation of transcription in response to hypoxia, regulation of mRNA stability, and NIK/NF-kappaB signaling (p-value 0.0000000000008; 0.0000000004; 0.0000000025; 0.000000012; Fig. 3.3B).

At 4 weeks post-repair the DE genes are no longer enriched for cellular components terms of mitochondrial components and instead for lipid droplet, phagocytic vesicle, postsynaptic cytosol, synaptic vesicle membrane, and cytoplasmic vesicle membrane (p-value 0.0022; 0.0043; 0.0134; 0.0162; 0.0191; Fig. 3.3C). Molecular function at 4 weeks had similar DE gene enrichment for hormone and cofactor binding (p-value 0.0065; 0.0126) as 1 week post-repair, in addition to RNA polymerase II repressing transcription factor binding, estrogen receptor binding, and protein homodimerization activity (p-value 0.0141; 0.0032; 0.0015; Fig. 3.3C). DE genes were enriched for regulation of a range of processes dominates at 4 weeks in biological process including regulation of cholesterol storage, collagen biosynthetic process, and negative regulation of vascular smooth muscle cell proliferation, and cytokine secretion, and positive regulation of muscle cell apoptotic process (p-value 0.000067; 0.0002; 0.000067; 0.00052; 0.00031; Fig. 3.3C)

KEGG analyses highlight different pathways that were enriched at each time point (significantly enriched means p-value < 0.05, exact p-values can be found in Supplementary Data 3.4). At 1 week post-repair most terms in lipid, carbohydrate, amino acid, glycan and energy metabolism were significantly enriched. However, by 2 weeks there is over a 50% reduction of significantly enriched metabolism terms with even fewer enriched at 4 and 8 weeks post-repair (Fig. 3.4 – metabolism). One category to note of metabolism is energy metabolism, which was uniquely enriched from 1 to 4 weeks post-repair. Cell processes were mainly enriched over time for gap junctions and the proteasome, with the majority of terms enriched at 2 weeks including: mitophagy, mRNA surveillance pathway, regulation of actin cytoskeleton, cell adhesion, and

adherens junction (Fig. 3.4 – Cell processes). Receptor interaction for the ECM was enriched from 1 to 4 weeks post-repair, with cytokine and neuroactive ligand interactions enriched at few earlier time points. In the signal transduction category, MAPK signaling was enriched at all time points with the number of enriched pathways increasing at each time point. At 8 weeks post-repair, there were five uniquely enriched signaling pathways: longevity regulating, mTOR, NF-kappaB, p53, and ErbB (Fig. 3.4 – signaling transduction). The endocrine system terms were most enriched at 4 weeks post-repair where in particular, regulation of lipolysis in adipocytes was uniquely enriched (Fig. 3.4 – endocrine system). Meanwhile, at 2 weeks the most immune system terms were enriched and uniquely: chemokine signaling, leukocyte migration, phagocytosis, complement and coagulation cascades (Fig. 3.4 – immune system).

Gene programs of interest changes over time after repair – muscle specific

All programs, relating to myogenesis, anti-myogenic (suppressing muscle formation, cell death, degradation), adipogenesis, and fibrosis, had a few significant DE genes ($|logFC| > 1$ & adj. p-value < 0.05) at 1 week post-repair (Fig. 3.5A). At 2 weeks post-repair, there were even fewer significant DE genes for the myogenic and adipogenic categories, and more significant DE genes for the inflammation and fibrotic programs (Fig. 3.5B). In fact, at 4 weeks post-repair there were only significant DE genes in the anti-myogenic and adipogenic programs (Fig. 3.5C). There were no significant DE genes at 8 weeks post-repair and the corresponding magnitude of expression is also much lower compared to all other time points (Fig. 3.5D).

Transcriptional data correlations with phenotypic traits

WGCNA revealed gene modules significantly related to phenotype characteristics quantified by histology (Fig. 3.6). Transcriptional activity correlated significantly with histological traits such as fat, degeneration, fibrosis, and centralized nuclei (CN), oil red-O (ORO) and collagen

(Fig. 3.6). The most positively correlated module gene set for degeneration (module 7 corr 0.731864336; p-value 0.000770984) was enriched for TGF-B related pathways, and for fat (module 50 corr 0.722057657; p-value 0.001008972) was enriched for fatty acid metabolism, predominately catabolism (Fig. 3.6). Module 29 was positively correlated for CN (corr 0.562698044; p-value 0.021680671), fibrosis (corr 0.781338353; p-value 0.000155891), degeneration (corr 0.673602659; p-value 0.003210287), and fat (corr 0.658490829; p-value 0.004386982), and was enriched for vesicular transport and phosphatase binding (Fig. 3.6, Supplemental Data 3.7).

Discussion

The purpose of this study was to establish transcriptional changes as a function of time in a pre-clinical RC surgical repair model. We hypothesized, based on the typical behavior of reloading muscle, we would observe a hypertrophy growth and regenerative muscle response after surgical repair. However, the lack of a transcriptional regenerative/growth response, at any time point, and the lack of positive morphological changes measured in this model (Wu et al., 2022), suggest that surgical repair of the tendon after a chronic tear does not induce the expected anabolic responses in the muscle. Transcriptionally, it appears that, due to the previous tear injury, there is a reduced initial wound healing response and a quicker transition towards inflammation, fatty infiltration, apoptosis, and fibrosis compared to the tear alone model (Vasquez-Bolanos et al., 2021). Likewise, phenotypic traits correlated significantly with gene groupings in unbiasedly defined modules which were enriched for biological relevant pathways such as fatty acid metabolism and in particular catabolism.

After surgical repair there was a strong initial response of over 1000 differentially expressed (DE) genes which decreased to zero by 8 weeks post-repair where across each time point

the majority of DE genes were up-regulated (Fig. 3.1A-D, Fig. 3.3B). Of the time points with DE genes, there were more unique genes than genes shared between time points (Fig. 2A), highlighting that there were shifts in biological programs of the DE genes in the muscle at each time point. Broadly, functional enrichment determines that 1-week post-repair was primarily related to metabolism and energetic activity, cofactor/hormone binding, and mitochondrial translation (Fig. 3.3, 5). Meanwhile, for muscle specific genes there are various significant DE genes in each category except inflammation (Fig. 3.5). This differs from the 1 week post-tenotomy transcriptional response in a rabbit model, mouse model (1 week) and a rat tenotomy and denervation (10 days), where inflammatory genes were overexpressed and there was far less significant adipogenic genes (Vasquez-Bolanos et al., 2021, Lee et al., 2018; Gumucio et al., 2019). Similar enriched pathways to 1 week post-repair were present at 2 weeks post-repair, along with NIF/NF-kappaB signaling, transcription in response to hypoxia, and mRNA stability, making this time point the most transcriptionally diverse (Fig. 3.3-5). Histologically, the most muscle atrophy was observed at this time point, (Wu et al., 2022) although transcriptionally it is not obvious as to why that may be. Many KEGG terms are enriched across the board including cell processes such as mitophagy, and signal transduction such as JAK-STAT, phospholipase D, Ras, and TGF-B signaling pathways (Fig. 3.4). In particular, the immune system response is most pronounced at 2 weeks post-repair time point (Fig. 3.4) and unlike the response observed in previously mentioned rabbit (1, 2, 4, 8, 16 weeks) mouse (1 & 4 weeks) and rat (10, 30, 60 days) RC tear models investigating time-dependent transcriptional response, where the strongest immune system was at the first recorded time point, and decreased from there (Vasquez-Bolanos et al., 2021, Lee et al., 2018; Gumucio et al., 2019). This increase in inflammation related transcription may indicate the chronic inflammatory state in which repair is performed and the

possibility of further activating the immune system processes which continues to dysregulate the cellular environment. Additionally, there are enriched programs involved in mitochondrial energetics and the ECM, particularly related to collagen, where extracellular space and calcium binding was also enriched in a sheep RC tear model (Flück et al., 2017, 2020). Overall, 2 weeks post-repair was active for inflammation, cellular environment, and cellular homeostasis (likely apoptosis) programs with the beginning signs of fatty acid activity. This highlights the difference between RC tear transcriptional data across a range of animal models, adipogenic program terms are enriched as early as 1 week post-repair in comparison to about a month post-tear in other studies (Lee et al., 2018; Gumucio et al., 2019; Hu et al., 2019; Vasquez-Bolanos et al., 2021). This is unsurprising when comparing to torn human RC muscle, because of the characterization for high-fat (~ 40%) muscle (Gibbons et al., 2018), and animal models struggling to recapitulate a representative percentage of fat (ie. Rabbit ~ 10-15% fat), so seeing the transcriptional presence of adipogenesis supports the rabbit chronic tear and repair model's similarity to human.

The strongest shift towards lipids, fibrosis, hormones, apoptosis, and cytokine activity occurred at 4 weeks post-repair even with an overall decrease in the number of differentially expressed genes (Fig. 3.3, 5). At 8 weeks post-repair, there were no DE genes (Fig. 3.1, 3), possibly representing a steady state of gene expression. This decrease of expression and DE genes was also observed in a post-tenotomy model possibly representing a steady state reached after an invasive event such as tenotomy or repair (Vasquez-Bolanos et al., 2021). However, when considering significant genes that did not meet the log fold change minimum, KEGG enrichment could be assessed and terms related to fibrosis, energetics, cell fate, inflammation, highlighting general dysregulation with stress response (Fig. 3.4).

After describing the transcriptional profile at each time point post-repair, the key finding is that there is no growth/regenerative signal as one would expect from muscle (re)loading. Instead, there are energetic changes, inflammation, lipid metabolism, phagocytosis, and apoptosis, accentuating the reality that tendon repair does not induce the desired fundamental biological result. In addition, histological changes correlated with transcriptional results, although these changes were more general in observation, the transcriptional data provides the opportunity to sparse apart which programs may be active and when. However, the possibility of whether this state is permanent or reversible becomes an increasingly interesting future direction. Further validating studies to investigate in the future include; measuring muscle cell signaling responses to reloading, identifying the cell types present and activated by repair using immunohistochemistry or immunofluorescence, and exploring how the immune system interacts with muscle in this state of dysfunction. Similarly, using proteomic approaches to further validate transcriptional data will be important.

Limitations of this study include; the inability to determine direct cause-effect relationships with gene sets of interest, the need to validate the observed transcriptional profile with proteomic data, and the lack of comparative literature quantifying transcriptional data post-repair. This limits the ability to make specific conclusions and compare to well defined baselines or expected changes to reloading after chronic injury. Another limitation is the sample size and power of this study. In order to achieve a power of >80% with this sequencing depth, one would need a sample size of 7. As such, false negative rates could be higher than desired. However, the genes of interest (growth and regeneration) are clearly not differentially regulated and do not demonstrate variance structures that indicate lack of power in our primary hypothesis. Using only female rabbits is also a potential limitation as it relates to extrapolating to males. This could not be avoided because we

use animals that have reached skeletal maturity and sourcing is only available in females of this age. Likewise, the age of this rabbit model (~10 months at the end of the experiment) is not a direct analog to aging-related muscle changes that would be expected with the older human population experiencing a rotator cuff tear and delayed repair. Lastly, the amount of time that is allowed to pass between tenotomy and surgical repair could influence the findings (Uhthoff et al., 2014), this study aimed to use a duration (8 weeks) where characteristic pathophysiology is present and additional changes to the muscle are minimal.

Conclusion

Defining transcriptional changes in a preclinical RC surgical repair model such as rabbit allows for the possibility of further mechanistic studies to understand the role surgical repair plays on the muscle dysfunction leading to continued muscle atrophy and fatty infiltration observed. These data will also provide a scientific premise for future investigations aimed at understanding the effect of repair plus adjuvant therapeutics, and help tease apart the potential impact of adjuvant therapies versus surgical repair techniques. This study identifies the timeline of transcriptional changes in muscle after RC repair, which by itself, does not induce a growth or regenerative response as desired and instead is predominately related to metabolism/energetics changes at 1 week post-repair, unclear or asynchronous transcriptional diversity at 2 weeks post-repair, increased adipogenesis at 4 weeks post-repair, and a low transcriptional steady state or a dysregulated stress response at 8 weeks post-repair. Given the lack of a positive regenerative/growth response in the presence of mechanical reloading, future experiments are being directed at mechanical connectivity within the muscle, mechanical signaling processes, and epigenetic changes in myocytes that may individually (or collectively) preclude a positive muscle response to reloading.

Acknowledgements

This chapter, in full, is a reprint of the material as it appears in the Journal of Frontiers in Physiology, 2023. Laura S Vasquez-Bolanos, Michael C Gibbons, Severin Ruoss, Isabella T Wu, Mary C Esparza, Donald C Fithian, John G Lane, Anshuman Singh, Chanond A Nasamran, Kathleen M Fisch, Samuel R Ward. The dissertation author was the primary investigator of this material.

Figures

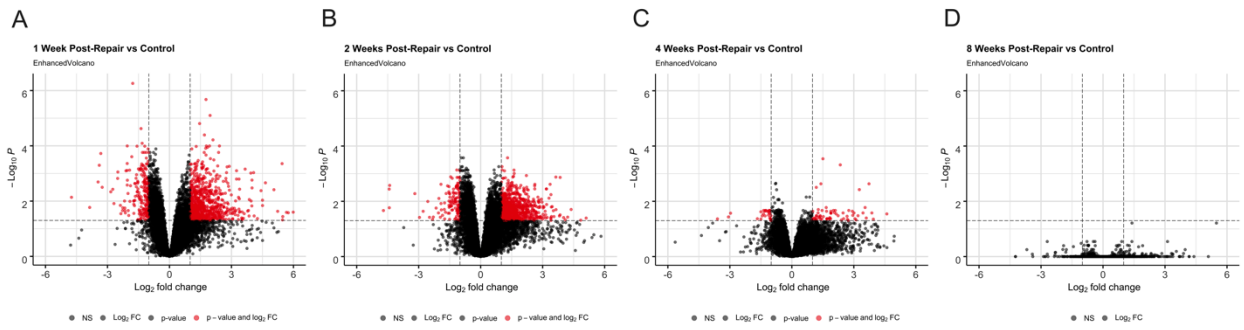

Figure 3.1: Post-Repair Volcano plots.

Volcano plots (A-D) highlight differentially expressed (DE) genes (red dots) at each time point post-repair defined as a |logFC| >1 and an adjusted p-value <0.05 (based on the moderated t-statistic using the Benjamini-Hochberg (BH).

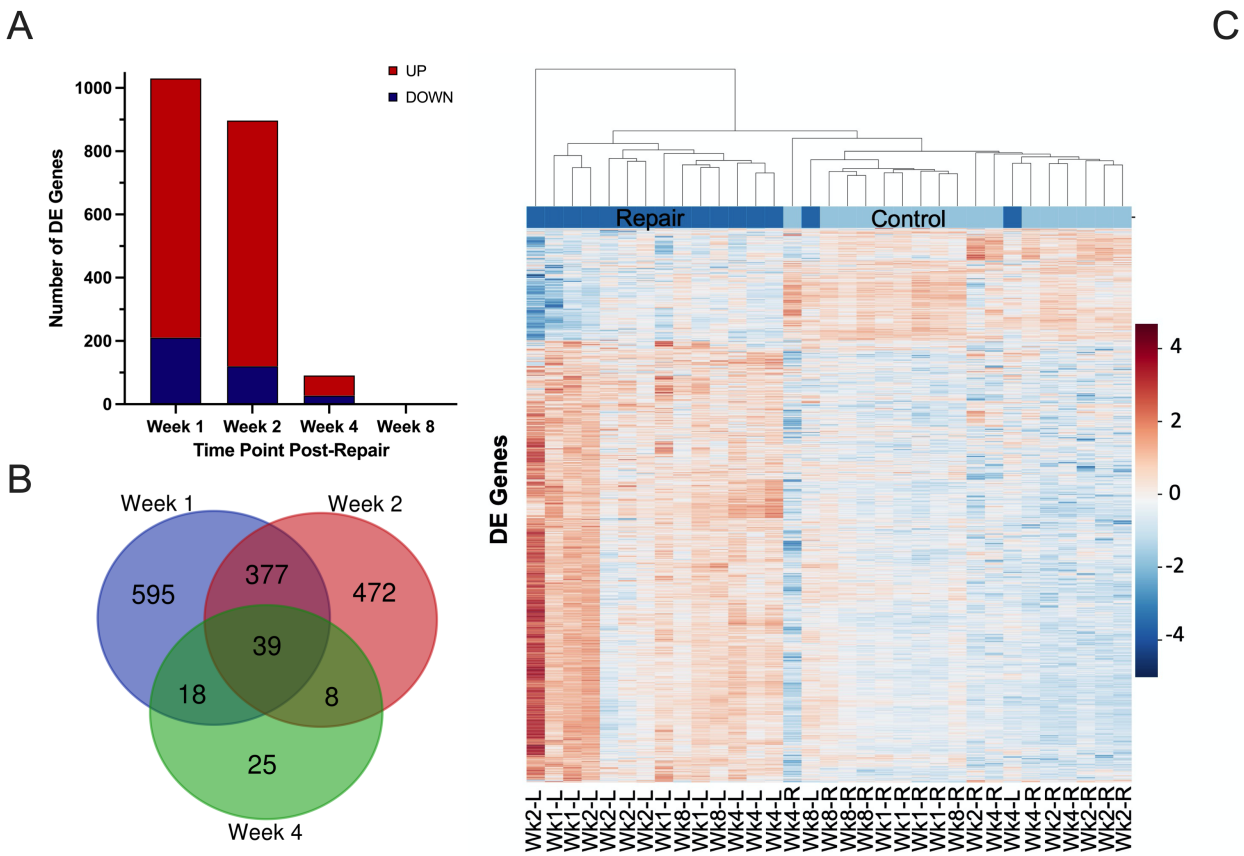

Figure 3.2: Post-Repair DE genes distribution across time.

Distribution of samples by repair vs control and DE genes over each time point post-repair. Venn diagram (A) highlights the DE genes at each time point and the overlap with other time points. The bar chart (B) displays the number of DE genes which are up or down regulated at each timepoint. Data in the heatmap (C) is presented as normalized expression for each repair (L=left) and control (R=right, unoperated shoulder) sample at each time point post-re with a z-score scale by rows and an average hierarchical clustering by columns.

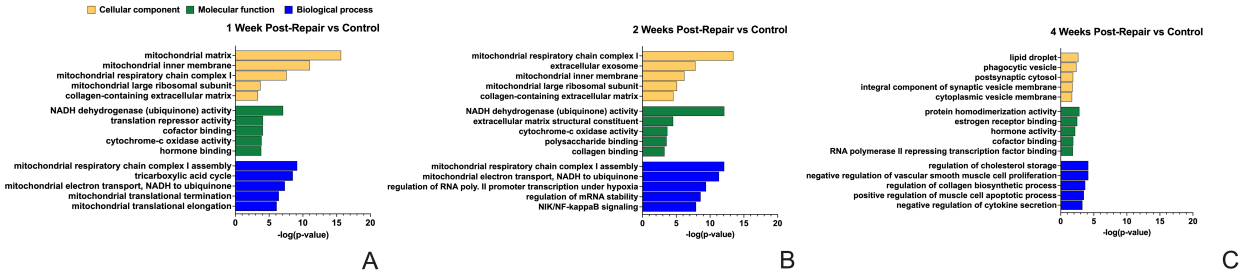

Figure 3.3: Post-Repair GO Enrichment analysis by timepoint.

GO enrichment analysis for (A) 1 week post-repair, (B) 2 weeks post-repair, and (C) 4 weeks post-repair. Data presented as top 5 most significant term in each category: cellular component (yellow), molecular function (green), biological process (blue) (Supplementary Data 3.3).

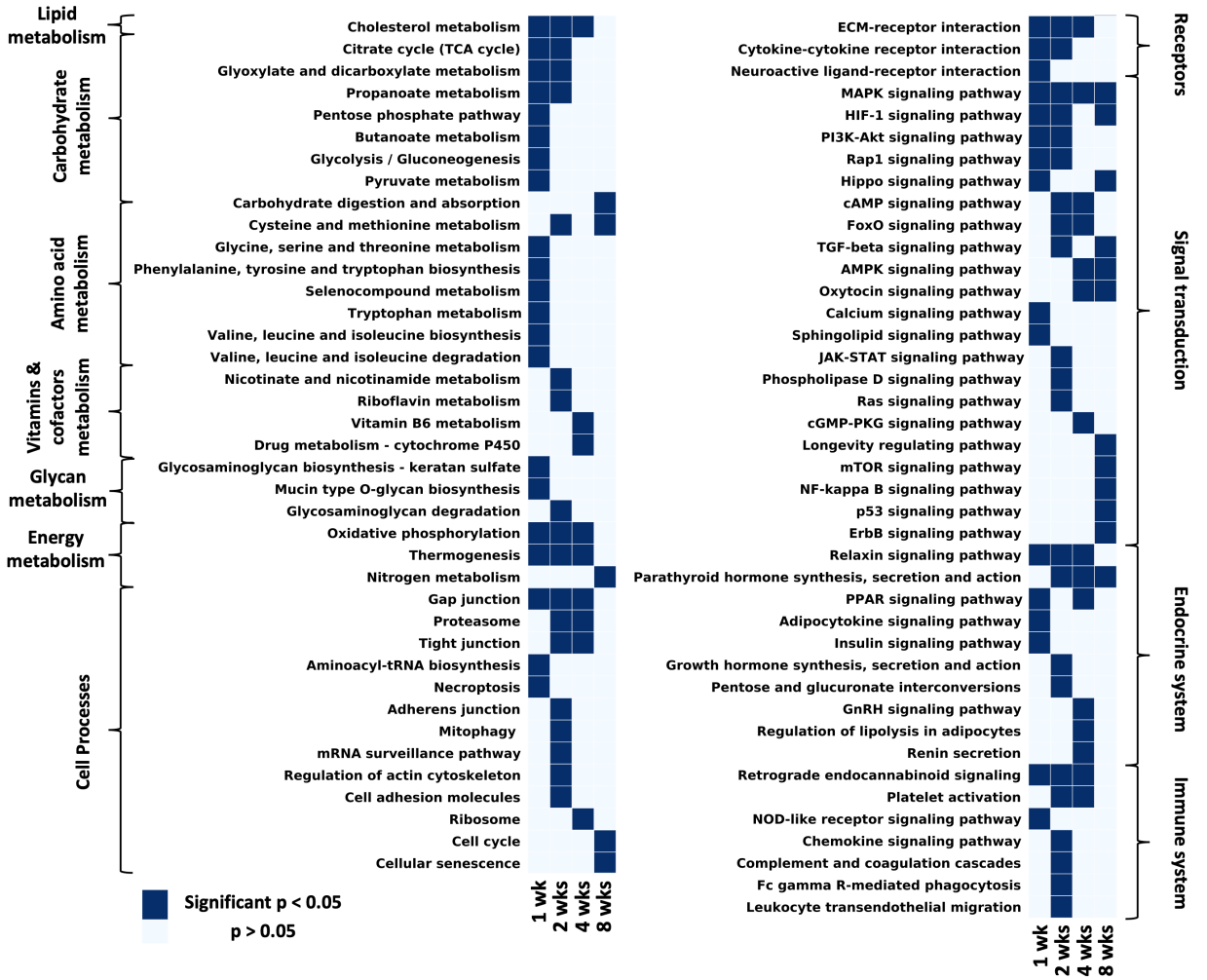

Figure 3.4: Post-Repair KEGG Enrichment analysis by timepoint.

Considering all pathways that have at least one time point with a significant p-value and filtering out disease/tissue specific pathways, the remaining pathways were grouped by KEGG hierarchy into amino acid metabolism, carbohydrate metabolism, vitamins and cofactors metabolism, energy metabolism, lipid metabolism, endocrine system, nervous system, immune system, signal transduction, cell processes (Supplementary Data 3.4).

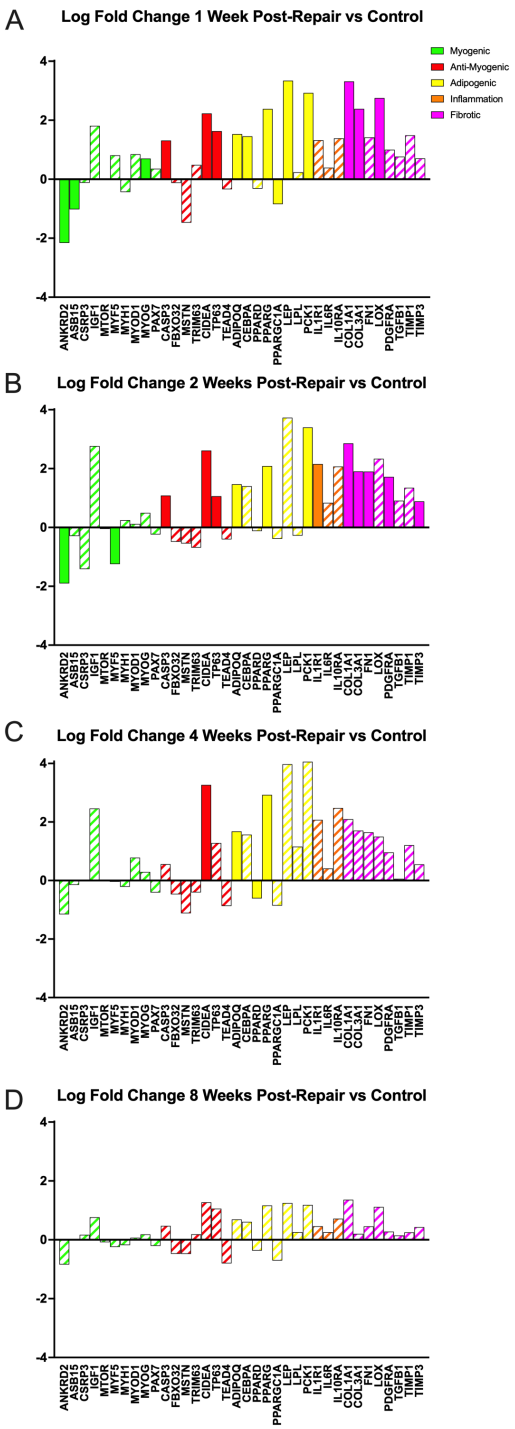

Figure 3.5: Post-Repair Literature based gene expression.

Considering all pathways that have at least one time point with a significant p-value and filtering out disease/tissue specific pathways, the remaining pathways were grouped by KEGG hierarchy into amino acid metabolism, carbohydrate metabolism, vitamins and cofactors metabolism, energy metabolism, lipid metabolism, endocrine system, nervous system, immune system, signal transduction, cell processes (Supplementary Data 3.4).

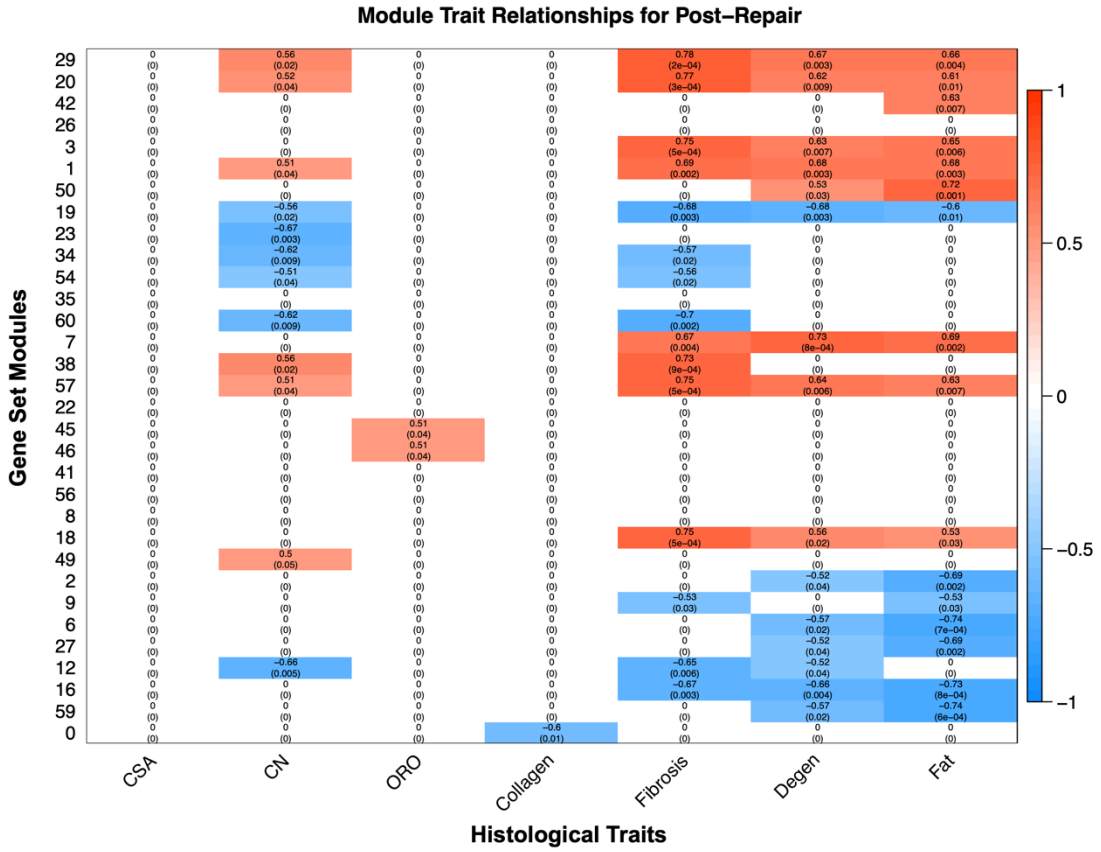

Figure 3.6: Post-Repair Module-trait relationship plot.

The modules, unbiased clustering of genes (described in Supplementary Data 3.8), on the left and the phenotypic traits are on the bottom. The scale bar represents the correlation coefficient and is the first number listed in each cell, and the number in parentheses is the p-value. Only cells with a p-value equal or less than 0.1 were selected to be displayed and the white cells with zeros represent cells with a p-value > 0.1 for clarity of which modules correlate with which phenotypic traits (Supplementary Data 3.6).

Chapter 4 CHRONIC STATE OF MUSCLE AFTER ROTATOR CUFF TEAR AND REPAIR

Abstract

Rotator cuff (RC) tears represent a significant health burden, often leading to shoulder pain and disability, particularly in the aging population. Despite various treatment options, persistent muscle atrophy and degeneration following surgical repair remain significant challenges. This study aims to elucidate the role of the immune system in the pathophysiology of RC tears and the subsequent repair process. We integrated transcriptional and histological analyses to investigate the temporal dynamics of the immune response in chronic RC tear and delayed surgical repair. Our findings revealed distinct patterns of differentially expressed genes at various timepoints post-tenotomy and post-repair, with more directly related immune response GO terms enriched in the post-tenotomy samples. Histological analyses corroborated these findings, with a significant increase in neutrophil numbers observed at 1 and 4 weeks post-tenotomy and none post-repair, meanwhile a significant increase in CD163+ (M2c) macrophages at 2 weeks post-tenotomy and 1 and 2 weeks post-repair. Interestingly, our study demonstrated a lack of a significant increase in KI-67 positive nuclei, a marker of cell proliferation, at any timepoint post-tenotomy or post-repair, and p53 only increased significantly at 1 week post-repair and at no timepoints post-tenotomy. Our study provides valuable insights into the role of the immune system in RC tear and repair, highlighting the dynamic and complex interplay between immune cells and muscle tissue during the progression of RC tear and repair. These findings underscore the need for further research to further elucidate these interactions.

Introduction

Rotator cuff (RC) tears are a common cause of shoulder pain and disability, affecting a significant proportion of the aging population (Lehman et al., 1995; Colvin et al., 2012;

Sayampanathan et al., 2017; Collin et al., 2019; Yamamoto et al., 2010). These injuries often result in substantial healthcare costs due to the range of treatment options, which include physical therapy, injectables, and surgical intervention (Galatz et al., 2004; Gladstone et al., 2007; Collin et al., 2018 & 2019). Despite these interventions, the persistence of muscle atrophy, degeneration, and fatty infiltration following surgical repair remains a significant challenge, highlighting the need for a deeper understanding of the underlying biological mechanisms involved in RC tears and their repair.

One such mechanism that has been gaining attention is the role of the immune system in the pathophysiology of RC tears and the subsequent repair process. The immune system plays a crucial role in tissue homeostasis, injury response, and repair (Nathan., 2002). In the context of musculoskeletal injuries, immune cells are among the first responders to the site of injury, where they participate in the clearance of cellular debris, orchestrate inflammation, and contribute to the initiation of muscle regeneration. They achieve this through activation and cueing differentiation of various cells including muscle satellite cells and fibro/adipogenic progenitors (FAPs) as well as a range of other programs such as apoptosis, adipogenesis, fibrosis (Scalier et al., 2013; Oprescu et al. 2010; Tidball et al., 2010; Jensen et al., 2020; Giannakis et al., 2019; Rogeri et al., 2020; Bernard et al., 2022). However, the specific role of the immune response in the progression of RC tear and repair remains poorly understood.

Recent studies have begun to shed light on the potential involvement of various immune cells in RC disease (Abraham et al., 2017). For instance, macrophages, key players in inflammation and tissue repair, have been found in increased numbers in muscles following injury as well as in regions of fatty degeneration (Gibbons et al., 2017; Gumucio et al., 2012). Similarly, proteomic neutrophil granulation signatures have been identified in human RC muscle (Frich et al., 2021)

and strong immune system signatures have been identified transcriptionally in chronic rabbit rotator cuff tear and delayed repair models out to 16 weeks post-tenotomy (Vasquez-Bolanos et al., 2021 & 2023). In a rat tenotomy experiment studying the acute temporal dynamics of the immune system, maximal hematopoietic (CD45+) cells were found around 5-7 days post-tenotomy (Stengaard et al., 2022).

The transition from the M1 (pro-inflammatory) and M2 (anti-inflammatory) macrophage populations, plays a crucial role in muscle healing (Tidball et al., 2010). An imbalance of one or both of these phases has been identified for possible involvement in muscle degeneration and fibrosis as subtypes of macrophages coexist and fail to encourage muscle regeneration (Rigamonti et al., 2014; Watanabe et al., 2019). As an example, CD163+, a marker of M2c macrophages, are a key player in the anti-inflammatory/resolution phase aiding muscle regeneration and when added in-vitro increase myoblast proliferation (Deng et al., 2012; Villalta et al., 2009; Massimino et al., 1997). However, in both mouse aging muscle and a *mdx* muscular dystrophy model, models of chronic inflammation, CD163+ M2c macrophages are found to accumulate over time and encourage fibrosis by an upstream reaction with arginase that leads to overproduction of collagen and fibrosis (Villalta et al., 2009; Wehling-Henricks et al., 2010; De Santa et al., 2019; Wang et al., 2015; Wang et al., 2022). Despite the possible fibrotic or antifibrotic role of CD163+ M2c macrophages, the precise role, timing, and crosstalk of this and other immune cells in the pathogenesis of RC tear and repair remains unclear.

This study aims to investigate the role of the immune system in RC tear and repair, by integrating transcriptional and histological analyses, in order to begin to elucidate the key cell types and temporal dynamics involved. We hypothesize that there will be a prolonged initial presence of neutrophils and a delayed appearance of CD163+ M2c macrophages that will then

persist to much later timepoints post-tear and post-repair with supporting proliferation (KI-67+) and increases in cell stress markers (p53). Likewise, CD163+ (M2c) macrophages will correlate with muscle morphology changes related to dysfunctional rotator cuff muscle, such as muscle degeneration, fibrosis, and fat. These findings will improve our understanding of the role of the immune system in the pathophysiology of RC disease and help move us toward the development of targeted therapeutic strategies to improve surgical outcomes and patient quality of life.

Materials & Methods

Animals

This study is a tertiary analysis, leveraging data previously collected and analyzed in the Vargas-Vila et al. (2021) and Wu et al. (2022) papers, to further explore and synthesize the findings within a broader context. In this study 67 skeletally mature female New Zealand White rabbits (~6 months, Western Oregon Rabbit Company, Philomath, OR) were used, 30 to evaluate post-tenotomy and 37 to evaluate post-repair transcriptional changes over time. Females were used due to housing safety concerns regarding mixing gender and the ease of sourcing older female animals. All protocols were approved by the University of California, San Diego Institutional Animal Care and Use Committee (protocol #S11246). All animals were assigned a number ID and individual cage location upon arrival and then at time of harvest were randomized to one of the study groups. Animals were single housed with food and water ad lib, environmental and food enrichment, and visual access to other animals. These tissues were also used in a prior study of histology (Vargas-Vila et al., 2021; Wu et al., 2022).

Surgical Procedures

Rabbits were anesthetized with a subcutaneous injection of ketamine and xylazine (35 mg/kg ketamine/5 mg/kg xylazine, MWI Veterinary Supply, Boise, ID). Following intubation, 2-

4% isoflurane (VetOne, Boise, ID) was utilized to keep the animals under anesthesia for the duration of the surgery. The left supraspinatus muscle served as the experimental side in all animals, with the right shoulder as an unoperated control for 21 animals in the repair study and for the 30 animals in the tenotomy study, a sham surgery was performed on the contralateral limb of the tenotomy to serve as a control for the procedure where only the skin was cut, tendon isolated, and then stitched up as normal., as described previously (Vargas-Vila et al., 2021). In brief, an open anterior approach was performed on the left shoulder, followed by sharp transection of the left supraspinatus tendon from its footprint on the greater tuberosity of the humerus. The surrounding soft tissues were bluntly dissected to allow unhindered retraction of the tendon stump and distal muscle. After securing a Penrose drain to the tendon stump to prevent scar formation between the tendon and surrounding soft tissue, the incision was closed in layers. Rabbits were then allowed individual cage activity with routine post-operative care. A fentanyl patch was placed on the back for pain control for 3 days, and the animals were monitored daily for 2 weeks post-operatively (Vargas-Vila et al., 2021). Then 21 rabbits continued after this point and at 8 weeks post-tenotomy, underwent an open repair of the torn tendon. The repair was performed using a modified locking suture with anterior and posterior bone tunnels to restore the tendon footprint to the humeral head. The same anesthesia (subcutaneous injection of ketamine and xylazine), surgical approach and closure, and post-operative protocols (fentanyl patch and daily monitoring) were used for the surgical repair operations (Wu et al., 2022).

Muscle Harvesting

After the study, 30 animals were euthanized at 5 time points; 1 week, 2 weeks, 4 weeks, 8 weeks and 16 weeks post-tenotomy and in the repair study 21 animals were euthanized at 4 time points; 1 week, 2 weeks, 4 weeks, and 8 weeks post-repair. At the specified time points, animals

were euthanized with an intravenous overdose of pentobarbital (Beuthanasia, 120 mg/kg, MWI Veterinary Supply, Boise, ID). The supraspinatus muscles from both shoulders were harvested and divided into four regions with the central tendon serving as the muscle midline between the anterior and posterior sides of the muscle. These four regions included anterior lateral (A1), posterior lateral (P1), anterior medial (A2), and posterior medial (P2), and one full-muscle thickness fragment was harvested from each location. The harvested muscle regions were pinned to in vivo length and flash frozen in liquid nitrogen-chilled isopentane for storage at -80 C degrees (Wu et al., 2022).

RNA Extraction, Sequencing, and Analyses

These methods have been defined and described previously by Vasquez-Bolanos et al. (2021 & 2023).

Enrichment Analysis Immune Specific

The total genes (~10,000) for tenotomy and repair study were filtered to immune specific genes (~2000) determined by using InnateDB (Bruere et al., 2013). Differentially expressed genes were defined as those with adj. p-value < 0.05. Overrepresentation of functional categories was calculated for immune specific DE genes as compared with the corresponding 'background' genes, and significant GO terms were identified as those having p-value <0.05. Figure 4.2 highlights the top 5 GO terms with the lowest p-value at each timepoint and then the heatmap describes the significance of each pathway at each timepoint.

Correlation Analysis

Pearson correlation analysis was conducted using GraphPad Prism software. The data sets were imported into the software and organized into corresponding rows and columns. The software was set to provide both the correlation coefficient (r) and the two-tailed p-value. A p-value < 0.05 was considered statistically significant. The results were visualized using a correlation matrix and

top correlations of interest were highlighted with a scatterplot where a line of best fit was used and r^2 was calculated and labeled on the figure.

Weighted correlation network analysis (WGCNA) was performed using WGCNA R package (v. 1.70-3) (Langdelder & Horvath, 2008) with transcriptional and phenotypic data from both studies (Vasquez-Bolanos et al., 2021 & 2023) with the tenotomy and sham samples and the repair and control samples in order to correlate histological traits. This analysis identified unbiased modules or sets of genes that are clusters of highly correlated genes. In the combined analysis (both repair and control groups) only two modules correlated significantly with fat and none with experimental assays (CD163, Neutrophils, KI67, p53) for tear and sham groups. This analysis works by building an unbiased network of modules which represents a cluster of genes, and then correlations can be investigated with phenotype traits through gene membership. GO enrichment analysis was then performed by GoEnrichmentAnalysis function within the WGCNA R package and returns the top 10 GO terms of each module (Supp. Data 1). The phenotypic data included in this study is fiber area, central nucleation, fat quantification, collagen content, and degeneration, all of which are reported in detail elsewhere (Vargas-Vila et al., 2021; Wu et al., 2022) but are from the same animals used in this study.

Tissue Collection

Supraspinatus muscles were harvested, and a full-muscle thickness segment was dissected from P1 region described above. These segments were then pinned to in-vivo length, and snap-frozen in liquid nitrogen-cooled isopentane before being stored at −80°C. Frozen muscle segments were then embedded in OCT and sectioned in a cryostat to obtain axial sections. They were then sectioned at thickness of 10 um serially.

Histology

We preformed immunofluorescence stains using anti-Neutrophil (1:100 dilution, Clone RPN3/57), anti-CD68 (Clone 514H12), anti-CD163 (1:100 dilution, Clone EDHu-1), anti-KI-67 (1:100 dilution, Clone 8D5), anti-p53 (1:100 dilution, Clone PAb421) on muscle sections embedded in OCT. In brief, sections were taken out of the freezer, and allowed to reach room temperature. If a nuclear stain was used, an additional step of fixation with 4% PFA followed by heat induced epitope retrieval by using 0.01 M citrate buffer pH 6.0 on a heat plate for 15 mins, otherwise the section was permeabilized with PBS-T (0.1% triton-X), then washed with PBS (3 changes). Sections were then blocked with 10% goat serum for 1 hour, washed with PBS (3 changes), then the primary antibody was diluted with 0.1% BSA/PBS and incubated overnight at 4 C, then rinsed with PBS (3 changes). The secondary was then diluted similarly to the primary and left to incubate for 1 hour, washed with PBS (3 changes), then wheat germ agglutinin (1:2000; Alexa Fluor 594; Invitrogen) was added, washed with PBS again, and coverslipped with mounting medium with 4′,6-diamidino-2-phenylindole (Vectashield Antifade mounting medium with DAPI; VectorLabs). Appropriate positive and negative controls were included with the study sections for each stain anti-Neutrophil (spleen; (Anderson, K. et al., 2014), anti-CD163 (tonsil; Glavind, E. et al., 2020), anit-KI-67 (tonsil; Hsu, C. et al., 2013), anti-p53 (degenerated skeletal muscle; Stocks, B. et al., 2017). CD68 did not pass positive and negative control screening, so it is not reported in the Results.

Image Collection

Multi-channel (.lif) stack images were obtained using a Leica microscope (Leica DM6000B microscope with DCF365FX camera on x10 setting (x100 total magnification)) equipped with a 10x objective lens. The microscope was set to capture images in three separate channels corresponding to red (647 nm), green (488 nm), and blue (350 nm). The red channel was

used to capture the respective assay, the green channel was used for Wheat Germ Agglutinin (WGA) – marker for membrane/laminin equivalent, and the blue channel was used for 4',6-diamidino-2-phenylindole (DAPI) – identify nuclei. The microscope settings were adjusted to ensure optimal signal-to-noise ratio for each channel using the positive and negative control for each batch, so the same settings were used across each batch. A grid capturing the whole section of muscle was mapped out and then images were captured sequentially to avoid bleed-through between channels at each position until the whole grid had been imaged. The captured images were saved in a stack .lif format for subsequent analysis. The process was repeated for all the samples, ensuring consistent settings across all the images.

Image Analysis

ImageJ/FIJI software was utilized for automated quantification of particles in the blue (DAPI) and red (Assay) channels of .lif files. The Bio-Formats plugin was employed to open the .lif files in the software. For each image, the channels were separated, and the analysis was performed independently for the DAPI and Assay channels. A custom macro was developed to automate the process. The macro first applied an auto-thresholding technique to each image to distinguish particles from the background. For the Assay channel, the auto-thresholding method that best suited the assay was chosen, either MaxEntropy or Otsu (Sezgin & Sankur, 2004), based on the image characteristics. For the DAPI channel, the Otsu method was consistently used across all samples. The 'Watershed' function was then used to separate touching particles. Following this, the 'Analyze Particles' function was used to quantify the particles in each image. This function provides a count of the particles, as well as measurements of their area. For nuclei calculation a mathematical operation was used to merge the assay and DAPI channels using the "AND" operation and then similarly 'Analyze Particles' function was used. The results were saved and

exported for further analysis. The macro was run on all samples, ensuring a consistent and unbiased quantification process.

Regional assessment of CD163 positive cells in degenerated and healthy regions of muscle was performed manually by observation in only post-repair samples. Signs of muscle degeneration were defined as hypercellularity (i.e., myophagocytic fibers with multiple nonperipheral nuclei), disrupted muscle fiber membranes, irregularly shaped fibers, or split muscle fibers for over 50% of a field of view (Vargas-Vila et al., 2022; Gibbons et al., 2017). If in a given field of view there were 50% or more of healthy muscle on section, the section was defined as healthy, non-degenerated.

Statistical Analysis

For the nuclei data, which involved multiple groups and factors, a two-way analysis of variance (ANOVA) was conducted. This test was used to examine the main effects of two independent variables, as well as the interaction effect between them. The two-way ANOVA was followed by a post-hoc Tukey's Honest Significant Difference test to correct for multiple comparisons and identify specific differences between group means. Given the non-normal variance structure of immunofluorescence data, we employed non-parametric statistical tests for analysis. Specifically, the Wilcoxon rank-sum test was used due to its robustness against non-normality and its ability to compare distributions based on rank, making it suitable for our data structure. All statistical analyses were performed using GraphPad Prism software, and a p-value < 0.05 was considered statistically significant. The results were presented as mean values with standard error of the mean, and all graphs were generated within GraphPad Prism to visually represent these findings.

Results

Transcriptionally, of the immune specific genes identified, 2136 were shared between post-tenotomy and post-repair, while 66 were unique to post-tenotomy and 87 were unique to post-repair. (Fig. 4.1). GO enrichment of immune-related programs identified terms relating to the immune system directly, and other biological programs such as extracellular matrix (ECM), fibrosis, adipogenesis, mechanosensing, and metabolism (Fig. 4.2). Post-tenotomy, of the top 5 significantly enriched terms for each timepoint, 10 out of 25 GO terms directly related to the immune system (Fig. 4.2A), while post-repair only 5 out of 20 related to the immune system (Fig. 4.2B). The immune transcript signature for post-tenotomy muscle consisted of an innate immune response with strong differential regulation of IL-6, IFN-gamma, TNF-alpha, and protein kinase-B, while post-repair was significantly enriched for IL-10, NF-kappaB, metabolism (glucose, cholesterol, catabolism), and mechanical sensing (Fig. 4.2).

Average nuclei numbers were quantified per field of view and differences between tear and repair, and their respective controls were compared (Fig. 4.3). Post-tenotomy, there was a significant increase compared to the sham-operated controls at 1, 8, and 16 weeks post-tenotomy (Fig. 4.4A) (p-value = 0.0062; p-value =0.0109; p-value = 0.0399). When these numbers were normalized to the average number of muscle cells per field (muscle fibers are atrophying) these differences largely disappeared, with the exception of 1 week post tenotomy, where it remained elevated (Fig. 4.4B). Although there was a significant increase in nuclei between post-repair and control muscles at all timepoints (Fig. 4.4C) (p-value <0.001; p-value <0.001; p-value =0.001; p-value <0.001), these numbers only remained elevated at 1 and 8 weeks (p-value = 0.023; p-value = 0.016) post-repair when average fiber number (atrophy) was considered (Fig. 4.4D).

Neutrophil numbers were increased significantly at 1 (p-value = 0.031) and 4 weeks (p-value = 0.031) post-tenotomy compared to sham-operated control samples with an average number of neutrophils per field of view of 10 and 1.55 respectively (Fig. 4.3A). There were no significant differences at any other timepoints post-tenotomy (Fig. 4.5A). When results were normalized by the average number of nuclei per field of view, similar results were found post-tenotomy for normalized neutrophil numbers (Fig. 4.5B). For post-repair samples there were no significant differences compared to control at any timepoint (Fig. 4.5C). This carried through the normalized results post-repair as well (Fig 4.5D).

CD163+ cells (M2c macrophages) trended (p-value = 0.063) towards being increased at 1 week post-tenotomy and were significantly elevated at 2 weeks post-tenotomy (p-value = 0.031) with an average number of CD163 per field of view of 38.45 and 3.94 respectively (Fig. 4.3B & 4.6A). Normalized post-tenotomy samples had the same behavior as non-normalized data (Fig. 4.6B). For post-repair, 1 (p-value = 0.031) and 2 weeks (p-value = 0.016) were significantly increased compared to control and there was a trend at 8 weeks (p-value = 0.011) but none at 4 weeks (Fig. 4.6C). Average CD163+ cell numbers were 19.5, 24.5, 0.54, and 10.45 respectively (Fig. 4.6C). Normalized results post-repair were similar to non-normalized result with the exception that at 1 week the increase is not significantly different (p-value = 0.063; Fig. 4.6D).

KI-67+ nuclei were measured, and the data was found to be highly variable across all timepoints post-tenotomy and post-repair (Fig. 4.3C & 4.7A-D). The observed trend, although not statistically significant, is increased KI-67+ nuclei for post-tenotomy samples across all timepoints compared to sham control (Fig. 4.7A). This trend continued slightly at 1 week post-repair, but not at any other timepoints post-repair (Fig. 4.7B). Similar observations were made for post-tenotomy and post-repair normalized data compared to non-normalized results (Fig 4.7).

Cytoplasmic and nuclear p53 demonstrated similar trends across post-tenotomy and post-repair (Fig. 4.3D, 4.8, 4.9). Nuclear p53 however did have a trending increased difference at 2 weeks post-tenotomy (p-value = 0.063) compared to sham-operated control and none at any other timepoint (Fig 4.9A). This increased trend carried over to the normalize post-tenotomy result (Fig 4.8B). Meanwhile, for post-repair there was a significant increase at 1 week post-repair (p-value = 0.031) for nuclear p53 counts compared to control and not at any other timepoints (Fig. 4.9C), which similarly carried over to the normalized representation of the data (Fig. 4.9D).

WGCNA revealed gene modules significantly related to immune cell and cell cycle markers quantified by histology (Fig. 4.10). Transcriptional activity correlated significantly with the presence of neutrophils, CD163+ macrophages, and p53, but not KI-67 for post-tenotomy samples and only CD163 and p53 for post-repair samples (Fig. 4.10). For post-tenotomy WGCNA, module 51 was positively correlated for neutrophils (r = 0.57; p-value = 0.0009; Fig. 4.10A) and CD163 (r = 0.66; p-value = 0.00006) and was enriched for GO terms related to innate immune response and type I interferon (Supp. Data 4.1). Additionally for post-tenotomy WGCNA, module 52 was negatively correlated for p53 (r = 0.57; p-value = 0.0005; Fig. 4.10A) and was enriched for GO terms related to nucleus activity and chromatin and histone modifications (Supp. Data 4.1). For post-repair WGCNA, module 50 was negatively correlated for CD163 (r = 0.66; p-value = 0.015) and was enriched for GO terms related to immune response, T-cell activity, and apoptotic signaling (Supp. Data 4.1). Additionally for post-repair WGCNA, module 18 was negatively correlated for p53 (r = 0.57; p-value = 0.036) and was enriched for GO terms related to kinase activity (AMPK, NADPH) and receptor activity (Supp. Data 4.1). Module 14 was negatively correlated in post-repair for both CD163 (r = 0.57; p-value = 0.0075) and p53 (r = 0.57; p-value =

0.0075), and was enriched for GO terms related to leukocytes and T-cell adhesion, activation, and differentiation (Supp. Data 4.1).

Using previously collected muscle morphological data (Vargas-Vila et al., 2021; Wu et al., 2022), and newly collected immune cell and cell cycle markers, a Pearson correlation matrix was calculated, and only significant correlations are highlighted (Fig. 4.10). The strongest correlation in post-repair samples was the morphological trait of degeneration and immune cell marker CD163 with a significant correlation post-repair (r^2 =0.71; Fig. 4.10C). In addition, CD163 was also significantly correlated with fat (r^2 = 0.25; Fig. 4.10E) post-repair. Fibrosis also correlated with CD163 significantly (r^2 =0.38; Fig. 4.10D) post-repair, and to a lesser extent CSA (r^2 = 0.22; Fig. 4.10F) post-repair. Focusing on specific immune cell markers correlations, post-tenotomy there is a strong correlation between neutrophil and CD163 results (r =0.88; Fig. 4.10A). Meanwhile, post-repair this relationship decouples a bit between neutrophils and CD163 numbers (r= 0.50; Fig. 4.10B).

Considering the strong correlations and regional implications of degeneration post-repair, we quantified CD163+ in a regional manner by subcategorizing CD163+ cells found in healthy and degenerated muscle (Fig. 4.12). At almost all timepoints (1, 2, 4 weeks post-repair) there was a significant increase in CD163+ macrophages found in degenerated regions of muscle compared to CD163 macrophages found in non-degenerated regions of muscle (p-value = 0.016, p-value = 0.016, p-value =0.0078), with similar trend at 8 weeks post-repair (p-value = 0.063; Fig. 4.13).

Discussion

The purpose of this study was to investigate the role of the immune system in rotator cuff (RC) tear and repair, with a specific focus on the temporal dynamics of the immune response. We hypothesized that neutrophils would have a prolonged initial presence with a delayed appearance

of CD163+ M2c macrophages that would then persist to much later timepoints post-tear and post-repair with supporting proliferation (KI-67+) and increases in cell stress markers (p53) over time. Likewise, CD163+ (M2c) macrophages would correlate with muscle morphology changes related to dysfunctional rotator cuff muscle, such as muscle atrophy, degeneration, fibrosis, and fat. Neutrophils did not behave as hypothesized for post-repair where no timepoints were different and CD163+ M2c macrophages dominated early on, but did not persist at much later timepoints post-tear and post-repair as hypothesized. Meanwhile CD163+ M2c macrophage results correlated with muscle morphology changes related to dysfunctional rotator cuff muscle, such as muscle atrophy, degeneration, fibrosis, and fat supporting our initial hypotheses.

Our transcriptional analysis revealed distinct patterns of enriched GO terms at various timepoints post-tenotomy and post-repair. Interestingly, the acute immune response was more pronounced in the post-tenotomy samples compared to the post-repair samples, based on the number and type of GO terms significantly enriched across time post-tenotomy compared to post-repair (Fig. 4.2), suggesting a differential immune response to injury and repair. These findings aligned with previous studies that have reported an early and robust immune response following musculoskeletal injuries, which gradually subsides during the repair process (Scalier et al., 2013; Oprescu et al. 2010; Tidball et al., 2010; Jensen et al., 2020; Giannakis et al., 2019; Rogeri et al., 2020; Bernard et al., 2022).

Meanwhile, our histological analyses further supported these transcriptional findings, with a significant increase in neutrophil numbers observed at 1 and 4 weeks post-tenotomy with none post-repair, and a significant increase in CD163+ M2c macrophages at 2 weeks post-tenotomy and 1 and 2 weeks post-repair. The presence and difference of these immune cells at these specified timepoints suggests a dynamic and complex interplay between the immune system and the muscle

tissue during the progression of RC tear and repair. Remarkably, despite discovering a strong immune system resurgence of transcriptional activity at 16 week post-tenotomy, of the assays quantified in this study, none support this previous observation. Suggesting a complex interplay between genetic expression and actual physiological manifestation as well as possible limitation of the sample numbers available at 16 weeks post-tenotomy due to sample supply.

Our study also revealed a lack of significant increase in KI-67 positive nuclei, a marker of cell proliferation, at any timepoint post-tenotomy or post-repair. This finding contrasts with the expected regenerative response following acute muscle injury, which typically involves a surge in cell proliferation as part of the repair process (Close, 1972). This discrepancy may suggest a dysregulated regenerative response in the context of RC tear and repair, potentially due to the chronic inflammatory state induced by the injury and the subsequent repair process. Meanwhile, cytoplasmic and nuclear p53 changes across post-tenotomy and post-repair have little to no pattern, but does correlate strongly with transcriptional results, suggesting an alternative explanation that is not obviously clear.

Gene modules were identified in this study that were significantly associated with the immune cell and cell cycle markers quantified by histology. Specifically for post-tenotomy, transcriptional results correlated with neutrophils, CD163 macrophages, and p53, however for post-repair the transcriptional correlation observed between neutrophils and CD163 macrophages was decoupled with only CD163 and p53 correlating significantly post-repair. These modules were enriched for biological processes related to the immune response, cell cycle regulation, and chromatin modification, further underscoring the intricate interplay between the immune system and the cellular machinery during RC tear and repair.

Despite these significant findings, our study had several limitations. First, the utilization of a rabbit animal model, although relevant, presents challenges as there are significantly fewer biological tools available compared to more commonly used models across science such as mice. Second, our focus on only two types of immune cells among a vast array of different immune cells and subtypes may have led to an incomplete understanding of the immune response. The complexity of the immune system involves numerous cell types and interactions, and our study is not capable of cover all critical components of this intricate network. Third, the temporal resolution of our study may not fully capture the dynamics of the immune system, as our first time point was at 1 week post-tear and post-repair. This design overlooks potential immune changes occurring between day 0 and day 7, possibly missing early critical events in the immune response. Finally, the inter-subject variability due to the heterogeneous nature of the immune system may have introduced increased variance in our findings. Individual differences in immune response could have affected the results, leading to challenges in generalizing our conclusions. These limitations should be considered when interpreting the findings of this study and should guide future research efforts to provide a more comprehensive understanding of the immune system's role in rotator cuff pathology.

Conclusion

In conclusion, our study provides valuable insights into the role of the immune system in RC tear and repair. Our investigation revealed unexpected behaviors of neutrophils and CD163+ M2c macrophages during different stages of injury and repair, challenging our initial hypotheses. Specifically, the neutrophil results did not align with expectations post-repair, with no significant differences observed at any timepoints, contrasting with the significant increase in neutrophil numbers at 1 and 4 weeks post-tenotomy. The early dominance of CD163+ M2c macrophages,

heterogenous increase presence in degenerated/healthy muscle, and their correlation with muscle morphology changes such as atrophy, degeneration, fibrosis, and fat accumulation emphasize their potential role in RC dysfunction. The transcriptional analysis further illuminated the differential immune response to injury and repair, with acute immune activation more pronounced post-tenotomy. Histological findings supported these transcriptional patterns, highlighting the temporal dynamics of immune cells during RC tear and repair. The lack of significant increase in KI-67 positive nuclei post-tenotomy or post-repair points to a potential dysregulated regenerative response, possibly influenced by chronic inflammation. The identification of gene modules associated with immune cells and cell cycle markers, and their enrichment in biological processes related to immune response and cell regulation, further underscores the intricate interplay between the immune system and cellular machinery in RC tear and repair. The study's findings not only contribute to our understanding of the immunological aspects of RC pathology but also open new avenues for therapeutic interventions targeting the immune response to enhance muscle recovery and repair. The observed discrepancies between transcriptional activity and in vivo manifestations, as well as the limitations related to sample numbers at specific timepoints, call for further research to unravel the complex interactions between genetic expression and physiological manifestation in the context of RC tear and repair.

Acknowledgements

This chapter, in full, is a reprint of the material being prepared for submission for publication. Laura S Vasquez-Bolanos, Severin Ruoss, Mary C Esparza, Donald C Fithian, John G Lane, Anshuman Singh, Elsa Sanchez-Lopez, Samuel R Ward. The dissertation author was the primary investigator of this material.

Figures

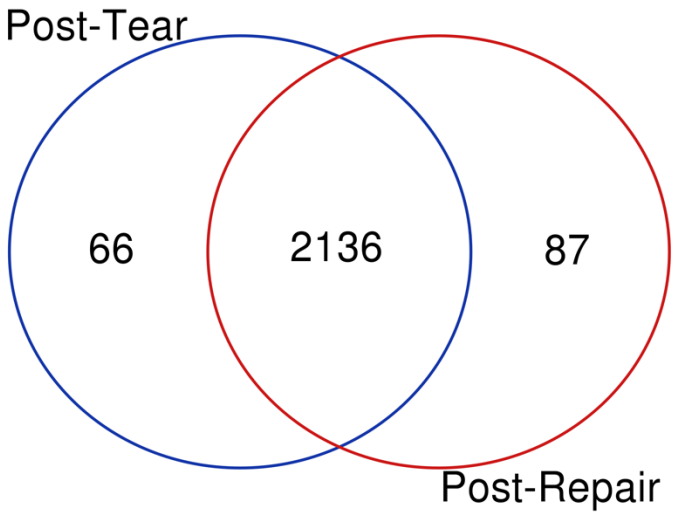

Figure 4.1: Venn diagram of immune specific genes.

Venn Diagram of immune specific genes isolated from InnateDB for post-tenotomy and post-repair studies across all timepoints.

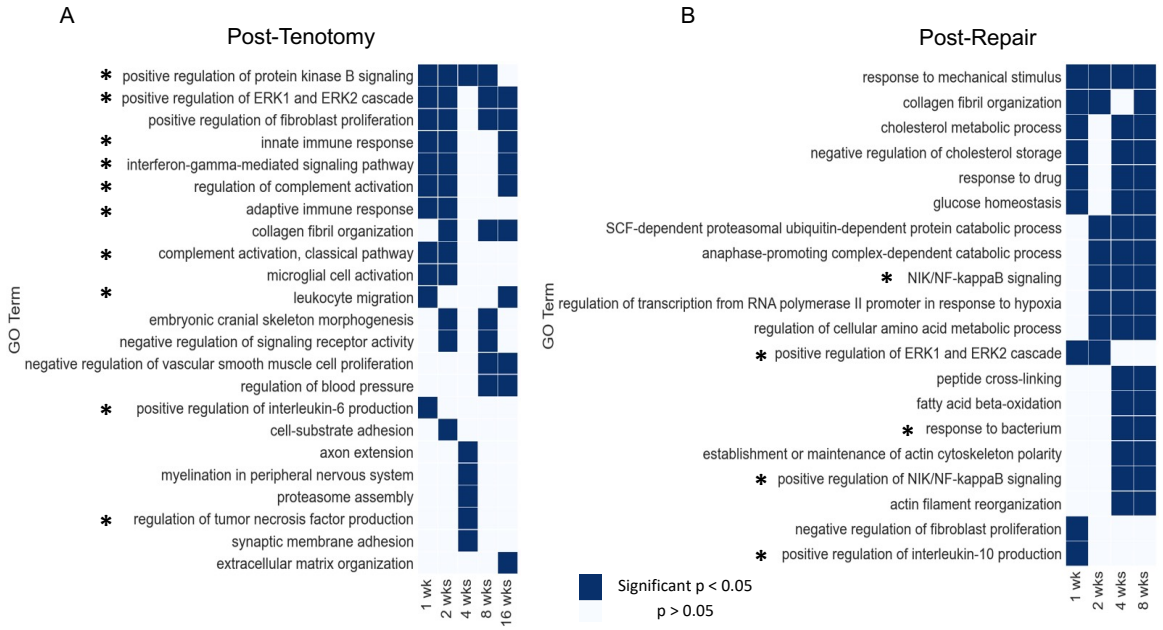

Figure 4.2: Immune specific KEGG enrichment analysis.

Heatmap of top GO terms at each timepoint across post-tenotomy and post-repair. Significant terms are highlight with dark blue (p-value<0.05). Immune specific terms are highlighted by an Asterix.

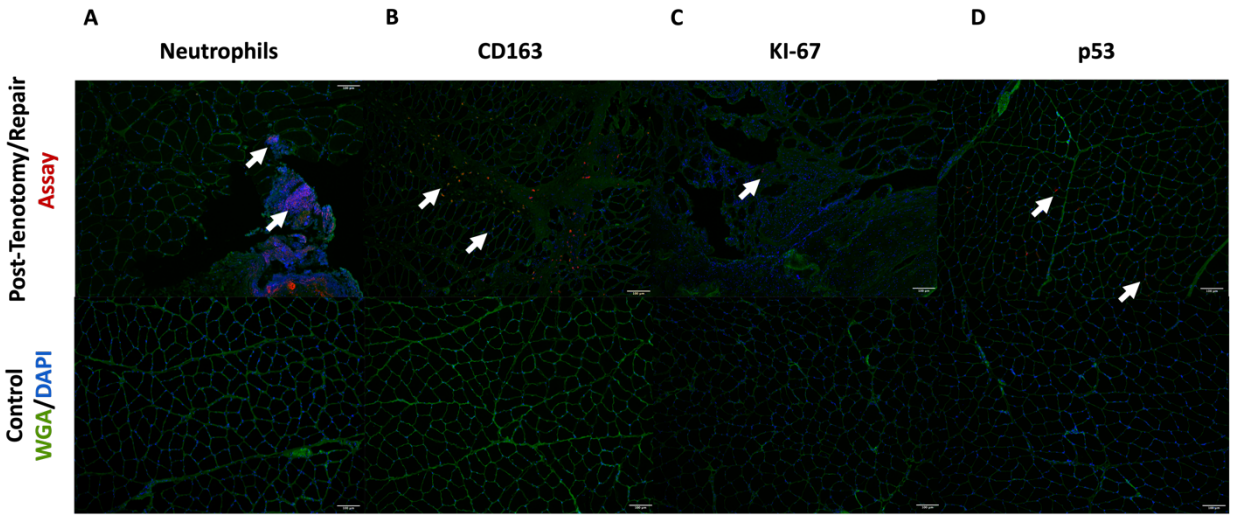

Figure 4.3 Post-Tenotomy & Post-Repair Immunofluorescence Examples

Sample of control tissue and positive for post-tenotomy and post-repair for each assay (in red) quantified: neutrophils (A), CD163 (B), KI-67(C), p53 (D). Where blue represents DAPI labeling nuclei and green represent WGA, a marker for membranes.

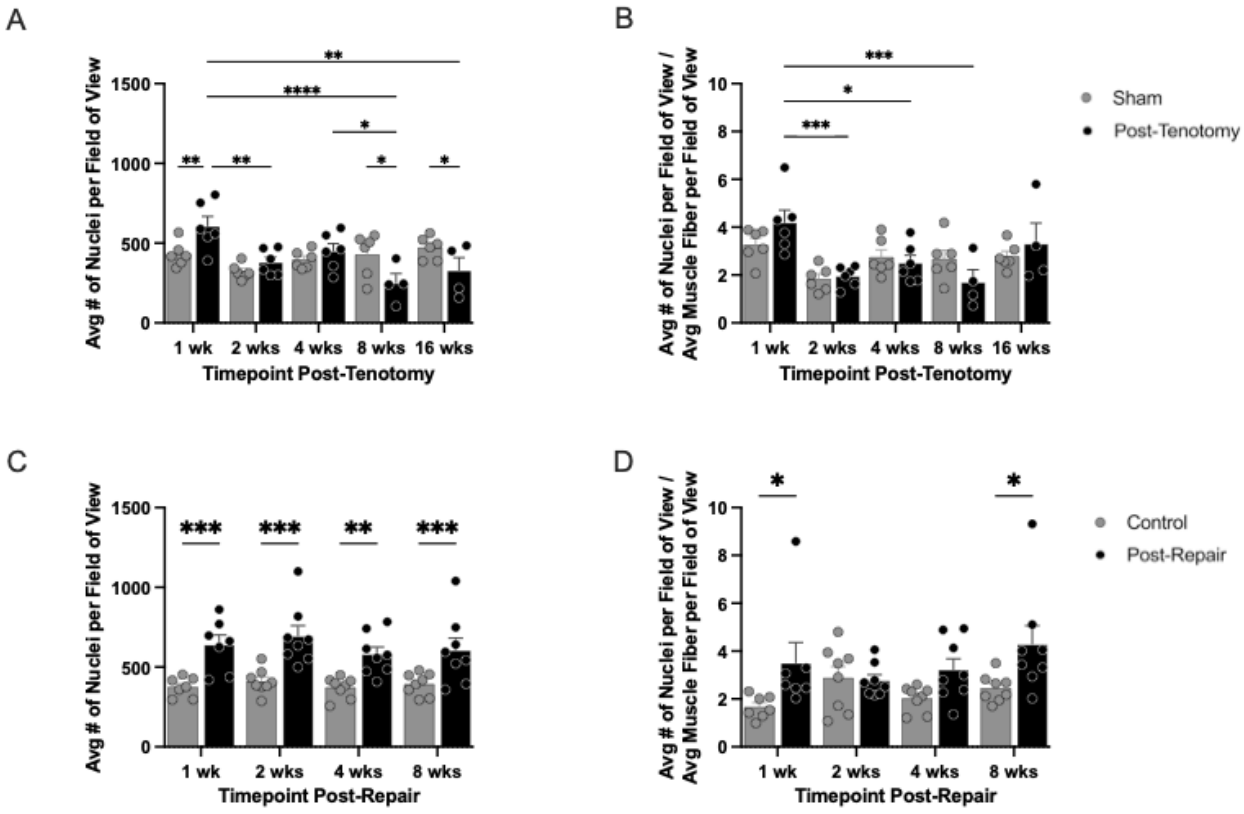

Figure 4.4: Post-Tenotomy & Post-Repair Average nuclei numbers.

Bar plot of average nuclei counts per field of view and normalized by average muscle fibers per field of view results for post-tenotomy (A-B) and post-repair (C-D). * Indicates p-value < 0.05 (2-way ANOVA, post-hoc tukey).

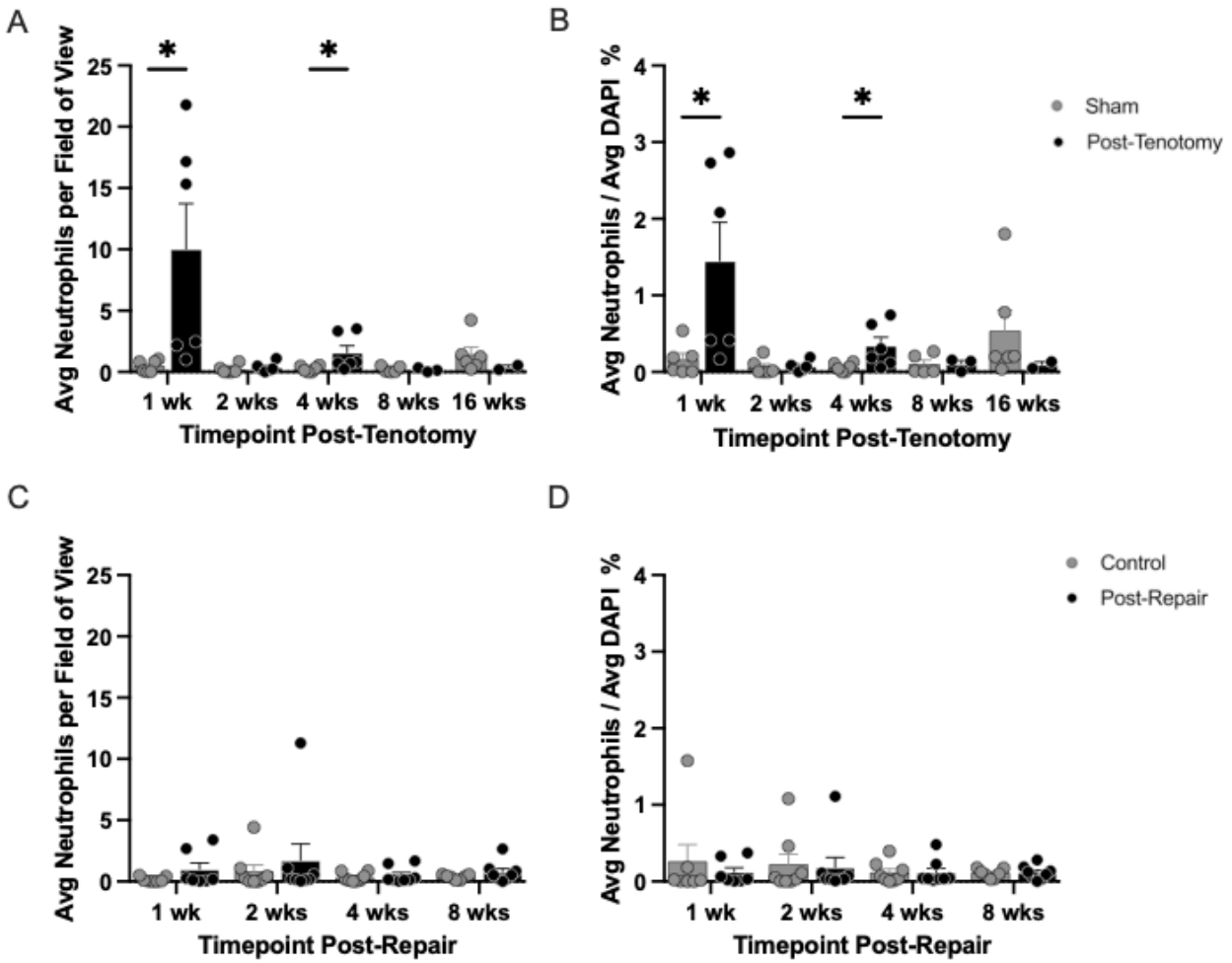

Figure 4.5: Post-Tenotomy & Post-Repair Average neutrophil cell numbers.

Bar plot of average neutrophil counts per field of view and normalized result for post-tenotomy (A-B) and post-repair (C-D). * Indicates p-value < 0.05 (Wilcoxon tests).

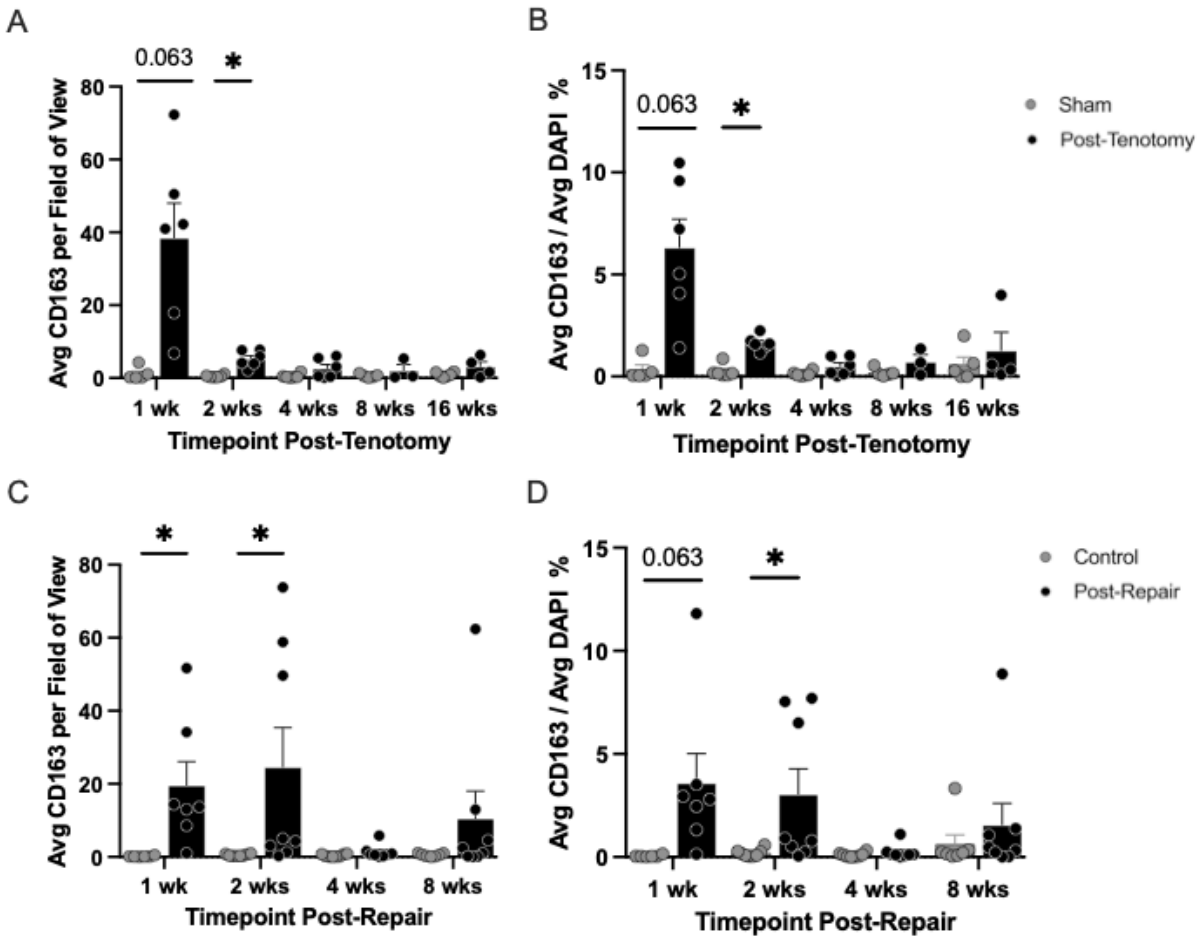

Figure 4.6: Post-Tenotomy & Post-Repair Average CD163 cell numbers.

Bar plot of average CD163 counts per field of view and normalized result for post-tenotomy (A-B) and post-repair (C-D). * Indicates p-value < 0.05 (Wilcoxon tests).

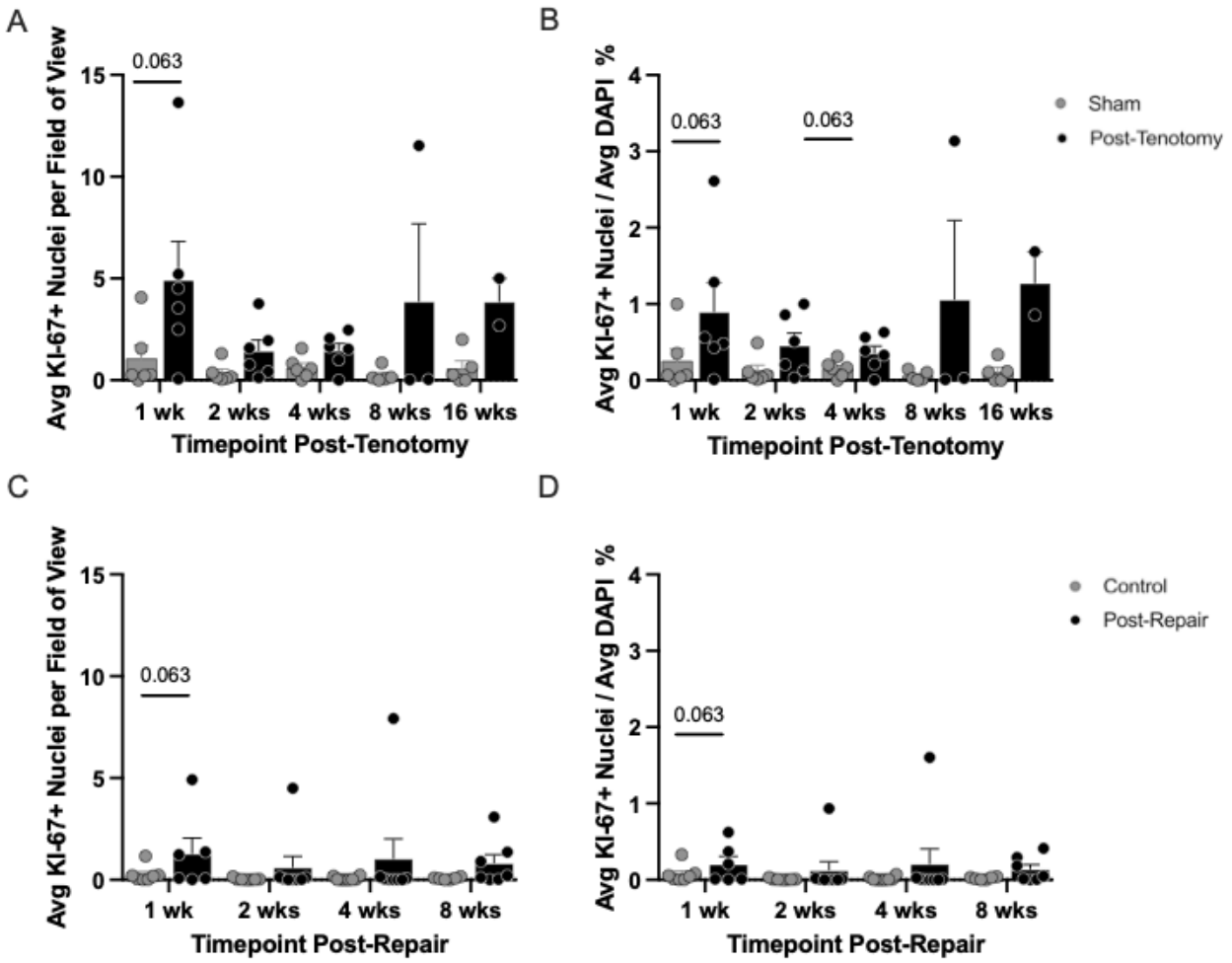

Figure 4.7: Post-Tenotomy & Post-Repair Average KI-67+ nuclei numbers.

Bar plot of average KI-67+ nuclei counts per field of view and normalized result for post-tenotomy (A-B) and post-repair (C-D). * Indicates p-value < 0.05 (Wilcoxon tests).

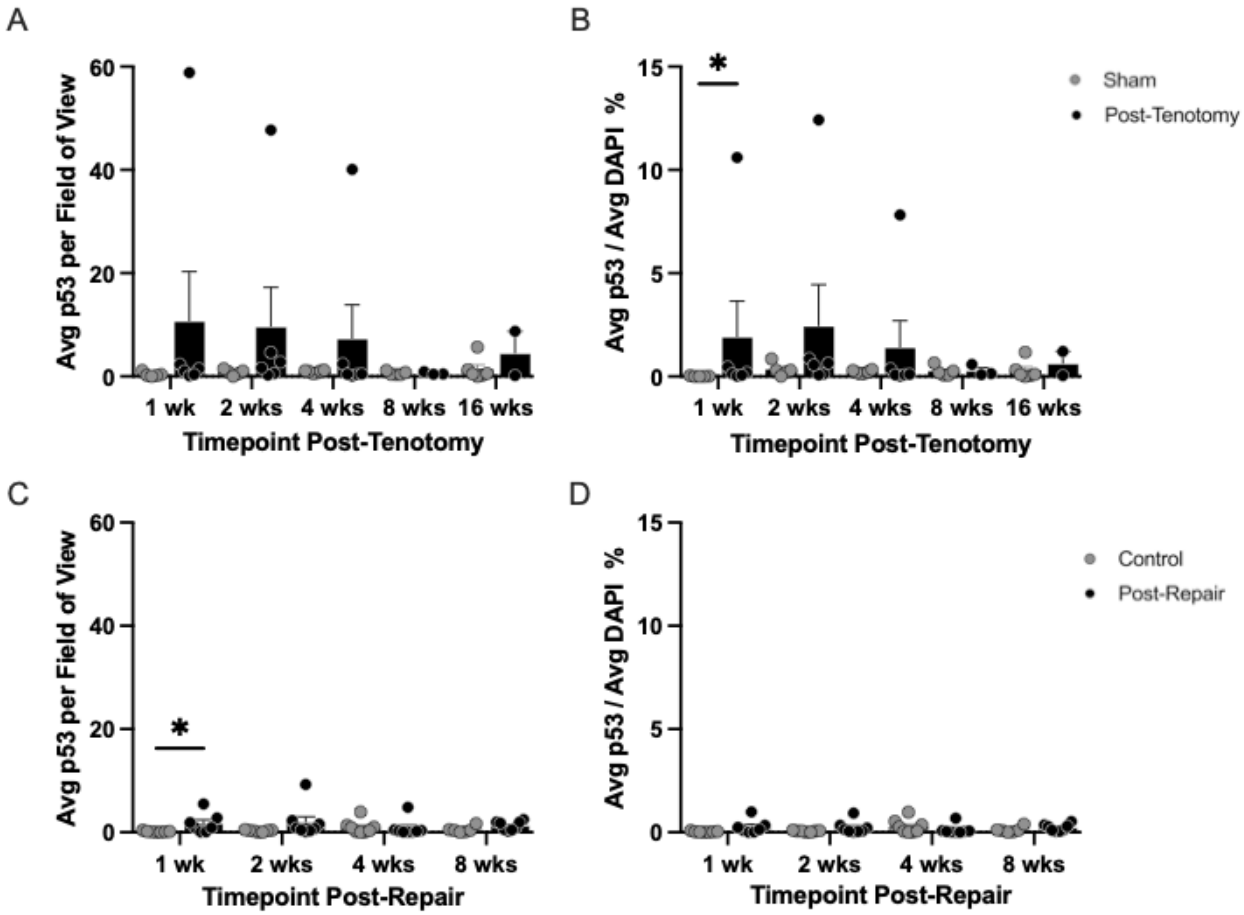

Figure 4.8: Post-Tenotomy & Post-Repair Average cytoplasmic p53.

Bar plot of average cytoplasmic p53 counts per field of view and normalized result for post-tenotomy (A-B) and post-repair (C-D). * Indicates p-value < 0.05 (Wilcoxon tests).

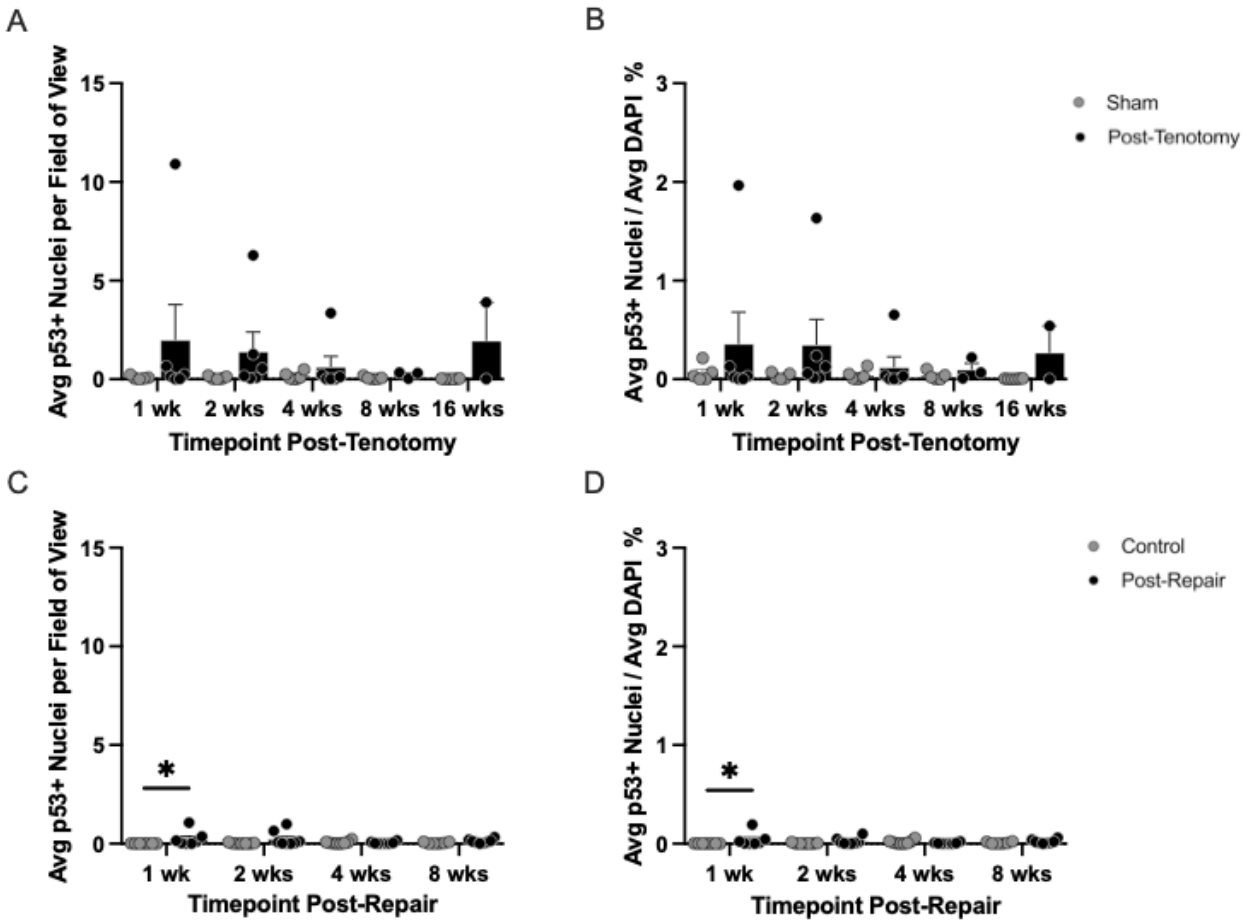

Figure 4.9: Post-Tenotomy & Post-Repair Average nuclear p53.

Bar plot of average nuclear p53 counts per field of view and normalized result for post-tenotomy (A-B) and post-repair (C-D). * Indicates p-value < 0.05 (Wilcoxon tests).

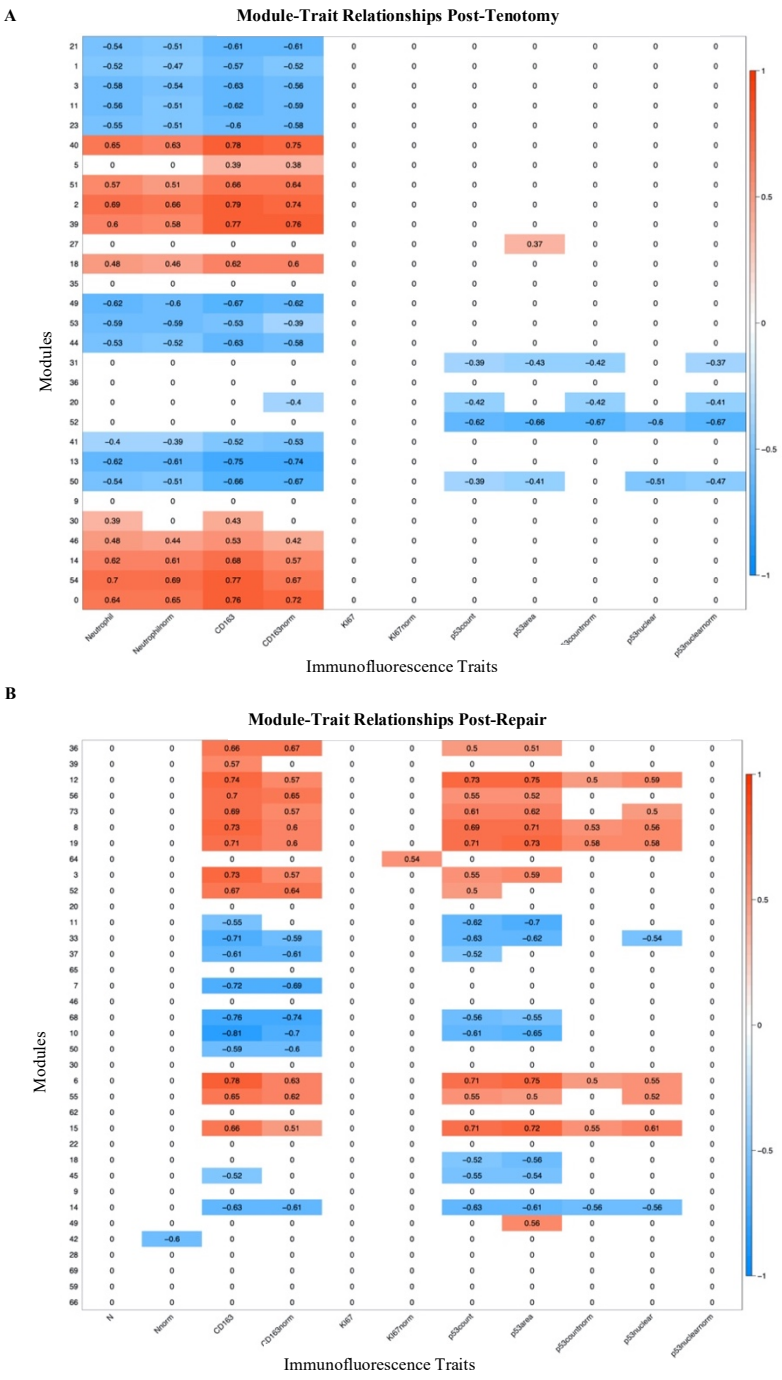

Figure 4.10: Post-Tenotomy & Post-Repair Module-trait relationship plots for immunofluorescence traits.

The modules, unbiased clustering of genes, on the left and the immunofluorescence traits are on the bottom. The scale bar represents the correlation coefficient and is the first number listed in each cell, and the number in parentheses is the p-value. Only cells with a p-value equal or less than 0.1 were selected to be displayed and the white cells with zeros represent cells with a p-value > 0.1 for clarity of which modules correlate with which traits.

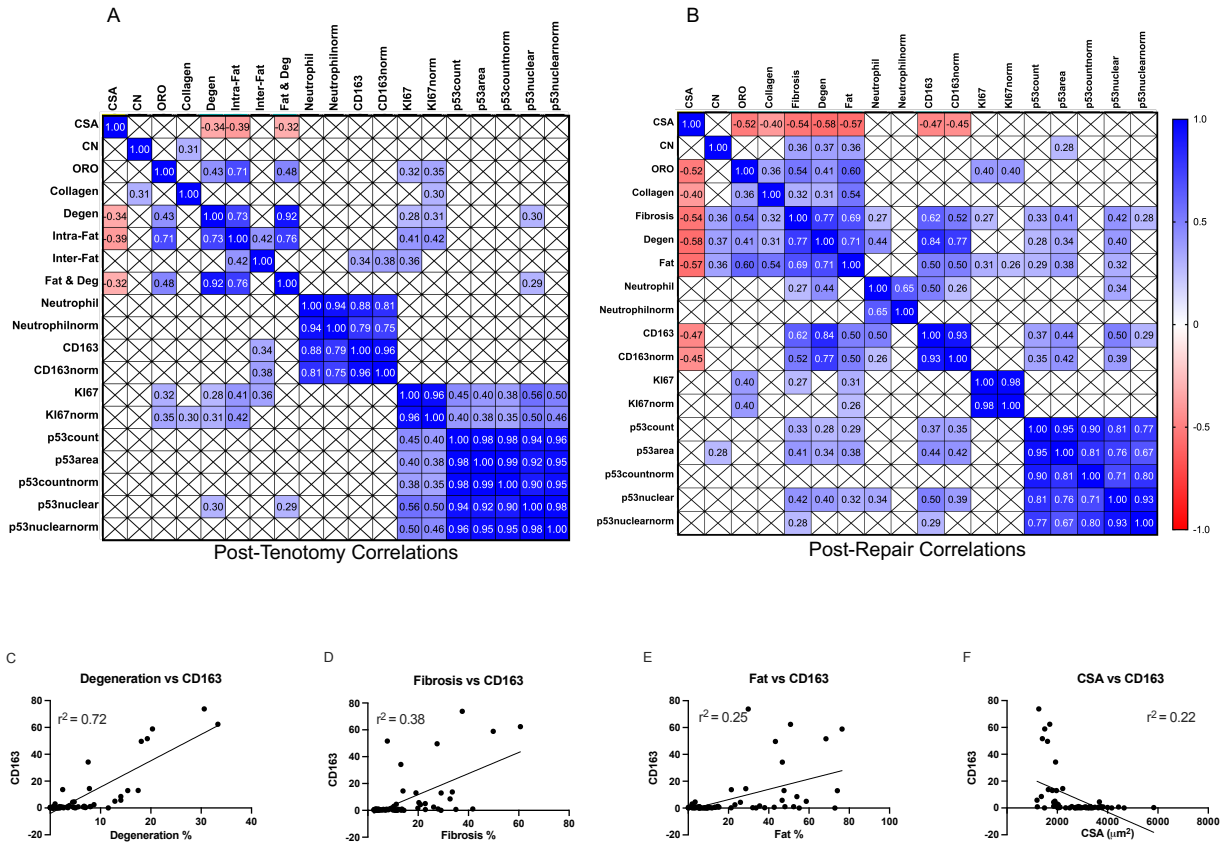

Figure 4.11: Post-Tenotomy & Post-Repair Pearson correlation matrix.

Pearson correlation matrix (r) of all phenotypic and immunofluorescence traits. Only relationships with a significant p-value < 0.05 are displayed. Top scatterplots and linear regression (r^2) values are listed for identified traits.

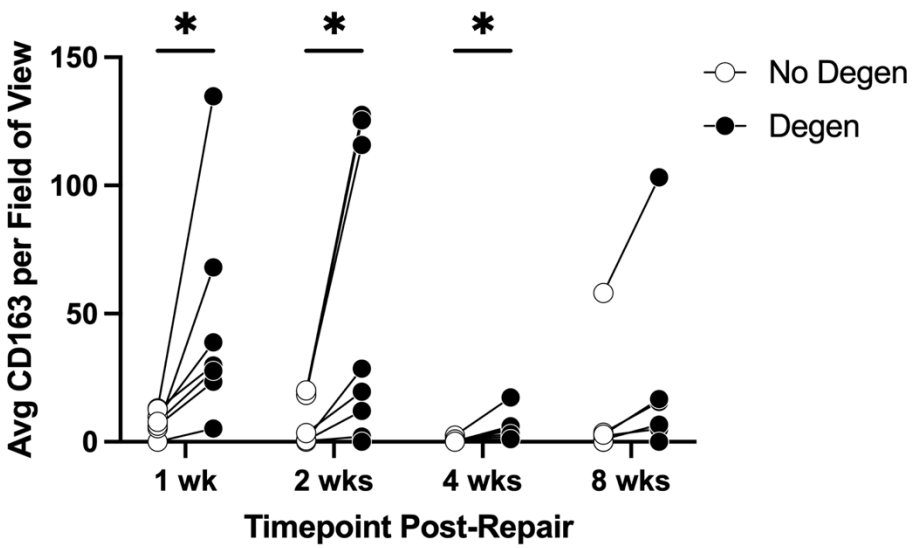

Figure 4.12: Post-Repair Regional CD163 plot.

Regional CD163 counts in degenerated and non-degenerated muscle. * Indicates p-value < 0.05 (Wilcoxon tests).

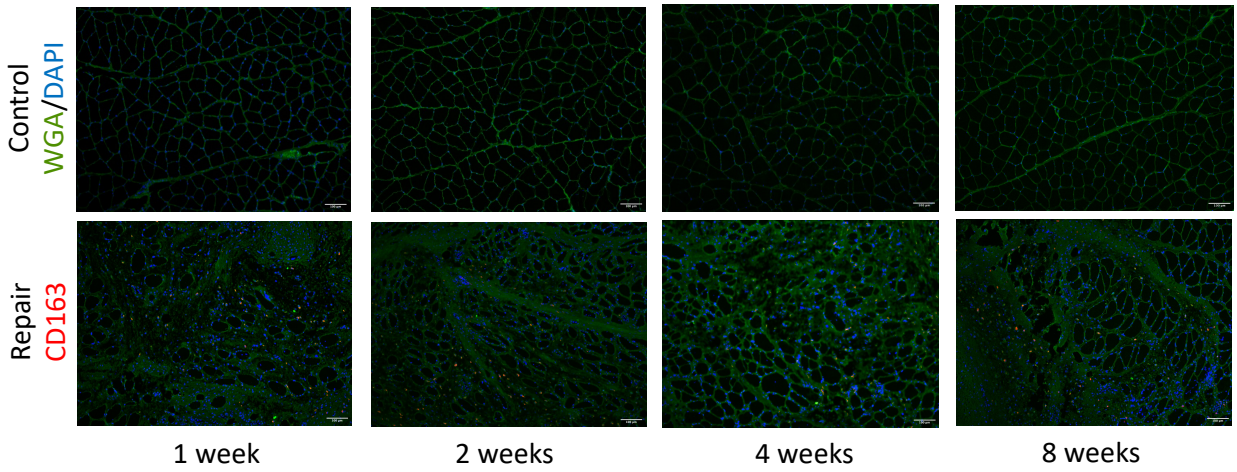

Figure 4.13: Post-Repair Regional CD163 Visualization

Post-repair compared to control. Channels are CD163 (red), membrane/WGA (green) and nuclei/DAPI (blue).

Chapter 5 DISCUSSION

The purpose of Aim 1 was to determine the time-dependent transcriptional profile in muscle after a rotator cuff tear/tenotomy in a rabbit animal model. We hypothesized, based on morphological changes previously observed in this model, that transcriptional activity of certain genes would be time dependent. Early changes demonstrate upregulation of atrophy and inflammation programs, but late changes would demonstrate upregulation of fatty infiltration, degeneration, and fibrosis programs. We sequenced rotator cuff muscles from the posterior region closest to the tendon tear by RNAseq. We measured gene expression at 1, 2, 4, 8, and 16 weeks post-tenotomy, revealed significant wide-spread differential gene expression level at 1 week post-tenotomy compared to sham operated controls, but this transcriptional activity was reduced to minimal expression by the 8 week post-tenotomy time point. There was a resurgence in differential gene expression at 16 weeks post-tenotomy (Figure 2.2). After performing GO and KEGG enrichment analyses, we described the signature of biological programs active at each timepoint (Figure 2.4 & 2.5). There were clear transcriptional differences between each time point, which support the concept of differential timing of inflammation, adipogenesis, fibrosis, and cell death programs that lead to muscle atrophy, degeneration, and fatty infiltration. Lastly, we used weight correlation analysis (WGCNA) to relate morphological characteristics (Vargas-Vila et al., 2021) with transcriptomics and demonstrated that these assays were significantly correlated in these post-tenotomy samples. In summary, this aim provided an overview of the differentially regulated transcriptional programs, their respective time courses, and established that these programs were correlated with the muscle pathology observed in the rabbit rotator cuff tenotomy model.

The purpose of Aim 2 was to determine the time-dependent transcriptional profile after a chronic tear and delayed rotator cuff surgical repair (8 weeks post-tenotomy) in a rabbit animal

model. We hypothesized that surgical repair would induce transcriptional activity associated with hypertrophy in the muscle because it was mechanically re-loaded via tendon repair. We sequenced samples of rotator cuff muscle from the posterior region closest to the tendon repair by RNAseq using methods previously described (Vasquez-Bolanos et al., 2021). We measured gene expression at 1, 2, 4, and 8 weeks post-repair, which demonstrated significant differential gene expression compared to contralateral control muscles at 1 and 2 weeks post-repair, and then reduced to minimal expression by 8 week post-repair (Figure 3.2). After performing GO and KEGG enrichment analysis, we described the signature of biological programs active at each timepoint (Figure 3.4 & 3.5). This signature refuted our hypothesis as there was no hypertrophic or anabolic biological activity observed transcriptionally, instead inflammation, adipogenesis, and fibrosis dominated. Using weight correlation analysis (WGCNA), we determined that histological traits (Wu et al, 2023) and transcriptomics were correlated in the post-repair samples. In summary, this aim provided an overview of the time-dependent transcriptional changes that occur in the rabbit rotator cuff post delayed repair.

The objective of Aim 3 was to dive deeper into a specific biological program that emerged in both transcriptional profiles of Aims 1 and 2, and could possibly be contributing to the irreversible state of rotator cuff muscle observed with muscle atrophy, fibrosis, and fatty infiltration. We hypothesized that the immune system could be contributing to chronic muscle degeneration through the persistence of immune cells (and immune cell activity) at longer time points, along with abnormal cell cycle control and stress signaling. Using immune system specific transcriptional results and immunofluorescent markers for neutrophils (early immune cell), CD163 (M2c macrophage), KI-67 (proliferation marker), and p53 (stress/division marker) we elucidated the possible behavior of the immune system over time post-tenotomy and post-repair. Neutrophils

were increased at 1 and 4 weeks post-tenotomy, while CD163 positive cells were increased at higher numbers compared to controls at 1 and 2 weeks post-tenotomy and post-repair (Fig. 4.3, 4.4) Importantly, we demonstrated significant heterogeneity in the immune cell responses between samples, which was surprising given the standardized procedures and genetic similarity between animals. Leveraging this high degree of variance, we were able to correlate number of CD163+ with morphological traits of degeneration, fat, fibrosis, and CSA (Fig. 4.9). Overall, these results refuted our initial hypothesis which was that there would be persistence of immune cells at later time points after intervention. However, we did identify a significant regional relationship between the presence of CD163+ cells and degenerated muscle when compared to the non-degenerated equivalent muscle. In summary, this aim provided a closer look into the presence of immune system cells post-tenotomy and post-repair and possible relationship with muscle changes over time that may be regionally dependent.

There are limitations to the studies presented in this dissertation. While the rabbit animal model is advantageous for recapitulating the morphology observed in chronic human rotator cuff disease, it is also a challenging model because of the lack of biological tools available compared to mouse and rat. For example, many antibodies are raised in rabbit, which make cross-reactivity an issue for immunofluorescence and consequently, fewer immune cell number could be readily quantified. Likewise, despite having an exceptional set of time course data (4 to 5 time points over 2-3 months) post-tenotomy and post-repair, for a biological program as highly time sensitive as the immune system, it is possible that the temporal resolution of these studies is insufficient to truly capture the shifts occurring in the immune system activity.

In summary, this dissertation explored the time-dependent transcriptional profiles and probed the immune system presence after rotator cuff tear and chronic repair in a rabbit animal

model. The emergence of a unique transcriptional profile late after repair was a key finding. Similarly, the lack of predictable transcriptional responses after chronic repair is important and should steer future research towards the mechano-sensitivity of these chronically torn muscles, or towards the immune system as we have done here. Given the strong immune system transcriptional signature in these muscles across time, and some of the data indicating differential immune cell presence, the relationship between the immune system and other resident cells in skeletal muscle deserves further investigation. Improved access to immune system specific assays and higher temporal resolution would be advantageous for future experiments aimed at understanding the presence of a wide range of immune cells and rotator cuff disease severities. Identifying biological programs and their temporal behavior after rotator cuff injury and repair allows further investigation into potential therapeutics, or adjuvant therapies to surgery, which may improve the state of the muscle and outcomes of surgical repair in the future.

REFERENCES

Alexa A, Rahnenfuhrer J. (2020). topGO: Enrichment Analysis for Gene Ontology. R package version 2.40.0

Andrews, S. (2010). FastQC: a quality control tool for high throughput sequence data.

Benjamini Y, Drai D, Elmer G, Kafkafi N, Golani I. (2001). Controlling the false discovery rate in behavior genetics research. Behav Brain Res. 125(1-2):279-284. Doi:10.1016/S0166-4328(01)00297-2

Bodine SC, Stitt TN, Gonzalez M, Kline WO, Stover GL, Bauerlein R, Zlotchenko E, Scrimgeour A, Lawrence JC, Glass DJ, Yancopoulos GD. (2001). Akt/mTOR pathway is a crucial regulator of skeletal muscle hypertrophy and can prevent muscle atrophy in vivo. Nature cell biology, 3(11), 1014–1019. https://doi.org/10.1038/ncb1101-1014

Bolotta A, Filardo G, Abruzzo PM, Astolfi A, Sanctis PD, Martino AD, Hofer C, Indio V, Kern H, Löfler S, Marcacci M, Zampieri S, Marini M, Zucchini C. (2020). Skeletal Muscle Gene Expression in Long-Term Endurance and Resistance Trained Elderly. Vol 21. doi:10.3390/ijms21113988

Carlson M. (2019). org.Hs.eg.db: Genome wide annotation for Human. R package version 3.8.2.

Chaudhury S, Xia Z, Thakkar D, Hakimi O, Carr AJ. (2016). Gene expression profiles of changes underlying different-sized human rotator cuff tendon tears. J Shoulder Elb Surg. 25(10):1561-1570. doi:10.1016/j.jse.2016.02.037

Cho NS, Rhee YG. (2009). The factors affecting the clinical outcome and integrity of arthroscopically repaired rotator cuff tears of the shoulder. Clin Orthop Surg 1:96-104.

Choo A, McCarthy M, Pichika R, Sato EJ, Lieber RL, Schenk S, Lane JG, Ward SR. (2014). Muscle gene expression patterns in human rotator cuff pathology. J Bone Jt Surg - Am Vol. 96(18):1558-1565. doi:10.2106/JBJS.M.01585

Chung SW, Song BW, Kim YH, Park KU, Oh JH. (2013). Effect of platelet-rich plasma and porcine dermal collagen graft augmentation for rotator cuff healing in a rabbit model. Am J Sports Med 41:2909-2918.

Coenye T. (2021). Do results obtained with RNA-sequencing require independent verification?. Biofilm, 3, 100043. https://doi.org/10.1016/j.bioflm.2021.100043

Coleman SH, Fealy S, Ehteshami JR, MacGillivray JD, Altchek DW, Warren RF, Turner AS. (2003). Chronic rotator cuff injury and repair model in sheep. The Journal of bone and joint surgery. American volume, 85(12), 2391–2402. https://doi.org/10.2106/00004623-200312000-00018

Collin P, Thomazeau H, Walch G, Gerber C, Mansat P, Favard L, Colmar M, Kempf JF, Hervé A, Betz M. (2019). Clinical and structural outcome twenty years after repair of isolated supraspinatus tendon tears. Journal of shoulder and elbow surgery, 28(1), 196–202. https://doi.org/10.1016/j.jse.2018.07.023

Dalbo VJ, Roberts MD, Sunderland KL, Poole CN, Stout JR, Beck TW, Bemben M, Kerksick CM. (2011). Acute loading and aging effects on myostatin pathway biomarkers in human skeletal muscle after three sequential bouts of resistance exercise. The journals of gerontology. Series A, Biological sciences and medical sciences, 66(8), 855–865. https://doi.org/10.1093/gerona/glr091

Davidson PA, Rivenburgh DW. (2000). Rotator cuff repair tension as a determinant of functional outcome. J Shoulder Elbow Surg.9(6):502-6. doi: 10.1067/mse.2000.109385.

Derwin KA, Baker AR, Iannotti JP, McCarron JA. (2010). Preclinical models for translating regenerative medicine therapies for rotator cuff repair. Tissue Eng Part B Rev 16:21-30.

Dobin A, Davis CA, Schlesinger F, Drenkow J, Zaleski C, Jha S, Batut P, Chaisson M, Gingeras TR. (2013). STAR: ultrafast universal RNA-seq aligner. Bioinformatics. 29, 15–21.

Egerman MA, Glass DJ. (2014). Signaling pathways controlling skeletal muscle mass. Critical reviews in biochemistry and molecular biology, 49(1), 59–68. https://doi.org/10.3109/10409238.2013.857291

Farshad, M., Gerber, C., Snedeker, J. G., Frauenfelder, T., & Meyer, D. C. (2011). Structure of retracted tendons after staged repair following continuous traction. Knee surgery, sports traumatology, arthroscopy : official journal of the ESSKA, 19(12), 2131–2137. https://doi.org/10.1007/s00167-011-1430-3

Feng, L., Liu, H., Liu, Y., Lu, Z., Guo, G., Guo, S., Zheng, H., Gao, Y., Cheng, S., Wang, J., Zhang, K., & Zhang, Y. (2010). Power of deep sequencing and agilent microarray for gene expression profiling study. Molecular biotechnology, 45(2), 101–110. https://doi.org/10.1007/s12033-010-9249-6

Flück, M., Schmutz, S., Wittwer, M., Hoppeler, H., & Desplanches, D. (2005). Transcriptional reprogramming during reloading of atrophied rat soleus muscle. American journal of physiology. Regulatory, integrative and comparative physiology, 289(1), R4–R14. https://doi.org/10.1152/ajpregu.00833.2004

Flück, M., Ruoss, S., Möhl, C. B., Valdivieso, P., Benn, M. C., von Rechenberg, B., Laczko, E., Hu, J., Wieser, K., Meyer, D. C., & Gerber, C. (2017). Genomic and lipidomic actions of nandrolone on detached rotator cuff muscle in sheep. Journal of Steroid Biochemistry and Molecular Biology, 165(August), 382–395. https://doi.org/10.1016/j.jsbmb.2016.08.005

Flück M, Fitze D, Ruoss S, Valdivieso P, Rechenberg BV, Neuenschwander AB, Opitz L, Hu J, Laczko E, Wieser K, Gerber C. (2020). Down-Regulation of Mitochondrial Metabolism after Tendon Release Primes Lipid Accumulation in Rotator Cuff Muscle. Am J Pathol. 190(7):1513-1529. doi:10.1016/j.ajpath.2020.03.019

Fisch, K. M., Gamini, R., Alvarez-Garcia, O., Akagi, R., Saito, M., Muramatsu, Y., Sasho, T., Koziol, J. A., Su, A. I., & Lotz, M. K. (2018). Identification of transcription factors responsible for dysregulated networks in human osteoarthritis cartilage by global gene expression analysis. Osteoarthritis and cartilage, 26(11), 1531–1538. https://doi.org/10.1016/j.joca.2018.07.012

Galatz LM, Ball CM, Teefey SA, Middleton WD, Yamaguchi K.. (2004). The outcome and repair integrity of completely arthroscopically repaired large and massive rotator cuff tears. J Bone Joint Surg Am 86:219-224.

Ge, Z., Tang, H., Lyu, J., Zhou, B., Yang, M., Tang, K., & Chen, W. (2020). Conjoint analysis of lncRNA and mRNA expression in rotator cuff tendinopathy. Annals of translational medicine, 8(6), 335. https://doi.org/10.21037/atm.2020.02.149

Gerber, C., Schneeberger, A. G., Perren, S. M., & Nyffeler, R. W. (1999). Experimental rotator cuff repair. A preliminary study. The Journal of bone and joint surgery. American volume, 81(9), 1281–1290. https://doi.org/10.2106/00004623-199909000-00009

Gerber, C., Fuchs, B., & Hodler, J. (2000). The results of repair of massive tears of the rotator cuff. The Journal of bone and joint surgery. American volume, 82(4), 505–515. https://doi.org/10.2106/00004623-200004000-00006

Gerber C, Meyer DC, Schneeberger AG, Hoppeler H, von Rechenberg B. (2004). Effect of tendon release and delayed repair on the structure of the muscles of the rotator cuff: an experimental study in sheep. J Bone Joint Surg Am. 86(9):1973-1982.

Gerber C, Meyer DC, Frey E, Rechenberg BV, Hoppeler H, Frigg R, Jost B, Zumstein MA. (2009). Neer Award 2007: Reversion of structural muscle changes caused by chronic rotator cuff tears using continuous musculotendinous traction. An experimental study in sheep. Journal of shoulder and elbow surgery, 18(2), 163-171.

Gibbons MC, Singh A., Anakwenze O, Cheng T, Pomerantz M, Schenk S, Engler AJ, Ward SR. (2017). Histological Evidence of Muscle Degeneration in Advanced Human Rotator Cuff Disease. The Journal of bone and joint surgery. American volume, 99(3), 190–199. https://doi.org/10.2106/JBJS.16.00335

Gibbons MC, Fisch KM, Pichika R, Cheng T, Engler AJ, Schenk S, Lane JG, Singh A, Ward SR. (2018). Heterogeneous muscle gene expression patterns in patients with massive rotator cuff tears. PLoS One. 13(1):1-17. doi:10.1371/journal.pone.0190439

Gibbons MC, Singh A, Engler AJ, Ward SR. (2018). The role of mechanobiology in progression of rotator cuff muscle atrophy and degeneration. J Orthop Res. 36(2):546-556. doi:10.1002/jor.23662

Gladstone JN, Bishop JY, Lo IKY, Flatow EL. (2007). Fatty infiltration and atrophy of the rotator cuff do not improve after rotator cuff repair and correlate with poor functional outcome. Am J Sports Med. 35(5):719-728. doi:10.1177/0363546506297539

Glass D. J. (2005). Skeletal muscle hypertrophy and atrophy signaling pathways. The international journal of biochemistry & cell biology, 37(10), 1974–1984. https://doi.org/10.1016/j.biocel.2005.04.018

Gumucio, J. P., Qasawa, A. H., Ferrara, P. J., Malik, A. N., Funai, K., McDonagh, B., & Mendias, C. L. (2019). Reduced mitochondrial lipid oxidation leads to fat accumulation in myosteatosis. FASEB journal : official publication of the Federation of American Societies for Experimental Biology, 33(7), 7863–7881. https://doi.org/10.1096/fj.201802457RR

Honda H, Gotoh M, Kanazawa T, Ohzono H, Nakamura H, Ohta K, Nakamura KI, Fukuda K, Teramura T, Hashimoto T, Shichijo S, Shiba N. (2017). Hyaluronic Acid Accelerates Tendon-to-Bone Healing After Rotator Cuff Repair. Am J Sports Med 45:3322-3330.

Hu P, Jiang L, Wu L. (2019). Identify differential gene expressions in fatty infiltration process in rotator cuff. J Orthop Surg Res. 14(1):1-10. doi:10.1186/s13018-019-1182-1

Hyman, S. A., Norman, M. B., Dorn, S. N., Bremner, S. N., Esparza, M. C., Lieber, R. L., & Ward, S. R. (2020). In vivo supraspinatus muscle contractility and architecture in rabbit. Journal of applied physiology (Bethesda, Md. : 1985), 129(6), 1405–1412. https://doi.org/10.1152/japplphysiol.00609.2020

Kobayashi, M., Itoi, E., Minagawa, H., Miyakoshi, N., Takahashi, S., Tuoheti, Y., Okada, K., & Shimada, Y. (2006). Expression of growth factors in the early phase of supraspinatus tendon healing in rabbits. Journal of shoulder and elbow surgery, 15(3), 371–377. https://doi.org/10.1016/j.jse.2005.09.003

Kwon J, Kim YH, Rhee SM, Kim TI, Lee J, Jeon S, Oh JH,. (2018). Effects of Allogenic Dermal Fibroblasts on Rotator Cuff Healing in a Rabbit Model of Chronic Tear. Am J Sports Med 46:1901-1908.

Langfelder, P., & Horvath, S. (2008). WGCNA: an R package for weighted correlation network analysis. BMC bioinformatics, 9, 559. https://doi.org/10.1186/1471-2105-9-559

Law CW, Chen Y, Shi W, Smyth GK. (2014). Voom: Precision weights unlock linear model analysis tools for RNA-seq read counts. Genome Biol.15(2):1-17. doi:10.1186/gb-2014-15-2-r29

Lee YS, Kim JY, Kim HN, Lee DW, Chung SW. (2018). Gene expression patterns analysis in the supraspinatus muscle after a rotator cuff tear in a mouse model. Biomed Res Int. 21-25. doi:10.1155/2018/5859013

Li, B. & Dewey, C. N. (2011). RSEM: accurate transcript quantification from RNA-Seq data with or without a reference genome. BMC Bioinformatics 12, 323

Li X, Shen P, Su W, Zhao S, Zhao J. (2018). Into-Tunnel Repair Versus Onto-Surface Repair for Rotator Cuff Tears in a Rabbit Model. Am J Sports Med 46:1711-1719.

MacDermid, J. C., Ramos, J., Drosdowech, D., Faber, K., & Patterson, S. (2004). The impact of rotator cuff pathology on isometric and isokinetic strength, function, and quality of life. Journal of shoulder and elbow surgery, 13(6), 593–598. https://doi.org/10.1016/j.jse.2004.03.009

Matsumoto F, Uhthoff HK, Trudel G, Loehr JF. (2002). Delayed tendon reattachment does not reverse atrophy and fat accumulation of the supraspinatus--an experimental study in rabbits. J Orthop Res 20:357-363.

McElvany MD, McGoldrick E, Gee AO, Neradilek MB, Matsen FA. (2015). Rotator cuff repair: published evidence on factors associated with repair integrity and clinical outcome. Am J Sports Med 43:491-500.

Ozbaydar M, Elhassan B, Esenyel C, Atalar A, Bozdag E, Sunbuloglu E, Kopuz N, Demirhan M. (2008). A comparison of single-versus double-row suture anchor techniques in a simulated repair of the rotator cuff: an experimental study in rabbits. J Bone Joint Surg Br 90:1386-1391.

Park JS, Park HJ, Kim SH, Oh JH. (2015). Prognostic Factors Affecting Rotator Cuff Healing After Arthroscopic Repair in Small to Medium-sized Tears. Am J Sports Med 43:2386-2392.

Perry, R. L., & Rudnick, M. A. (2000). Molecular mechanisms regulating myogenic determination and differentiation. Frontiers in bioscience : a journal and virtual library, 5, D750–D767. https://doi.org/10.2741/perry

Raudvere U, Kolberg L, Kuzmin I, Arak T, Adler P, Peterson H, Vilo J. (2019). G:Profiler: A web server for functional enrichment analysis and conversions of gene lists (2019 update). Nucleic Acids Res. 47(W1):W191-W198. doi:10.1093/nar/gkz369

Reardon, K. A., Davis, J., Kapsa, R. M., Choong, P., & Byrne, E. (2001). Myostatin, insulin-like growth factor-1, and leukemia inhibitory factor mRNAs are upregulated in chronic human disuse muscle atrophy. Muscle & nerve, 24(7), 893–899. https://doi.org/10.1002/mus.1086

Ren YM, Duan YH, Sun YB, Yang T, Tian MQ. (2018). Bioinformatics analysis of differentially expressed genes in rotator cuff tear patients using microarray data. J Orthop Surg Res. 13(1):1-9. doi:10.1186/s13018-018-0989-5

Ritchie ME, Phipson B, Wu D, Hu Y, Law CW, Shi W, Smyth GK. (2015). Limma powers differential expression analyses for RNA-sequencing and microarray studies. Nucleic Acids Res. 43(7):e47. doi:10.1093/nar/gkv007

Robinson MD, McCarthy DJ, Smyth GK. (2010). edgeR: A Bioconductor package for differential expression analysis of digital gene expression data. Bioinformatics. 26(1):139-140. doi:10.1093/bioinformatics/btp616

Robinson MD, and Oshlack A. (2010). A Scaling Normalization Method for Differential Expression Analysis of RNA-seq data. Genome Biology. 11: R25.

Rowshan K, Hadley S, Pham K, Caiozzo V, Lee TQ, Gupta R. (2010). Development of fatty atrophy after neurologic and rotator cuff injuries in an animal model of rotator cuff pathology. J Bone Joint Surg Am. 92(13):2270-2278.

Rubino, L. J., Sprott, D. C., Stills, H. F., Jr, & Crosby, L. A. (2008). Fatty infiltration does not progress after rotator cuff repair in a rabbit model. Arthroscopy : the journal of arthroscopic & related surgery : official publication of the Arthroscopy Association of North America and the International Arthroscopy Association, 24(8), 936–940. https://doi.org/10.1016/j.arthro.2008.03.004

Rudrappa SS, Wilkinson DJ, Greenhaff PL, Smith K, Idris I, Atherton PJ. (2016). Human skeletal muscle disuse atrophy: Effects on muscle protein synthesis, breakdown, and insulin resistance-A qualitative review. Front Physiol. 1-10. doi:10.3389/fphys.2016.00361

Ruoss, S., Kindt, P., Oberholzer, L., Rohner, M., Jungck, L., Abdel-Aziz, S., ... & Flück, M. (2018). Inhibition of calpain delays early muscle atrophy after rotator cuff tendon release in sheep. Physiological reports, 6(21), e13833.

Ruoss S, Möhl CB, Benn MC, von Rechenberg B, Wieser K, Meyer DC, Gerber C, Flück M. Costamere protein expression and tissue composition of rotator cuff muscle after tendon release in sheep. J Orthop Res 36: 272–281, 2018. doi:10.1002/jor.23624.

Sayampanathan AA, Andrew (2017). THC. Systematic review on risk factors of rotator cuff tears. J Orthop Surg (Hong Kong). 25(1):1-9. doi:10.1177/2309499016684318

Shah SA, Kormpakis I, Cavinatto L, Killian ML, Thomopoulos S, Galatz LM. (2017). Rotator cuff muscle degeneration and tear severity related to myogenic, adipogenic, and atrophy genes in human muscle. J Orthop Res. 35(12):2808-2814. doi:10.1002/jor.23593

Shahidi, B., Fisch, K. M., Gibbons, M. C., & Ward, S. R. (2020). Increased Fibrogenic Gene Expression in Multifidus Muscles of Patients With Chronic Versus Acute Lumbar Spine Pathology. Spine, 45(4), E189–E195. https://doi.org/10.1097/BRS.0000000000003243

Steinbacher P, Tauber M, Kogler S, Stoiber W, Resch H, Sänger AM. (2010). Effects of rotator cuff ruptures on the cellular and intracellular composition of the human supraspinatus muscle. Tissue Cell. 42(1):37-41. doi:10.1016/j.tice.2009.07.001

Su W, Li X, Zhao S, Shen P, Dong S, Jiang J, Zhao J. (2018). Native Enthesis Preservation Versus Removal in Rotator Cuff Repair in a Rabbit Model. Arthroscopy 34:2054-2062.

Sun Y, Kwak JM, Kholinne E, Zhou Y, Tan J, Koh KH, Jeon IH. (2020). Small Subchondral Drill Holes Improve Marrow Stimulation of Rotator Cuff Repair in a Rabbit Model of Chronic Rotator Cuff Tear. Am J Sports Med 48:706-714.

Tashjian RZ, Lock I, Granger EK, Wang Y, Lee Y, Chalmers PN, Jones KB. (2020). Gene Expression in Torn Rotator Cuff Tendons Determined by RNA Sequencing. Orthop J Sport Med. 8(6):1-8. doi:10.1177/2325967120927480

Uhthoff HK, Coletta E, Trudel G. (2014). Effect of timing of surgical SSP tendon repair on muscle alterations. J Orthop Res 32:1430-1435.

Valencia AP, Lai JK, Iyer SR, Mistretta KL, Spangenburg EE, Davis DL, Lovering RM, Gilotra MN. (2018). Fatty Infiltration Is a Prognostic Marker of Muscle Function After Rotator Cuff Tear. Am J Sports Med. 46(9):2161-2169.

Van de Peer Lab. http://bioinformatics.psb.ugent.be/webtools/Venn/

Vargas-Vila MA, Gibbons MC, Wu IT, Esparza MC, Kato K, Johnson SD, Masuda K, Ward SR. (2021) Progression of muscle loss and fat accumulation in a rabbit model of rotator cuff tear. J Orthop Res. 10.1002/jor.25160. doi: 10.1002/jor.25160.

Vasquez-Bolanos LS, Gibbons MC, Ruoss S, Wu IT, Vargas-Vila M, Hyman SA, Esparza MC, Fithian DC, Lane JG, Singh A, Nasamran CA, Fisch KM and Ward SR (2021). Transcriptional Time Course After Rotator Cuff Tear. Front. Physiol. 12:707116. doi: 10.3389/fphys.2021.707116

Vasquez-Bolanos, L. S., Gibbons, M. C., Ruoss, S., Wu, I. T., Esparza, M. C., Fithian, D. C., Lane, J. G., Singh, A., Nasamran, C. A., Fisch, K. M., & Ward, S. R. (2023). Transcriptional time course after rotator cuff repair in 6 month old female rabbits. Frontiers in physiology, 14, 1164055. https://doi.org/10.3389/fphys.2023.1164055

Waskom, M. L., (2021). seaborn: statistical data visualization. Journal of Open Source Software, 6(60), 3021, https://doi.org/10.21105/joss.03021

Yamamoto, A., Takagishi, K., Osawa, T., Yanagawa, T., Nakajima, D., Shitara, H., & Kobayashi, T. (2010). Prevalence and risk factors of a rotator cuff tear in the general population. Journal of shoulder and elbow surgery, 19(1), 116–120. https://doi.org/10.1016/j.jse.2009.04.006

Yoon JP, Lee CH, Jung JW, Lee HJ, Lee YS, Kim JY, Park GY, Choi JH, Chung SW. (2018). Sustained Delivery of Transforming Growth Factor beta1 by Use of Absorbable Alginate Scaffold Enhances Rotator Cuff Healing in a Rabbit Model. Am J Sports Med 46:1441-1450.

Wu, I. T., Gibbons, M. C., Esparza, M. C., Vasquez-Bolanos, L. S., Hyman, S. A., Dorn, S. N., Singh, A., Lane, J. G., Fithian, D. C., Ruoss, S., & Ward, S. R. (2022). The "Second Hit" of Repair in a Rabbit Model of Chronic Rotator Cuff Tear. Frontiers in physiology, 13, 801829. https://doi.org/10.3389/fphys.2022.801829

Deng, B., Wehling-Henricks, M., Villalta, S. A., Wang, Y., & Tidball, J. G. (2012). IL-10 triggers changes in macrophage phenotype that promote muscle growth and regeneration. Journal of immunology (Baltimore, Md. : 1950), 189(7), 3669–3680. https://doi.org/10.4049/jimmunol.1103180

Watanabe, S., Alexander, M., Misharin, A. V., & Budinger, G. R. S. (2019). The role of macrophages in the resolution of inflammation. The Journal of clinical investigation, 129(7), 2619–2628. https://doi.org/10.1172/JCI124615

Sezgin, M., & Sankur, B. (2004). Survey over image thresholding techniques and quantitative performance evaluation. J. Electronic Imaging, 13, 146-168.

Lee, C., Agha, O., Liu, M., Davies, M., Bertoy, L., Kim, H. T., Liu, X., & Feeley, B. T. (2020). Rotator Cuff Fibro-Adipogenic Progenitors Demonstrate Highest Concentration, Proliferative Capacity, and Adipogenic Potential Across Muscle Groups. Journal of orthopaedic research : official publication of the Orthopaedic Research Society, 38(5), 1113–1121. https://doi.org/10.1002/jor.24550

Lee, Y. S., Kim, J. Y., & Chung, S. W. (2020). Rotator cuff muscle stem cells: the double-edged sword in the skeletal muscle. Annals of translational medicine, 8(11), 717. https://doi.org/10.21037/atm.2020.02.32

Bianco, S. T., Moser, H. L., Galatz, L. M., & Huang, A. H. (2019). Biologics and stem cell-based therapies for rotator cuff repair. Annals of the New York Academy of Sciences, 1442(1), 35–47. https://doi.org/10.1111/nyas.13918

Chung, S. W., Kim, S. H., Tae, S. K., Yoon, J. P., Choi, J. A., & Oh, J. H. (2013). Is the supraspinatus muscle atrophy truly irreversible after surgical repair of rotator cuff tears?. Clinics in orthopedic surgery, 5(1), 55–65. https://doi.org/10.4055/cios.2013.5.1.55

Shah, S. A., Kormpakis, I., Cavinatto, L., Killian, M. L., Thomopoulos, S., & Galatz, L. M. (2017). Rotator cuff muscle degeneration and tear severity related to myogenic, adipogenic, and atrophy genes in human muscle. Journal of orthopaedic research : official publication of the Orthopaedic Research Society, 35(12), 2808–2814. https://doi.org/10.1002/jor.23593

De Santa, F., Vitiello, L., Torcinaro, A., & Ferraro, E. (2019). The Role of Metabolic Remodeling in Macrophage Polarization and Its Effect on Skeletal Muscle Regeneration. Antioxidants & redox signaling, 30(12), 1553–1598. https://doi.org/10.1089/ars.2017.7420

Abraham, A. C., Shah, S. A., & Thomopoulos, S. (2017). Targeting Inflammation in Rotator Cuff Tendon Degeneration and Repair. Techniques in shoulder & elbow surgery, 18(3), 84–90. https://doi.org/10.1097/BTE.0000000000000124

Tidball, J. G., & Villalta, S. A. (2010). Regulatory interactions between muscle and the immune system during muscle regeneration. American journal of physiology. Regulatory, integrative and comparative physiology, 298(5), R1173–R1187. https://doi.org/10.1152/ajpregu.00735.2009

Kim, MG., Lim, K., Lee, Y.J. et al. M2 macrophages predict worse long-term outcomes in human acute tubular necrosis. Sci Rep 10, 2122 (2020). https://doi.org/10.1038/s41598-020-58725-w

Villalta, S. A., Nguyen, H. X., Deng, B., Gotoh, T., & Tidball, J. G. (2009). Shifts in macrophage phenotypes and macrophage competition for arginine metabolism affect the severity of muscle pathology in muscular dystrophy. Human molecular genetics, 18(3), 482–496. https://doi.org/10.1093/hmg/ddn376

Jensen, S. M., Bechshøft, C. J. L., Heisterberg, M. F., Schjerling, P., Andersen, J. L., Kjaer, M., & Mackey, A. L. (2020). Macrophage Subpopulations and the Acute Inflammatory Response of Elderly Human Skeletal Muscle to Physiological Resistance Exercise. Frontiers in physiology, 11, 811. https://doi.org/10.3389/fphys.2020.00811

Oprescu, S. N., Yue, F., Qiu, J., Brito, L. F., & Kuang, S. (2020). Temporal dynamics and heterogeneity of cell populations during skeletal muscle regeneration. IScience, 23(4).

Giannakis, N., Sansbury, B. E., Patsalos, A., Hays, T. T., Riley, C. O., Han, X., Spite, M., & Nagy, L. (2019). Dynamic changes to lipid mediators support transitions among macrophage subtypes during muscle regeneration. Nature immunology, 20(5), 626–636. https://doi.org/10.1038/s41590-019-0356-7

Frich, L. H., Fernandes, L. R., Schrøder, H. D., Hejbøl, E. K., Nielsen, P. V., Jørgensen, P. H., Stensballe, A., & Lambertsen, K. L. (2021). The inflammatory response of the supraspinatus muscle in rotator cuff tear conditions. Journal of shoulder and elbow surgery, 30(6), e261–e275. https://doi.org/10.1016/j.jse.2020.08.028

Stengaard, K., Hejbøl, E. K., Jensen, P. T., Degn, M., Ta, T. M. L., Stensballe, A., Andersen, D. C., Schrøder, H. D., Lambertsen, K. L., & Frich, L. H. (2022). Early-stage inflammation changes in supraspinatus muscle after rotator cuff tear. Journal of shoulder and elbow surgery, 31(7), 1344–1356. https://doi.org/10.1016/j.jse.2021.12.046

Gumucio, J. P., Davis, M. E., Bradley, J. R., Stafford, P. L., Schiffman, C. J., Lynch, E. B., Claflin, D. R., Bedi, A., & Mendias, C. L. (2012). Rotator cuff tear reduces muscle fiber specific force production and induces macrophage accumulation and autophagy. Journal of orthopaedic research : official publication of the Orthopaedic Research Society, 30(12), 1963–1970. https://doi.org/10.1002/jor.22168

Rogeri, P. S., Gasparini, S. O., Martins, G. L., Costa, L. K. F., Araujo, C. C., Lugaresi, R., Kopfler, M., & Lancha, A. H., Jr (2020). Crosstalk Between Skeletal Muscle and Immune System: Which Roles Do IL-6 and Glutamine Play?. Frontiers in physiology, 11, 582258. https://doi.org/10.3389/fphys.2020.582258

Bernard, C., Zavoriti, A., Pucelle, Q., Chazaud, B., & Gondin, J. (2022). Role of macrophages during skeletal muscle regeneration and hypertrophy-Implications for immunomodulatory strategies. Physiological reports, 10(19), e15480. https://doi.org/10.14814/phy2.15480

Ziemkiewicz, N., Hilliard, G., Pullen, N. A., & Garg, K. (2021). The Role of Innate and Adaptive Immune Cells in Skeletal Muscle Regeneration. International journal of molecular sciences, 22(6), 3265. https://doi.org/10.3390/ijms22063265

Minari, A. L. A., & Thomatieli-Santos, R. V. (2022). From skeletal muscle damage and regeneration to the hypertrophy induced by exercise: what is the role of different macrophage subsets?. American journal of physiology. Regulatory, integrative and comparative physiology, 322(1), R41–R54. https://doi.org/10.1152/ajpregu.00038.2021

Saclier, M., Cuvellier, S., Magnan, M., Mounier, R., & Chazaud, B. (2013). Monocyte/macrophage interactions with myogenic precursor cells during skeletal muscle regeneration. The FEBS journal, 280(17), 4118–4130. https://doi.org/10.1111/febs.12166

Walton, R.G., Kosmac, K., Mula, J. et al. Human skeletal muscle macrophages increase following cycle training and are associated with adaptations that may facilitate growth. Sci Rep 9, 969 (2019). https://doi.org/10.1038/s41598-018-37187-1

Howard, E. E., Pasiakos, S. M., Blesso, C. N., Fussell, M. A., & Rodriguez, N. R. (2020). Divergent Roles of Inflammation in Skeletal Muscle Recovery From Injury. Frontiers in physiology, 11, 87. https://doi.org/10.3389/fphys.2020.00087

Zúñiga-Pereira, A. M., Santamaría, C., Gutierrez, J. M., Alape-Girón, A., & Flores-Díaz, M. (2019). Deficient Skeletal Muscle Regeneration after Injury Induced by a Clostridium perfringens Strain Associated with Gas Gangrene. Infection and immunity, 87(8), e00200-19. https://doi.org/10.1128/IAI.00200-19

Yu, Y., Yue, Z., Xu, M., Zhang, M., Shen, X., Ma, Z., Li, J., & Xie, X. (2022). Macrophages play a key role in tissue repair and regeneration. PeerJ, 10, e14053. https://doi.org/10.7717/peerj.14053

Breuer, K., Foroushani, A. K., Laird, M. R., Chen, C., Sribnaia, A., Lo, R., Winsor, G. L., Hancock, R. E., Brinkman, F. S., & Lynn, D. J. (2013). InnateDB: systems biology of innate immunity and beyond--recent updates and continuing curation. Nucleic acids research, 41(Database issue), D1228–D1233. https://doi.org/10.1093/nar/gks1147

Nathan C. (2002). Points of control in inflammation. Nature, 420(6917), 846–852. https://doi.org/10.1038/nature01320

Rigamonti, E., Zordan, P., Sciorati, C., Rovere-Querini, P., & Brunelli, S. (2014). Macrophage plasticity in skeletal muscle repair. BioMed research international, 2014, 560629. https://doi.org/10.1155/2014/560629

Silldorff, M. D., Choo, A. D., Choi, A. J., Lin, E., Carr, J. A., Lieber, R. L., Lane, J. G., & Ward, S. R. (2014). Effect of supraspinatus tendon injury on supraspinatus and infraspinatus muscle passive tension and associated biochemistry. The Journal of bone and joint surgery. American volume, 96(20), e175. https://doi.org/10.2106/JBJS.M.01315

Wehling-Henricks, M., Jordan, M. C., Gotoh, T., Grody, W. W., Roos, K. P., & Tidball, J. G. (2010). Arginine metabolism by macrophages promotes cardiac and muscle fibrosis in mdx muscular dystrophy. PloS one, 5(5), e10763. https://doi.org/10.1371/journal.pone.0010763

Rigamonti, E., Zordan, P., Sciorati, C., Rovere-Querini, P., & Brunelli, S. (2014). Macrophage plasticity in skeletal muscle repair. BioMed research international, 2014, 560629. https://doi.org/10.1155/2014/560629

Wang, X., & Zhou, L. (2022). The Many Roles of Macrophages in Skeletal Muscle Injury and Repair. Frontiers in cell and developmental biology, 10, 952249. https://doi.org/10.3389/fcell.2022.952249

Arnold, L., Henry, A., Poron, F., Baba-Amer, Y., van Rooijen, N., Plonquet, A., Gherardi, R. K., & Chazaud, B. (2007). Inflammatory monocytes recruited after skeletal muscle injury switch into antiinflammatory macrophages to support myogenesis. The Journal of experimental medicine, 204(5), 1057–1069. https://doi.org/10.1084/jem.20070075

Frey, E., Regenfelder, F., Sussmann, P., Zumstein, M., Gerber, C., Born, W., & Fuchs, B. (2009). Adipogenic and myogenic gene expression in rotator cuff muscle of the sheep after tendon tear. Journal of orthopaedic research : official publication of the Orthopaedic Research Society, 27(4), 504–509. https://doi.org/10.1002/jor.20695

Wang, Y., Lu, J., & Liu, Y. (2022). Skeletal Muscle Regeneration in Cardiotoxin-Induced Muscle Injury Models. International journal of molecular sciences, 23(21), 13380. https://doi.org/10.3390/ijms232113380

Hirata, A., Masuda, S., Tamura, T., Kai, K., Ojima, K., Fukase, A., Motoyoshi, K., Kamakura, K., Miyagoe-Suzuki, Y., & Takeda, S. (2003). Expression profiling of cytokines and related genes in regenerating skeletal muscle after cardiotoxin injection: a role for osteopontin. The American journal of pathology, 163(1), 203–215. https://doi.org/10.1016/S0002-9440(10)63644-9

Villalta, S. A., Nguyen, H. X., Deng, B., Gotoh, T., & Tidball, J. G. (2009). Shifts in macrophage phenotypes and macrophage competition for arginine metabolism affect the severity of muscle pathology in muscular dystrophy. Human molecular genetics, 18(3), 482–496. https://doi.org/10.1093/hmg/ddn376

Mounier, R., Théret, M., Arnold, L., Cuvellier, S., Bultot, L., Göransson, O., Sanz, N., Ferry, A., Sakamoto, K., Foretz, M., Viollet, B., & Chazaud, B. (2013). AMPKα1 regulates macrophage skewing at the time of resolution of inflammation during skeletal muscle regeneration. Cell metabolism, 18(2), 251–264. https://doi.org/10.1016/j.cmet.2013.06.017

Gibbons, M. C., Sato, E. J., Bachasson, D., Cheng, T., Azimi, H., Schenk, S., Engler, A. J., Singh, A., & Ward, S. R. (2016). Muscle architectural changes after massive human rotator cuff tear. Journal of orthopaedic research : official publication of the Orthopaedic Research Society, 34(12), 2089–2095. https://doi.org/10.1002/jor.23256

Laumonier, T., & Menetrey, J. (2016). Muscle injuries and strategies for improving their repair. Journal of experimental orthopaedics, 3(1), 15. https://doi.org/10.1186/s40634-016-0051-7

Thomopoulos, S., Parks, W. C., Rifkin, D. B., & Derwin, K. A. (2015). Mechanisms of tendon injury and repair. Journal of orthopaedic research : official publication of the Orthopaedic Research Society, 33(6), 832–839. https://doi.org/10.1002/jor.22806